STRUCTURAL AND MINERALOGIC CHARACTERIZATION OF THE SOUTH PRAIRIE FAULT IN THE STILLWATER COMPLEX, BEARTOOTH MOUNTAINS, MONTANA

By

Jacob Oliver Thacker

A thesis submitted in partial fulfillment
of the requirements for the degree

of

Master of Science

in

Earth Sciences

MONTANA STATE UNIVERSITY
Bozeman, Montana

April 2014

©COPYRIGHT

by

Jacob Oliver Thacker

2014

All Rights Reserved

ACKNOWLEDGEMENTS

First and foremost I sincerely extend my gratitude to Dr. David R. Lageson for taking me on and guiding me as his student. The amount I have learned from Dave is extraordinary and from every facet of geology, especially structure and tectonics. Dr. David Mogk has also been invaluable with his consistent kindness and knowledge of mineralogy and metamorphic petrology. Thank you also to Colin Shaw for serving on my committee, and an immense thank you to Lowell Miyagi for selflessly helping me for uncounted hours. Thank you to Stillwater geologist Mike Pasecznyk for his help underground and insightful conversation, and Eric Kucinski for his photography. I also wish to collectively thank my peers for all their help: Christine Maday, Mel Baldwin, Eric Easley, Nick Atwood, Ryan Hillier, Dan Ross, and the rest of the structure crew. An immense thank you to Helen Lynn for her expertly written thesis, which served as a model for writing my own. I would also like to thank my mother Jill, Tania Thacker, Adam Mentkowski, Valerie Hansel, and the Yellowstone Association. A special thanks is indebted to my father, to whom I owe my love for the mountains. Unfortunately, there are too many people to thank for a project of this magnitude, and anyone left out is not intentional but rather a result of the overwhelming kindness received the last few years. For that, lastly, I wish to thank you all.

None of this work would have been possible without help from the Stillwater Mining Company and geologists Mike Koski and Paul Holick. I also wish to extend gratitude to the MSU Department of Earth Sciences, and the Tobacco Root Geological Society, Clay Minerals Society, and Colorado Scientific Society for funding this research.

TABLE OF CONTENTS

1. INTRODUCTION 1

2. GEOLOGIC BACKGROUND 5

Beartooth Mountains 5
The Stillwater Complex 6
General Structure of the Stillwater Complex 11
The South Prairie Fault 13

3. FAULT TERMINOLOGY USED IN THIS STUDY 15

Fault Zone Terminology 15
Fault Rock Terminology 16

4. PREVIOUS LARAMIDE FAULT STUDIES AND SIGNIFICANCE OF THE SOUTH PRAIRIE FAULT 19

5. METHODS 22

Outcrop Analysis 23
Fault Zone Descriptions 23
Fault Zone Measurements 23
Selection Method Fracture Analysis 25
Inventory Method Fracture Analysis 25
Core Analysis 26
Geometric and Kinematic Analysis 27
South Prairie Fault and Fracture Data 27
Regional Geometric Analysis 27
Balanced Cross-section 28
Sampling Methods 28
X-ray Diffraction Analysis 30
Powder Diffraction 30
Synchrotron Diffraction 31
Material Analysis Using Diffraction (MAUD) 31
Thin-section Microscopy and Petrographic Analysis 33

6. RESULTS AND DISCUSSION 36

Geometry and Kinematics of the SPF 36
Geometry 36
Kinematics 39

TABLE OF CONTENTS – CONTINUED

Balanced Cross-section 42
Extent of the Core and Damage Zone and the Architecture and Permeability of the SPF 45
Extent and Characteristics of the Core Zone and Damage Zone 45
Analysis of South Prairie Fault Fracture and Vein Orientations 50
Vein Characteristics within the South Prairie Fault 61
Architecture and Permeability of the South Prairie Fault 62
Role of Fluids within the South Prairie Fault 66
Mineralogy of the South Prairie Fault and How it Varies 69
Host Rock 71
Damage Zone 74
Veins 83
Core Zone 85
Synkinematic T/P Conditions and the Deformation Mechanisms 90
T/P Conditions within the South Prairie Fault 90
Pt/Pd Mobility within the South Prairie Fault 93
Deformation Mechanisms 97
Preferred Orientation of Fault Zone Rock and Material 101

7. CONCLUSIONS 104

Geometry and Kinematics of the South Prairie Fault 104
Extent of the South Prairie Fault's Core Zone and Damage Zone and its Architecture and Permeability 104
Mineralogy of the South Prairie Fault and How It Varies 106
Syn-kinematic T/P Conditions and the Deformation Mechanisms 108

REFERENCES 110

APPENDICES 119

APPENDIX A: Orientation Measurements of Beartooth Front Tectonic Features 120
APPENDIX B: Estimated Anorthite Concentrations 122

LIST OF TABLES

Table Page

1. Objectives, questions, and methods used to research the South Prairie fault.....4

2. Fault rock classification.....18

LIST OF FIGURES

Figure Page

1. Regional context 6

2. Geologic map of the Stillwater Complex.....9

3. Generalized stratigraphic column of the Stillwater Complex.....10

4. General geologic map overlay 14

5. Idealized fault zone structure 17

6. Fault zone measurement method 24

7. Inventory fracture analysis method.....26

8. Locations visited 32

9. 2600 level samples.....34

10. 4800 level samples.....35

11. Laramide regional stress-strain diagram (Brown, 1993) 37

12. Rose diagrams of geometric study.....38

13. Beartooth front structural features stereonet.....39

14. 3D schematic diagram of South Prairie fault kinematics.....41

15a. Balanced cross-section.....43

15b. Line-length restored cross section 44

16. Core zone vein at 2600 level.....46

17. HW-localized shear zone 48

18. FW-localized shear zone.....48

19. Internal folding of core zone gouge.....49

LIST OF FIGURES – CONTINUED

Figure Page

20. Rose diagram of fracture and vein orientations 51

21. Offset fractures at 4800 level 52

22. Stereonets of all fractures and veins from all locations visited 55

23. Stereonets of FW fractures by each level 56

24. Stereonets of core zone fractures by each level 57

25. Stereonets of HW fractures by each level 58

26. Stereonets compilation of all FW fractures 59

27. Stereonets compilation of all core zone fractures 59

28. Stereonets compilation of all HW fractures 59

29. 4800 HW Riedel R'-fractures 60

30. Widths of SPF architecture at 4800 level 64

31. Permeability estimate plot of SPF 65

32. Thin-section scans of FW host rocks at 2600 and 4800 level 73

33. Thin-section scan of HW-DZ at 4800 level 74

34. Photomicrograph of HW-DZ unstable and stable fractures 77

35. Photomicrograph of clinozoitization after plagioclase 79

36. Photomicrographs of serpentinized orthopyroxenes 81

37. Photomicrograph of undulose extinct quartz 81

38. Photomicrograph of altered clinopyroxene 82

39. Photomicrograph of vein fill 85

LIST OF FIGURES – CONTINUED

Figure Page

40. XRD results of 4800 CZ transect....87

41. Thin-section scan of CZ foliated gouge....88

42. Photomicrograph of sigma structure porphyroclast with vein fill material....89

43. Thin-section scan of HW-localized-shear zone....89

44. Photomicrograph of microfaults dying out into ductile matrix....99

45. Thin-section scan of cataclastic flow in 29w10200 core zone....100

46. Samples taken from core for synchrotron diffraction....103

ABSTRACT

The South Prairie fault (SPF) is a Laramide basement-involved fault located in the Archean ultramafic-mafic layered Stillwater Complex of the Beartooth Mountains, southern Montana. Laramide movement on the fault is suggested by the sub-greenschist alteration within the fault zone, as well as its similar strike geometry to the Laramide Horseman and Beartooth thrusts. The SPF is rarely visible in outcrop, but is exposed in the subsurface at several levels via active Pt/Pd mining by the Stillwater Mining Company to depths of 2400 feet below the Stillwater River. Thus, the SPF offers a unique and rare opportunity to study an in-situ basement fault never exposed to surface alteration processes, thereby giving a "pristine" look at the micro- and mesoscopic characteristics of a Laramide fault zone from which interpretations of Laramide fault behavior may be made. This study also offers the chance to characterize brittle deformation characteristics of mafic/ultramafic rocks. Both of these aspects have received little attention in previous Laramide fault studies, which have focused more on geometric and kinematic history or faulting in quartzo-feldspathic basement rocks.

To characterize the SPF, X-ray diffraction, thin-section analyses and subsurface observations have been conducted. Fracturing and alteration increase towards the heavily altered and cataclasized core zone. Width of the core zone is dependent on host rock. Mineralogy varies from essentially unaltered noritic and gabbronoritic compositions in the host rock to mainly tremolite, clinozoisite and serpentine/chlorite within the damage zone. Veins are composed of stilbite and minor carbonate with talc. The core zone is abundant in serpentine-chlorite, as evidenced by XRD. Plagioclase is observed to withstand heavy stable fracturing and minor alteration to clinozoisite at grain boundaries before complete alteration. Orthopyroxene succumbs to serpentinization much sooner at the same conditions. Evidence of pre-, syn- and post-kinematic fluids are abundant, and are consistent with the estimated architecture of the SPF. These characteristics observed suggest syn-kinematic sub-greenschist conditions of $T<300$ ºC and $P<400$ MPa, consistent with brittle to brittle-plastic deformation.

CHAPTER 1

INTRODUCTION

The South Prairie fault (SPF) is a backthrust located in the Archean age ultramafic-mafic cumulate layered Stillwater Complex of the Beartooth arch[1] in southern Montana. Surface outcrops of the fault are rare across its 20 km (12 mile) trace (Cox and Holick, 2008) and observation is restricted to the subsurface mining operations of the Stillwater Mining Company (SMC) near Nye, MT. At this location, the SPF is observed to intercalate with the Pt-/Pd-rich JM Reef of the Lower Banded Series that is currently being mined by the SMC. Geologic maps and early observations suggest that the above-ground continuation of the SPF displaces Cambrian strata at a high elevation above the Stillwater River Valley (Jones et al., 1961; Page and Nokleberg, 1974; Segerstrom and Carlson, 1982; Cooper et al., 2002). This suggests that the fault's most recent motion likely occurred during the Laramide orogeny and, therefore, offers a unique and rare opportunity to study the syn-kinematic characteristics of an in-situ Laramide basement fault that is essentially unaltered by post-kinematic processes such as weathering and erosion. Therefore, this contrasts with previous Laramide fault studies which have only been able to observe the characteristics of faults and fault rocks that crop out at the surface (Mitra and Frost, 1981; Miller, 1987; Evans, 1988; Smith, 1991).

---

[1] Arch is used herein instead of the term uplift, as suggested by Erslev (1993).

Much has been discussed and published about the macro-megascopic geometry (Brown, 1993) and kinematics (Erslev, 1993; Wise, 2000; Neely and Erslev, 2009) of the Laramide orogeny and major Laramide faults. These queries have even included analyses of the dynamics (stress field) associated with Laramide orogenesis (Bird, 1998; Lijun et al., 2010; Jones et al., 2011). However, there is disproportionately less written about the micro-mesoscopic aspects of Laramide faults and, when considered, most work has dealt with the characteristics of quartzofeldspathic rocks (Mitra and Frost, 1981; Mitra, 1984; Miller, 1987; Evans, 1988; Smith, 1991; Goddard and Evans, 1995). The aim of this study is to address the mechanical behavior and faulting characteristics of mafic and ultramafic rocks at sub-greenschist to greenschist conditions, and can be condensed into four main objectives (Table 1). These are to characterize:

(1) the geometry and kinematics of the SPF;

(2) the extent of the SPF's core and damage zone and its architecture and permeability;

(3) the mineralogy of the SPF and how it varies spatially;

(4) and the syn-kinematical mineral assemblage and its deduced T and P conditions, including deformation mechanisms associated at these conditions.

The specific questions regarding these objectives are shown in Table 1. How these results compare to other published results, and how the behavior and characteristics of these rock types compare to quartzofeldspathic rocks, has also been examined.

In order to address these goals, outcrop and core analysis, laboratory analyses, stereographic techniques, and analysis of a thin-section transect across the SPF were incorporated (Table 1). The role of phyllosilicates in the SPF is overwhelmingly apparent, and the observations associated with these minerals can be used to discern fluid-flow characteristics and faulting mechanisms. A lack of expanding clays, such as montmorillonite, also has interesting implications for the behavior of the SPF, and can be applied to civil engineering projects such as tunneling as well as extended mining activity within the Stillwater Complex and other ore bodies located in magmatic crystalline rocks.

Objectives	Questions	Methods
Geometry and kinematics of the SPF	Is this a Laramide fault?	Geometric and kinematic analysis, balanced cross-section, mineralogy
Extent of the SPF's core and damage zone and its architecture and permeability	What is the extent of the core and damage zone? What is the architecture and permeability? What was the role of fluids within the fault?	Outcrop analysis and measurements Caine et al. (1996) method Thin-section and outcrop analysis, mineralogy
Mineralogy of the SPF and how it varies	What is the mineral assemblage of the fault zone? What are the pre-, syn-, and post-kinematically derived phases?	XRD, thin-section analysis
Syn-kinematic T & P conditions and the deformation mechanisms	What were the syn-kinematic T & P conditions within the SPF? What were the deformation mechanisms? What is the degree of preferred orientation of fault zone rocks and material?	Mineralogy Thin-section analysis, outcrop analysis XRD synchrotron, MAUD

Table 1: Objectives, questions, and methods used to characterize the South Prairie fault.

CHAPTER 2

GEOLOGIC BACKGROUND

The Beartooth Mountains

The Beartooth range of Montana and Wyoming is a NW-SE trending, basement-involved Laramide foreland arch that is composed of four allochthonous blocks of various Precambrian origins (Wooden et al., 1988; Mogk, 1988) (Figure 1). These are the metasupracrustal North Snowy and Jardine (or South Snowy) blocks, the granitic-gneissic Beartooth block, and the ultramafic-mafic Stillwater Complex block. Assembly of these blocks most likely took place during the late Archean, with completion having occurred by the end of the Archean (Mogk, 1988). Episodes of tectonic activity and/or regional metamorphism after Archean assembly have been cited (Page, 1977; Page and Zientek, 1985), with the most recent and evident having occurred during the Cretaceous-Tertiary Laramide orogeny. Arching of the range occurred via the Beartooth thrust to the northeast and the Gardiner fault to the southwest. Eocene-age Absaroka volcanics are dispersed throughout the Beartooth Mountains from near Cooke City and in the Paradise Valley west of the arch and north of Yellowstone National Park. Neogene to recent crustal extension has down-dropped this edge of the Beartooth arch.

The Stillwater Complex

Cropping out as a 180 km^2 (70 mi^2) block of basement rock on the eastern Beartooth front, the Stillwater Complex is the upturned edge of a lopolith. Its dissected nature has precluded any determination of its original volume and true dimensions, but geophysical data to the northeast suggests that the remainder of the complex is up to

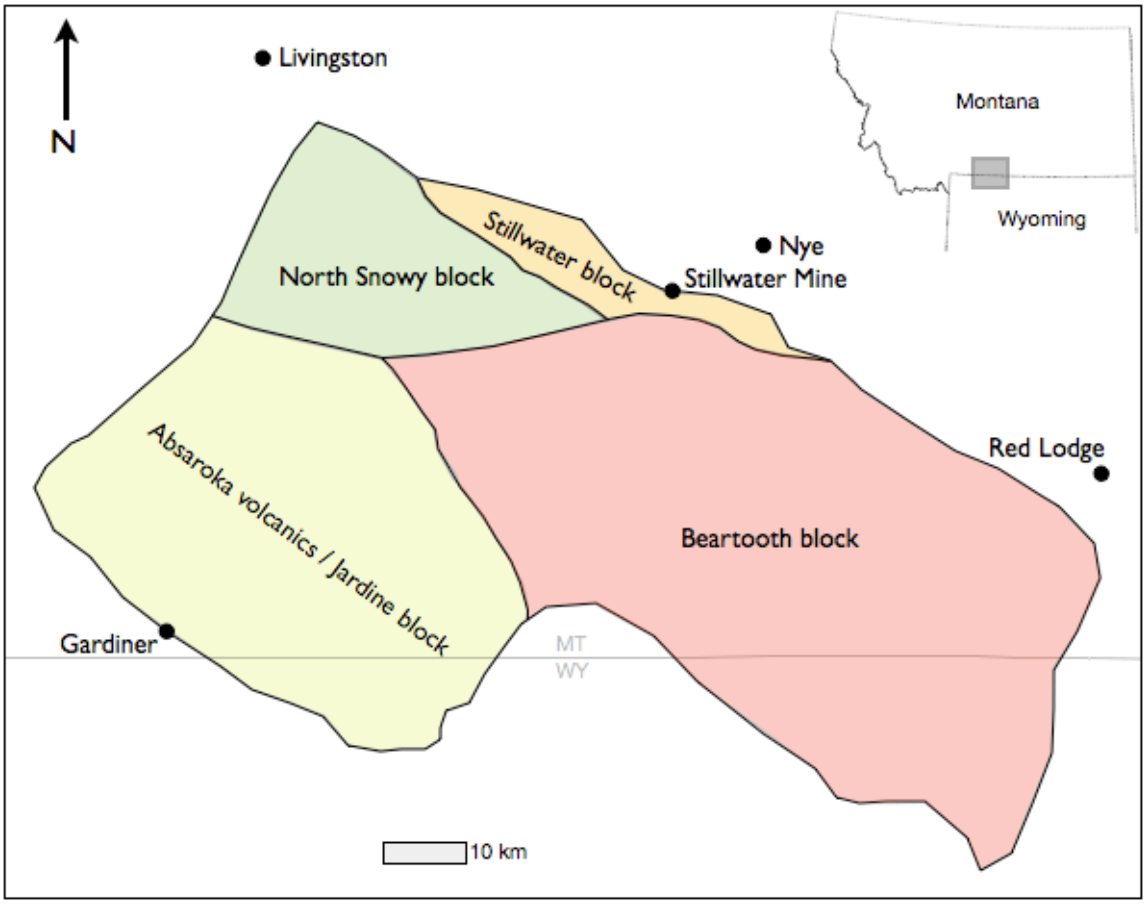


Figure 1: Regional context of the Beartooth Mountains showing allochthonous blocks including the Stillwater Complex. Accretion of the present-day Beartooth massif occurred by the late Archean (Mogk, 1988).

4400 km^2 (1700 mi^2) (Kleinkopf, 1985; Finn et al., 2013). Isotopic evidence has shown that the Stillwater intrusion formed after a major crust forming event that occurred approximately 2.8 Ga (Mueller et al., 2010), with intrusion of the Stillwater magmas occurring about 2701 Ma (DePaolo and Wasserburg, 1979). The intrusion of Stillwater magmas was into a regime of folded and slightly metamorphosed sedimentary rocks. These rocks were subsequently metamorphosed to a cordierite-pyroxene hornfels due to injection of the magmas above (Page, 1977). Field evidence has shown that the Stillwater Complex was not originally intruded into its present location along the Beartooth arch (Mogk and Geissman, 1984; Page, 1985; Geissman and Mogk, 1986), and it has been postulated that intrusion occurred somewhere south of its current location in what was most likely a tectonically quiescent (Page and Zientek, 1985) pull-apart basin (Mogk, 1988). Evidence for this quiescence is seen in the continuous stratiform nature of the layered cumulates, typically traceable for a majority of the exposed 46 km (29 mile) length of the complex. Faults that formed during magmatic intrusion (referred to as "growth faults") occasionally disrupt the linearity of these cumulates in the lower parts of the complex, and have experienced reactivated offset in the form of transverse faults as recently as the Laramide orogeny (Page, 1977). Their original geometry has been interpreted to be graben-style faults that allowed for thickening of certain successions of Stillwater magmas (Jones et al., 1960; Page and Zientek, 1985; Turner et al., 1985). This thickening has been observed in outcrop, and the faults have also been observed and inferred from outcrop and core observations.

Accretion to the main Beartooth block occurred in the Archean prior to intrusion of the 2500 Ma Mouat quartz monzonite, which crosscuts both the Beartooth block to the south and the Stillwater Complex. Gravity studies have also shown that the remainder of the complex may lie just to the northeast of the Beartooth front (Kleinkopf, 1985), meaning that transport of the unit may have kept it entirely or mostly intact. Active USGS research is currently assessing whether this buried portion of the complex is economic for subsurface drill mining (Finn et al, 2013).

It has been hypothesized by Page (1977), Geissman and Mogk (1986) and Mogk (1988) that transport of the complex occurred along an ancestral form of the Mill Creek-Stillwater fault zone, the "Centre fault" of Wilson (1936), with motion being left-lateral. This fault zone has been a major structural feature during the Beartooth arch's long history, and likely had recurrent activity through the Laramide orogeny with continued sinistral motion (Wise, 2000). Continuation of the complex in the subsurface to the northeast of the Beartooth front is also congruous with erupted fragments from Cretaceous volcanics and intrusives near the front containing phenocrysts of ultramafic-mafic Stillwater Complex rocks (Brozdowski, 1985). Post-juxtaposition low-grade metamorphism also occurred at least once, as determined by a penetrative serpentinization and greenschist facies mineralization (Page 1977; Page and Zientek, 1985; McCallum, 2002). As mentioned, Laramide deformation reactivated old syn-emplacement structures within the complex, and is also responsible for tilting the complex to its near-vertical and occasionally overturned position. Tilting of the complex

to this position during the Laramide is evidenced by similar geometry of Cambrian rocks in the Benbow area south of Nye, however other locations suggest tilting of the complex prior to Cambrian sedimentation. This is shown by high-angle angular unconformities between Stillwater rocks and Cambrian rocks in areas such as Picket Pin (Page and Nokleberg, 1974; Segerstrom and Carlson, 1982). This evidence suggests that tilting prior to Cambrian deposition was likely with further tilting having occurred during the Laramide.

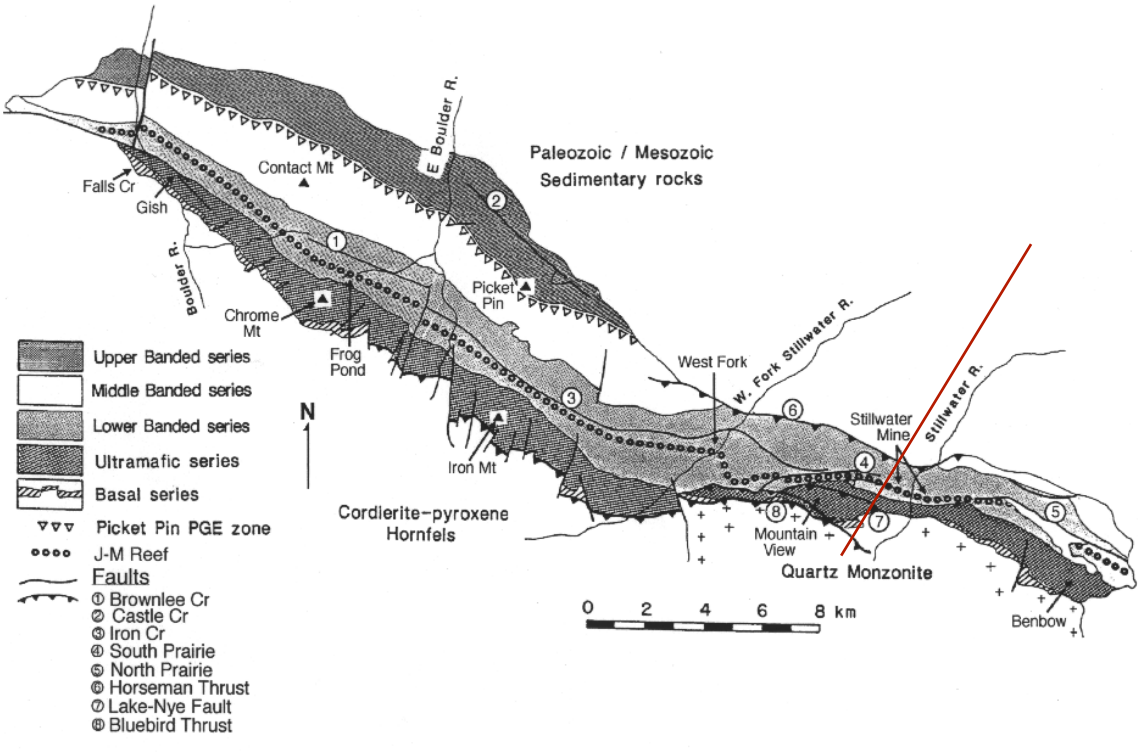


Figure 2: Geologic map of the exposed portion of the Stillwater Complex modified from McCallum, 2002 (refer to regional context in Figure 1). The South Prairie fault is represented by circle number 4 on the map. Figure 15 cross-section line is shown approximately by the red line.

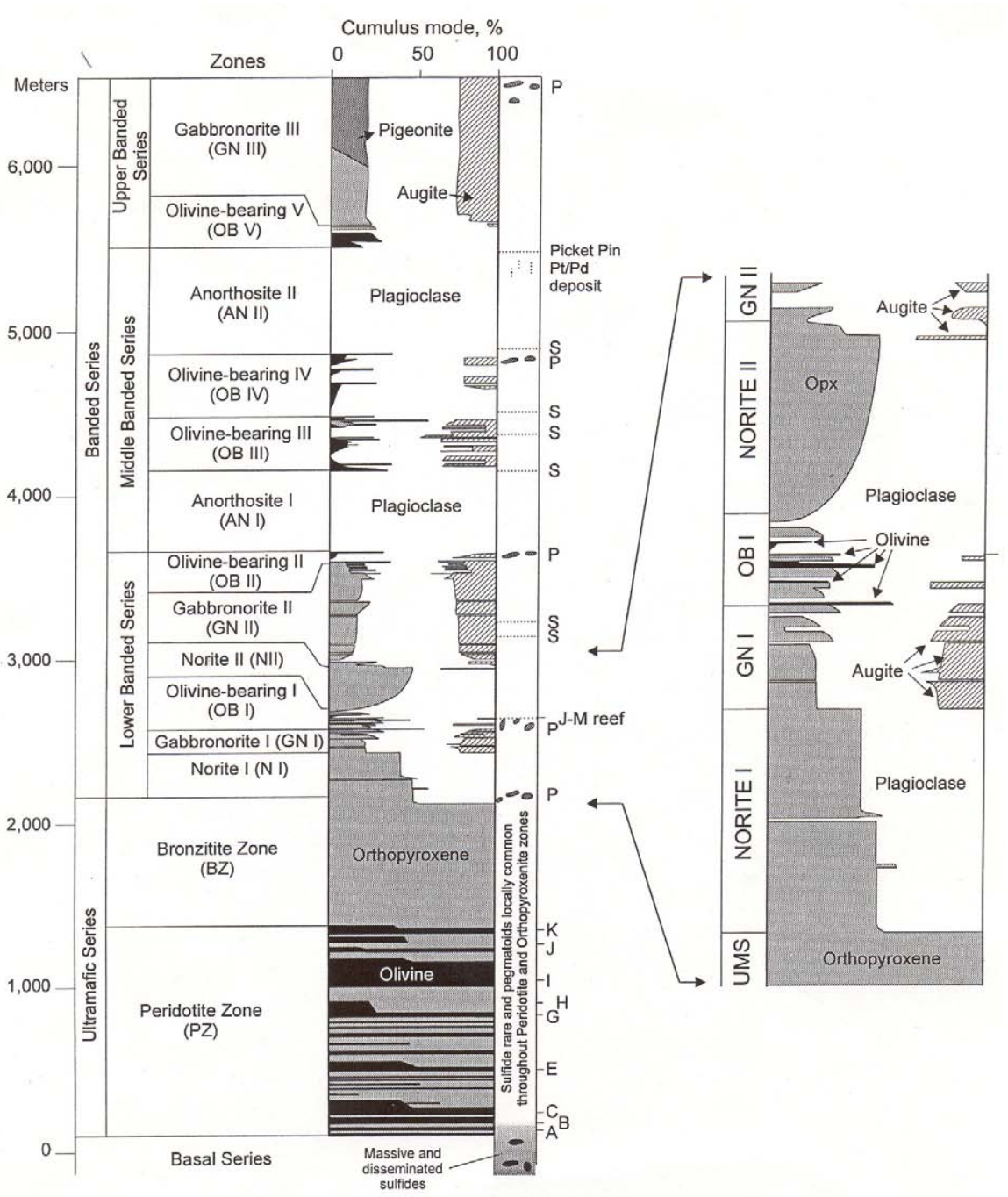


Figure 3: Generalized stratigraphic column of the Stillwater Complex (McCallum, 2002). The SPF occurs in the Lower Banded Series of the complex, coincident with the Pt-/Pd-rich JM Reef.

General Structure of the Stillwater Complex

An intricate series of faults are observed within the Stillwater Complex. Some of these faults, such as the syn-emplacement growth faults, have been intermittently active for the entire 2700 Ma existence of the complex. The prior-mentioned Mill Creek-Stillwater fault zone has been active for a large portion of the complex's history, and has also experienced motion as recent as the Laramide. The most pronounced structural effects to the complex most likely took place during the Laramide, with major frontal faults, such as the Beartooth and Horseman thrusts, forming. Other major faults observed within and near the complex also likely formed during Laramide orogenesis. Though these faults experienced motion during Laramide tectonism, the possibility of prior motion as early as the late Archean to early Proterozoic is likely. Therefore, reactivation during the Laramide must be considered.

Early work within the Stillwater Complex by Jones et al. (1960) recognized four distinct fault geometries. This generalization was also used by Page (1977):

Type 1: Longitudinal ramp and thrust faults striking N45-75W, dipping northeast.

Type 2: Longitudinal reverse and thrust faults striking nearly due west, dipping south.

Type 3: Possible strike-slip faults trending east-west, sinistral slip. South side raised.

Type 4: Transverse faults striking between N30E and N30W.

Type 1 faults are coincident with the dip of the complex's layers, and likely formed as a competency contrast within these cumulate layers. The South Prairie fault is an example of a Type 1 fault, and will be discussed below.

Examples of Type 2 faults include the Horseman, Bluebird and the main Beartooth thrust, which becomes a blind thrust in the vicinity of the Stillwater Complex. It is likely Type 2 faults represent Laramide faults, such as the Beartooth thrust and the Horseman thrust, which splays off the Beartooth thrust at depth (see Figure 15a, Chapter 6). The Bluebird thrust is likely Laramide as well, given its geometry and the reverse-drag style folding of Stillwater Complex layers near the Bluebird Peak area of the complex (see Figure 48 of Page, 1977).

Growth faults likely represent Type 3 and 4 faults. These faults formed during the intrusion of the Stillwater magmas and resulted in what have been called "basement irregularities" (Page and Zientek, 1985) that are seen in the cumulate layering. Footwall basins have been described as having a thicker succession of layering, as opposed to thinning and disappearance of some layering in the stratigraphically higher areas (Turner et al., 1985). The thickened sequences are postulated to have bounding faults on either side that acted as graben-style basins, thickening the intruding magmas at these localities. Three such growth faults have been observed, and drill cores have also supplemented the existence of these faults. Turner et al. (1985) considered some of these faults to have been the reactivated transverse faults mentioned above (Type 3 or 4). The Stillwater River valley has been shown to reside in one of these faults (the Stillwater Valley fault of Turner et al., 1985), and drill data has shown it to offset the South Prairie fault and the JM Reef left-laterally up to 120 meters across the valley.

The South Prairie Fault

According to the Reid (1913) fault classification, the South Prairie fault is a high-angle reverse fault (backthrust) that dips on average 63ºN, and has minor dextral oblique-slip as suggested by slickenlines measured along the fault face that give an average rake of R=78º from the west. In relation to the Stillwater Complex layering, the SPF is a strike-oriented fault, and is parallel to other faults within the complex and region, such as the Horseman, North Prairie, and main Beartooth thrusts. Jones et al. (1960) and Page's (1977) classification of Stillwater Complex faults places the SPF as a Type 1 fault that may have formed due to a competency contrast in the Lower Banded Series. This contrast most likely occurred in the Olivine Bearing zone 1 (OB I, Figure 3), between the lower Gabbronorite 1 (GN I) and the overlying Norite 2 (N II) layer. This is also the zone that comprises the JM Reef, which the SPF often cuts or repeats. Cox and Holick (2008) noted that ore located within gouge of the SPF can have platinum group metal (PGM) grades equal to or greater than relatively undeformed zones of the JM Reef. Subsurface mining of the JM Reef by the SMC has exposed cross-sectional views of the SPF at various levels of the mine (see Figure 8, Chapter 5), and continued diamond drilling has provided a three dimensional geometric view of the SPF at all depths of the mine. However, the layer-parallel geometry of the SPF has precluded any reliable determination of how much dip separation occurred along the SPF. Mineralized JM Reef strata duplexed by the SPF suggests a range of a few hundred feet to >2500 feet (>750 m).



Figure 4: GoogleEarth image with the SPF, Horseman thrust, inferred Stillwater River fault (Page, 1977), and major stratigraphic units generalized and overlain. View is to the south. No vertical exaggeration is used. Stillwater Complex rocks on the east (left) side of the Stillwater River are locally overturned whereas rocks on the west are high angle.

CHAPTER 3

FAULT TERMINOLOGY USED IN THIS STUDY

Fault Zone Terminology

Faults zones are discontinuities along which there is visible offset by shear displacement (Davis et al., 2012) within the brittle to brittle-ductile portion of the crust, and are encompassed by a hanging wall (HW) and footwall (FW). Zones of varying deformation typically encompass a fault (Caine et al., 1996) and can be gradational or sharp boundaries (Figure 5). Rock on the outer perimeter of these zones unaffected by deformation is termed the protolith or, as used herein, the host rock. The damage zone is a moderately to heavily brecciated zone that may be gradational from the host rock. Some faults exhibit a FW damage zone (FW-DZ) and a HW damage zone (HW-DZ), while others may have only one of these zones or neither. Due to brecciation, it is likely that damage zones are conduits for fluid-flow. Extensive veining within damage zones supports this claim.

Increased brecciation and cataclasis leads to a zone of pulverized rock (gouge) known as the core zone (CZ). The core zone is the zone of localized slip within a fault zone (Gudmundsson, 2011) and often contains a network of anastomosing fractures that partitions the amount of total slip within the core zone (Chester and Logan, 1986). The damage zone/core zone interface is typically a sharp contact (Gudmundsson, 2011). Clay minerals and clay-sized particles associated with the core zone typically cause it to be a

barrier to fluid-flow, unlike the brecciated damage zone. These mechanical contrasts affect the ability or inability of fluid to flow between the damage zone and core zone, and is thought to lead to fault rupture by causing fluid over-pressure within the fault zone (Scholz, 1992; Scholz, 1996; Babcock et al., 2013).

Fault Rock Terminology

Fault rocks are classified by the amount and size of cataclastic material they are composed of, and are separated by whether they are cohesive or incohesive as a function of the amount of cementation that has taken place since fault movement (Table 2). These fault rocks consist of breccia and gouge. The damage zone will typically consist of breccias that decrease in size from meter-scale to centimeter-scale towards the core zone. Core zones dominantly consist of gouge (foliated or non-foliated), but can have lenses of plucked host rock and damage zone material within them. At the microscopic scale, cataclastic flow textures can be observed within gouges. Pseudotachylytes are also common in the brittle crust and are the result of high heat from friction. It is likely that these form in fault zones that lack fluids (Sibson, 1977).

Alteration of minerals at varying conditions within gouge often leads to altered or recrystallized material that varies from the original host rock material. Gouge typically consists of clay minerals such as illite, smectite, serpentine, and chlorite, and can have a mix of any of these minerals. Host rock lithology seems to be the greatest influence on the gouge mineralogy present within a fault zone, but fluid-flow and temperature/pressure

conditions also contribute. Prior studies (Buatier et al., 2012 and references therein) have cited that gouge material has a weak preferred orientation texture of generally <2.5 multiples of a random distribution (m.r.d.), but as high as 7 m.r.d; shale samples can be 4-9 m.r.d. **(**Wenk et al., 2008**)**. This general lack of preferred orientation suggests that gouge has a tendency to "tumble" during fault movement, rather than glide (H.R. Wenk, personal communication), and has implications for fluid movement within a gouge zone. Gouge mineralogy and texture at specified temperature/pressure conditions was a large part of this study and will be discussed in Chapter 6.

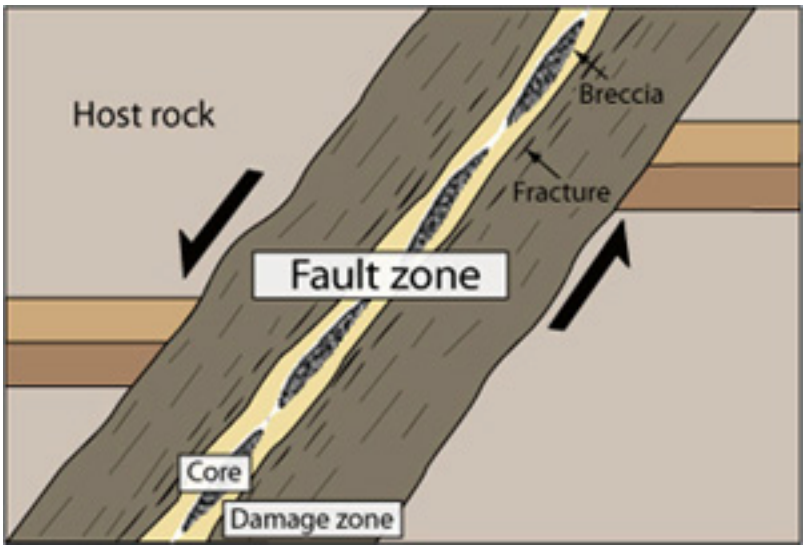


Figure 5: Idealized cross-sectional view of a fault zone showing the host rock, core, and damage zone. After Gudmundsson, 2011.

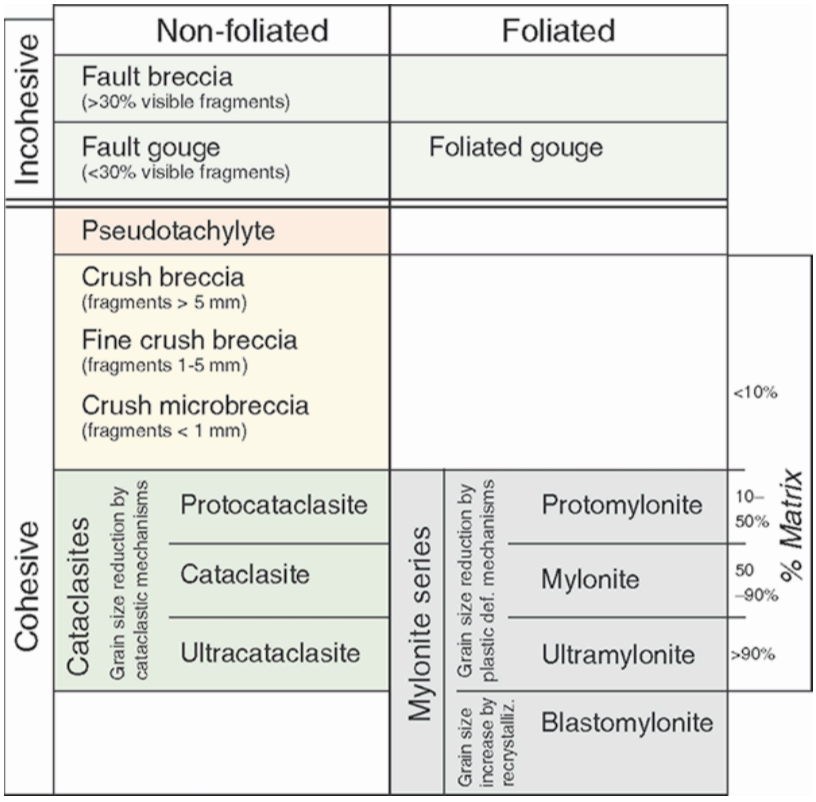


Table 2: Fault rock classification according to Sibson (1977) and modified by Scholz (1990).

CHAPTER 4

PREVIOUS LARAMIDE FAULT STUDIES AND SIGNIFICANCE OF THE SPF

Mesoscopic to microscopic characteristics of Laramide faults have been difficult to study in the past due to either a lack of exposure and/or weathering and erosion leading to post-kinematic alteration of the fault zone material. Therefore, microscopic-scale mechanisms of Laramide faulting has received little attention in the past (Miller, 1987). It is likely that subaerial exposure of faults obliterates gouge textures, such as preferred orientation, within fault zones, and can lead to incorrect interpretations on the behavior of fault zone material and the mechanics of faulting. Chester and Logan (1986) remarked that fracture intensity observed in subaerial fault zone exposures is dramatically reduced at just 0.5 to 1 m below the air-rock interface. Therefore, this warrants the implications of fracture patterns found in this study as they are subsurface and likely record syn-kinematically induced fractures. Subaerial obliteration of fault zone textures is also more likely in fault zone material that consists of expanding clays. Both of these situations are negated by the subsurface observations of the SPF provided by the Stillwater Mining Company.

The active mining operation at the Stillwater mine has produced exposures and abundant drill data of the SPF at levels up to three thousand feet below the Stillwater River Valley near Nye, MT. Given the fault's subsurface nature, it is likely that post-kinematic alteration to the fault zone's associated fractures and mineralogy has been

sufficiently minimal (meteoric fluid-flow is likely) so as not to destroy fragile features. From these observations, deductions on the mineral and fracture characteristics of the fault zone and interpretations of its behavior can be made. Therefore, the SPF allows a rare look into an in-situ Laramide basement fault that has remained virtually unchanged since the Laramide orogeny.

This research also differs from previous studies in that most or all Laramide basement fault studies have focused on quartzofeldspathic host rocks, the typical basement lithology of the Archean Wyoming Province. These studies have included the deformation mechanisms at greenschist and lower conditions (Mitra, 1984; Evans, 1988), mineral assemblages and deduced temperature-pressure conditions (Miller, 1987; Smith, 1991), as well as geochemical fluid-rock interactions (Goddard and Evans, 1995). All of these studies were conducted on subaerial exposures and samples collected from subaerial exposures. It is well understood that the characteristics of deformation will vary in differing host rocks. This variability extends to basement rocks of disparate lithologies as well, and the deformation of rocks that do not contain quartz should behave physically and chemically different from quartzofeldspathic rocks. This study is the first to be conducted on mafic-ultramafic rocks in a Laramide basement fault zone, as well as one conducted using samples from subsurface exposures. The most similar study to this one was conducted on subsurface faults in a tunnel boring site in the Gotthard Massif of Switzerland (Lützenkirchen, 2002; Lützenkirchen and Loew, 2011). Again, however, host

rock was quartzofeldspathic. Despite the different host rock, interesting similarities did occur between this study and the Gotthard Massif.

The San Andreas Fault Observatory at Depth (SAFOD) project is currently being conducted by a large number of researchers. This project lends many similarities to SAFOD by studying the *in-situ* physical-chemical characteristics of a fault zone (Zoback et al., 2011), and how it changes near and across the fault zone. However, study of the SPF differs from SAFOD mainly in that (1) the SPF is not an active fault, (2) earthquake dynamics such as nucleation and rupturing are not addressed, (3) the host rock of the San Andreas fault is essentially quartzofeldspathic, (4) seismic and well log characteristics are not being analyzed for the SPF, and (5) the SPF is not a plate-boundary fault. Similarities between the two faults are likely, though, and it is anticipated that inherent fault zone processes can explain these similarities and/or differences.

CHAPTER 5

METHODS

Characterization of the SPF was completed using a variety of field and lab-based techniques (Table 1). Structural characteristics are important for interpreting the behavior of faults during movement, as well as for understanding their likelihood of transporting or impeding fluids. Faults are also very important mechanically for the construction and longevity of civil engineering projects such as tunnel and road construction, and consequently merits analysis of the differing attributes of deformation within disparate lithologies. Therefore, fractures and veins associated with the fault were noted and measured, and their association with other fractures and fracture sets were also considered. In addition, the architecture of the SPF was measured and interpreted.

Alteration mineralogy of fault zones is important for deducing the conditions at which faulting took place, and can be used for interpreting how a fault behaved and responded to intrinsic and extrinsic variables. Extrinsic variables include, but are not limited to: fluid-flow, fluid overpressure, and overburden. Gouge formation, mechanical and rock competency contrasts, and T-P conditions are examples of intrinsic variables. Samples collected from the SPF were used to examine its mineralogy and the microscopic and sub-microscopic characteristics of deformation and alteration. The association of minerals with one another also has implications for fault zone processes,

and the cause of certain mineral assemblages was also examined to help better understand the behavior of the SPF during faulting.

Outcrop Analysis

Five exposures of the SPF were visited at three different levels within the mine (Figure 8). At each location the following procedures were conducted:

Fault Zone Descriptions

Overall descriptions of the fault zone were taken before sampling, measurements and fracture analyses were conducted. Where a water source was available, a dry description was first completed, then a wet description. Descriptions included color of the fault zone material, nature of the gouge zone (anastomosing, planar, etc), HW and FW color changes and qualitative sizes compared to the core zone, as well as how optimal the location was. Unique characteristics (such as apparent veining relationships) that differed from prior locations were also noted.

Fault Zone Measurements

At each locality, the SPF's width was measured and broken down into core zone and damage zone. The damage zones were described as the HW-DZ and FW-DZ. Strike and dip of the fault was measured by sighting at most locations due to lack of a discrete surface. At cross-sectional views, a tape measure was laid across the floor of the access connecting the CZ-DZ contact and measured by lining up the compass with the tape

measure and sighting the dip. An overhanging face of the SPF was available at the 26w8000 location, and also provided slickenlines for rake measurements.

Widths of the core and damage zones were measured perpendicular to the strike of the SPF at specific locations. An azimuth was measured to ensure an approximate perpendicular reading for true thicknesses. A tape measure was then used against the face of the fault to record the measurement (Figure 6). Changes in width were noted and given as a range. Where exposures were not ideal, an exposed thickness was measured. In some cases, a thickness could not be estimated due to lack of exposure of the damage zone on the opposite face of the access.



Figure 6: Example of core and damage zone measurements at the 2600 level (refer to Figure 8). Tape length is approximately 1.5 meters. Geologist is Mike Pasecznyk.

Selection Method Fracture Analysis

Fractures were analyzed first using a selection method (Van der Pluijm and Marshak, 2004) in which major fracture sets were noted, sketched, and then individually measured. This method characterizes the major fractures and fracture sets within and encompassing the fault zone.

Inventory Method Fracture Analysis

Fractures were then measured using an inventory fracture analysis method (Van der Pluijm and Marshak, 2004) with a one square meter grid (Figure 7). In this method, every fracture inside the grid was noted, sketched, and measured. Vein-filled fractures were noted as such, and their aperture was measured. Fractures measured in the selection method were typically left out and noted as being a selection method fracture. An inventory transect across the SPF at the 48w8400 location was partially completed, but unable to be finished due to subsequent inaccessibility. During this inventory analysis, fractures from the selection method were measured again and noted to their corresponding set from the selection method.

Three of the sites only partially exposed the SPF and were not conducive for comprehensive fracture analyses. The two cross-sectional views were at the 4800 level about 50 feet apart from each other. These localities provided a perpendicular exposure across the entire SPF from undamaged FW host rock through to the HW. However, due to time restrictions in the mine, only one of the 48w8400 localities was able to be fully

analyzed. At the partially exposed locations, fractures were measured and were still used for statistical analyses (presented in Chapter 6).

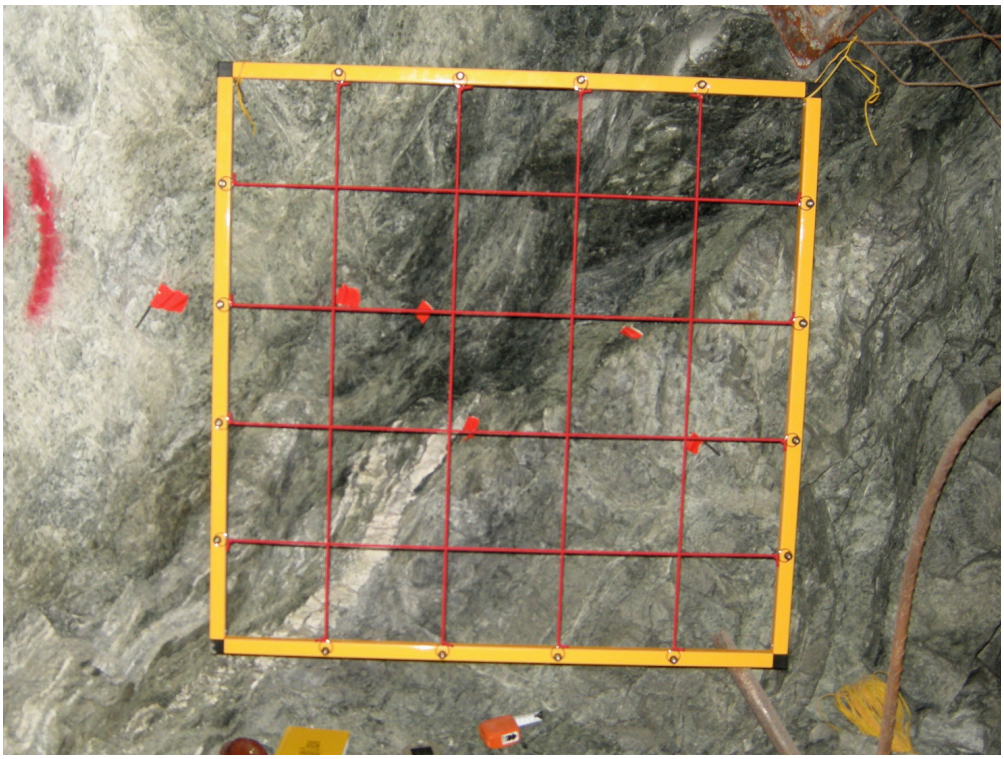


Figure 7: Example of the inventory fracture analysis with the one square meter grid. Orange flags represent sample locations.

Core Analysis

Cores through the SPF at the 2300 and 2000 foot levels (Figure 8) were provided by the Stillwater Mining Company. These were analyzed to estimate the width of the fault zone and also used for XRD and XRD-synchrotron analyses. Selection and inventory fracture analyses were not possible on these cores, however fracture and vein characteristics were noted.

Geometric and Kinematic Analysis

South Prairie Fault and Fracture Data

Fracture and fault orientation data were plotted on equal area lower hemisphere stereonets and rose diagrams using Rockware Stereostat for the purpose of geometric, kinematic and statistical analyses. Kamb contoured plots of fracture and vein data were made from poles to planes figures. These contoured plots aid in identifying statistically significant populations of data and are scaled to the sample size (Lynn, 2012). Kamb plots were used to deduce any dominant fracture patterns in the HW, FW, and core zone of the SPF by each level and by each zone.

Regional Geometric Analysis

To test the validity of the SPF's trend with published estimates of the Laramide shortening direction, trends of structures in proximity to the Beartooth front near the Stillwater Complex to just south of Red Lodge, MT were measured on the Montana Bureau of Mines and Geology Red Lodge 1:100,000 geologic map (Lopez, 2001). These data were then plotted on rose diagrams using Rockware Stereostat (Figure 12); the resultant vectors were subsequently taken and plotted on a stereonet. Results are presented in Chapter 6 (Figure 13). Dip values on the resultant stereonet were given as 90º on all features (except for thrust faults) to show the general trend of the feature being considered. Thrust faults were given an assumed 30º dip for the purpose of visual reference.

Balanced Cross-section

A cross-section was constructed using data from USGS (Page and Nokleberg, 1974; Segerstrom and Carlson, 1982) and Montana Bureau of Mines and Geology (Lopez, 2001; Geraghty, 2013) maps and reports, as well as data collected during this study. Drill data from Geragthy (2013) was also utilized. Assumption was made via slickenline measurements that out-of-plane motion was minimal enough for the cross-section to be balanced. Consistent bed thickness was used during construction and a hand-drawn section was line-length balanced (Marshak and Mitra, 1988).

Sampling Methods

Exposures of the SPF varied within the mine at each locality. However, in all SPF exposures, the following sampling criteria was attempted:

(1) Vein-filled fractures

(2) Damage zone(s) (FW and HW)

(3) Core zone(s)

(4) Unaltered host rock

Not all of these attributes were present or visible within individual exposures, and therefore sampling strategy was based upon the exposure quality at each spot visited. Two general types of exposure were observed within the mine:

(1) Along strike: These exposures were areas drilled along the length of the SPF where the JM Reef was in close contact with or within the SPF, and included the

29w10200 and 26w8000 accesses. The 26w8000 access also offered a partial cross-sectional view. At these localities, cross-sectional sampling from unaltered FW to unaltered HW was constricted to only one half or less of the SPF from an evident core zone to partially exposed damage zone. Sampling within the criteria was done as best as possible in these non-ideal exposures.

(2) Cross-sectional: Two of the five exposures were fully cross-sectional, and only one was able to be sampled incrementally across the fault zone due to time restrictions and subsequent shotcreting of the access. The partial cross-sectional view at the 26w8000 access was sampled across the SPF from HW to FW. The 48w8400 access allowed the most comprehensive sampling of the SPF and was sampled incrementally across each zone of the entire SPF from undamaged FW to the brecciated HW. The extensive HW and limited underground access did not allow for an unaltered host rock sample of the HW.

In most cases, oriented samples were taken so shear sense could be discerned in thin-section. Where oriented samples were not possible (clay gouge), the orientation of any foliation within the gouge relative to the dip of the main fault body was noted. The 2600 level location provided ample slickensided surfaces for kinematic measurements. Due to time restrictions in the mine, only a few were measured. Oriented samples of the slickensides were taken and rake measurements were subsequently measured from these samples in the lab with a protractor.

X-ray Diffraction Analysis

X-ray Powder Diffraction

Eleven samples were processed for XRD analysis at Montana State University's Imaging and Chemical Analysis Laboratory (ICAL). Three samples were from core, four gouge samples from the shotcreted 48w8400 locality, and another four core zone gouge samples from the sampling transect done at the 48w8400 locality. Random oriented mounts were made for all eleven samples, while oriented mounts were made from only the three core samples to preliminarily test for clay minerals present. Methods of random and oriented sample preparation and analysis followed the USGS Open File Report 01-041 (Poppe et al., 2002) and used the USGS XRD Clay Mineral Identification Flow Diagram present in the publication. Samples were ground with a mortar and pestle. The ground material was mixed with water into a slurry, then vacuum filtered onto an absorbent pad with a vacuum flask. The residue pad was pressed onto a glass slide and peeled off, leaving the residue on the slide. One oriented slide was allowed to air dry, while another oriented mount was baked at 380-400ºC for an hour and a half. The final oriented sample was heat treated at 70ºC in an oven with ethylene glycol for eight hours. XRD was then performed the following day using a SCINTAG X1 Diffraction System. Random oriented mounts were scanned in increments of 2º per minute from 3º to 73º. The oriented mounts were scanned at 2º per minute from 2º to 22º. Samples were analyzed in ICAL with the program Diffraction Management System for NT (DMSNT). The software MAUD (Material Analysis Using Diffraction) was attempted for analysis of

the powder XRD samples, but the resolution of the data proved too low to be accurately analyzed.

X-Ray Synchrotron Diffraction

Two areas of core provided by the Stillwater Mining Company were utilized for analysis at Sector 11-ID-C of the Advanced Photon Source at Argonne National Laboratories for the degree of preferred orientation. A monochromatic X-ray beam was used with a wavelength of 0.10803 Å and 0.5 mm diameter. A Perkin-Elmer image plate detector 3450 x 3450 pixels large was placed approximately 2139 mm from the sample and was used to record the diffraction images. Samples were prepared by cutting a section of the core to ≈2 mm thick, and were subsequently mounted to a goniometer. During exposure, samples were rotated in 15º increments from -45º to 45º.

Material Analysis Using Diffraction (MAUD)

The program MAUD was used to analyze synchrotron data and calculate the degree of preferred orientation. Diffraction data were analyzed for preferred orientation using the Rietveld method in MAUD which uses a least-squares Rietveld refinement approach to calculate a modeled diffraction pattern from the experimental diffraction data. Instrumental parameters, background, crystal structure, microstructure and weight fraction were refined on all data. Diffraction peak shapes and widths were modeled by refining the crystallite size and microstrain. Preferred orientation was modeled using the EWIMV algorithm. A similar method for analysis was used in Buatier et al. (2012).

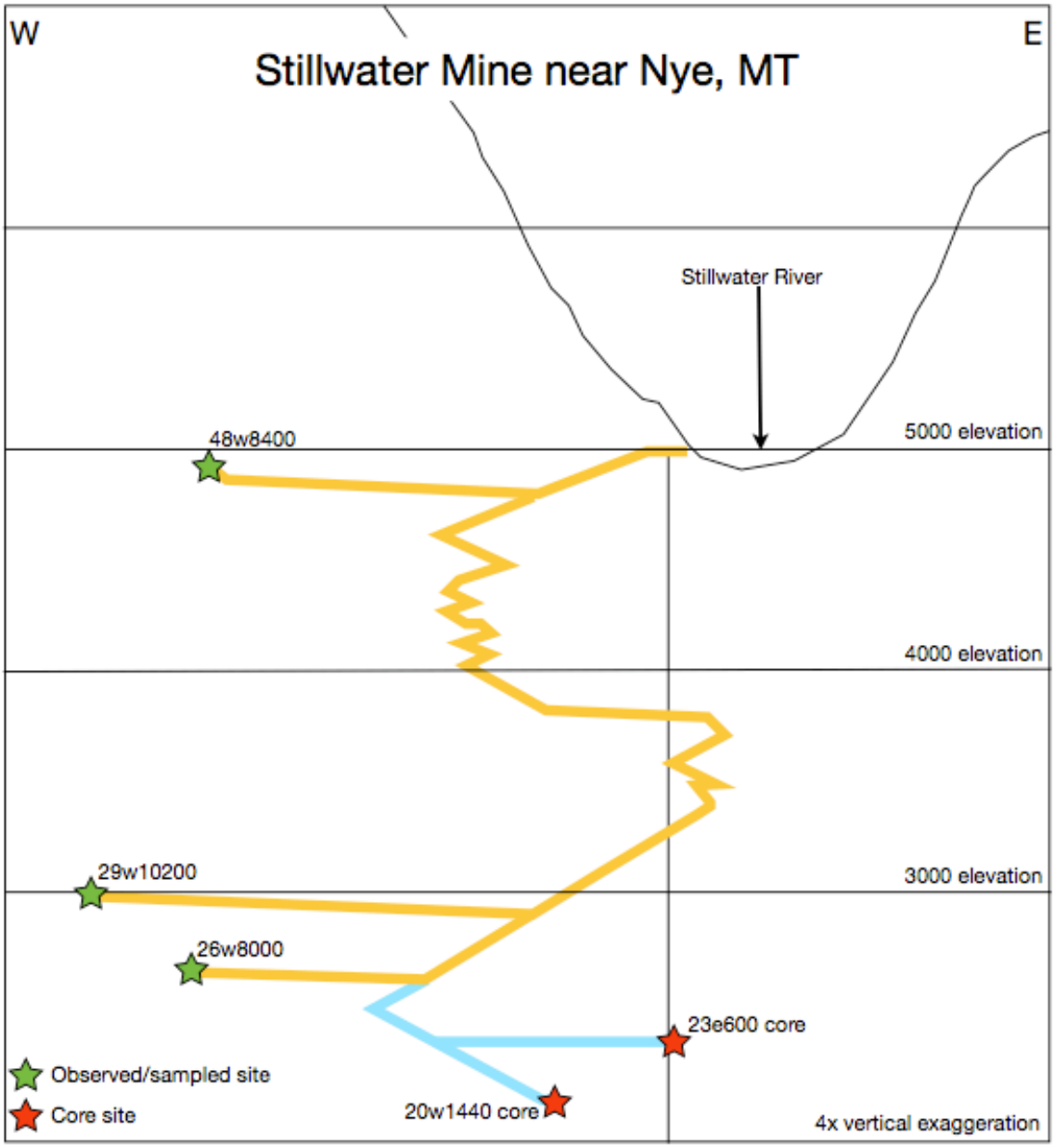


Figure 8: Observed and sampled localities within the Stillwater Mine near Nye, MT. Also shown are drill core locations for cores provided by the Stillwater Mining Company. Locations and levels are named for elevation above sea level. The 26w8000 level, for example, stands for an elevation of 2600 feet and 8000 feet due west of the 0-foot mine grid.

Thin-Section Microscopy and Petrographic Analysis

Samples collected in a transect across the SPF at the 26w8000 (Figure 9) and 48w8400 (Figure 10) localities were used for thin-sections to study how the deformation and mineralogy changed across the fault zone. Twenty five thin-sections were produced by Spectrum Petrographics: five thin-sections from the 2600 level, one thin-section from the 29w10200 core zone, and nineteen thin-sections across the exposure at the 4800 level. Oriented samples were marked on the section for kinematic interpretations. Non-oriented samples, such as foliated gouge, were made perpendicular to the foliation. Foliation in samples was always observed to be sub-parallel to the dip of the fault and still proved useful for kinematic interpretations (though relative shear sense could not be deciphered locally within the sample).

Whole thin-section images were created using a Nikon photo-negative scanner. Two polarizers perpendicular to each other were used to obtain a cross-polarized image; plane polarized scans were also taken. This process of scanning and analyzing whole thin-section images proved very useful in discerning the overall microstructure in a slide, as opposed to a limited view of one part of the microstructural system. Photomicrographs were taken at various areas of interest such as mineral alteration zones, fractures, and alteration products. Anorthite concentrations of plagioclase were estimated using the Michel Levy lamellae twinning extinction angle method. At least six grains were examined per slide. Results of these estimates are shown in Appendix B.

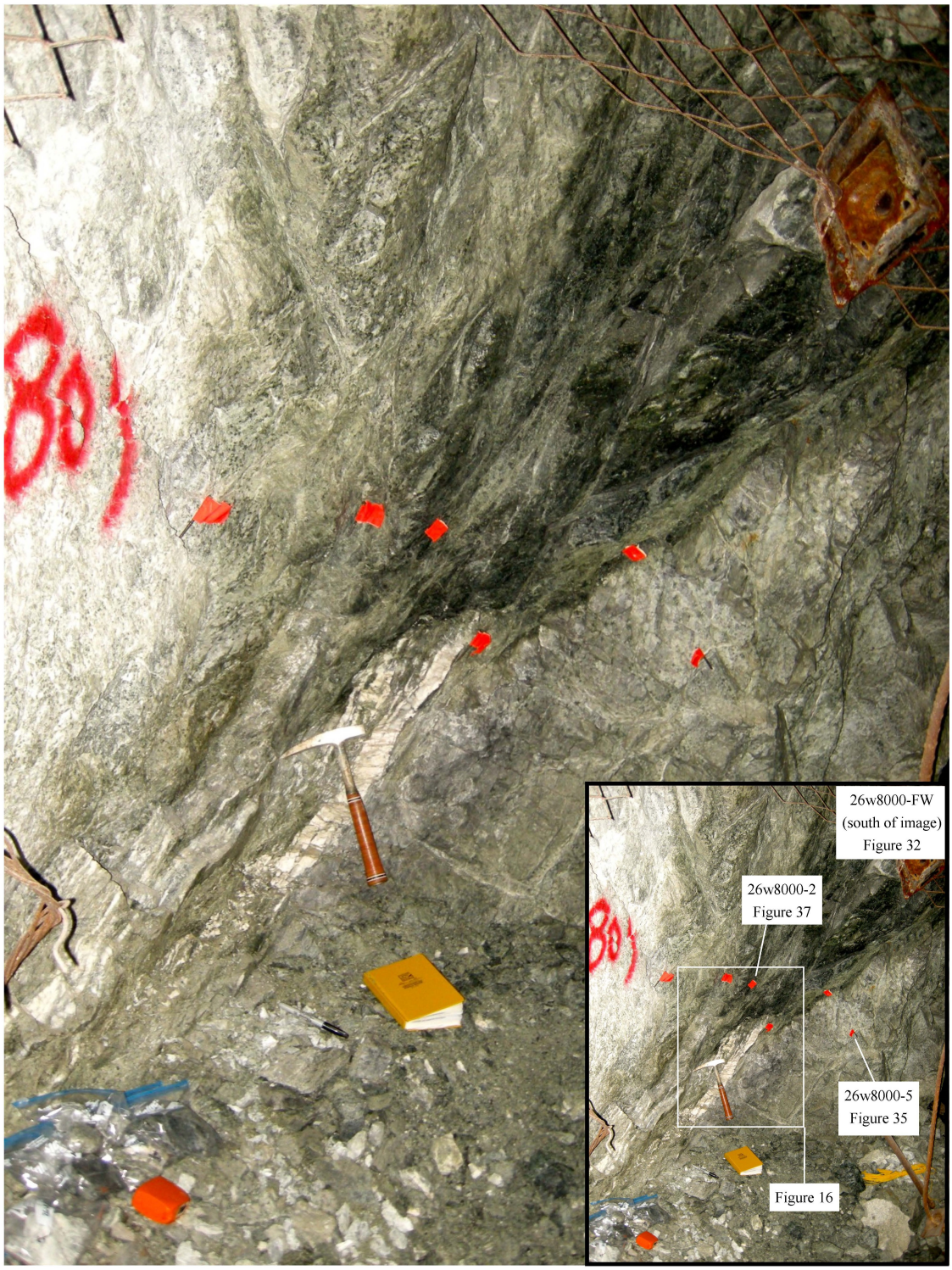


Figure 9: SPF at the 2600 level with orange flags showing locations of samples used for thin-sections. Rock hammer and field book for scale. View is looking east.

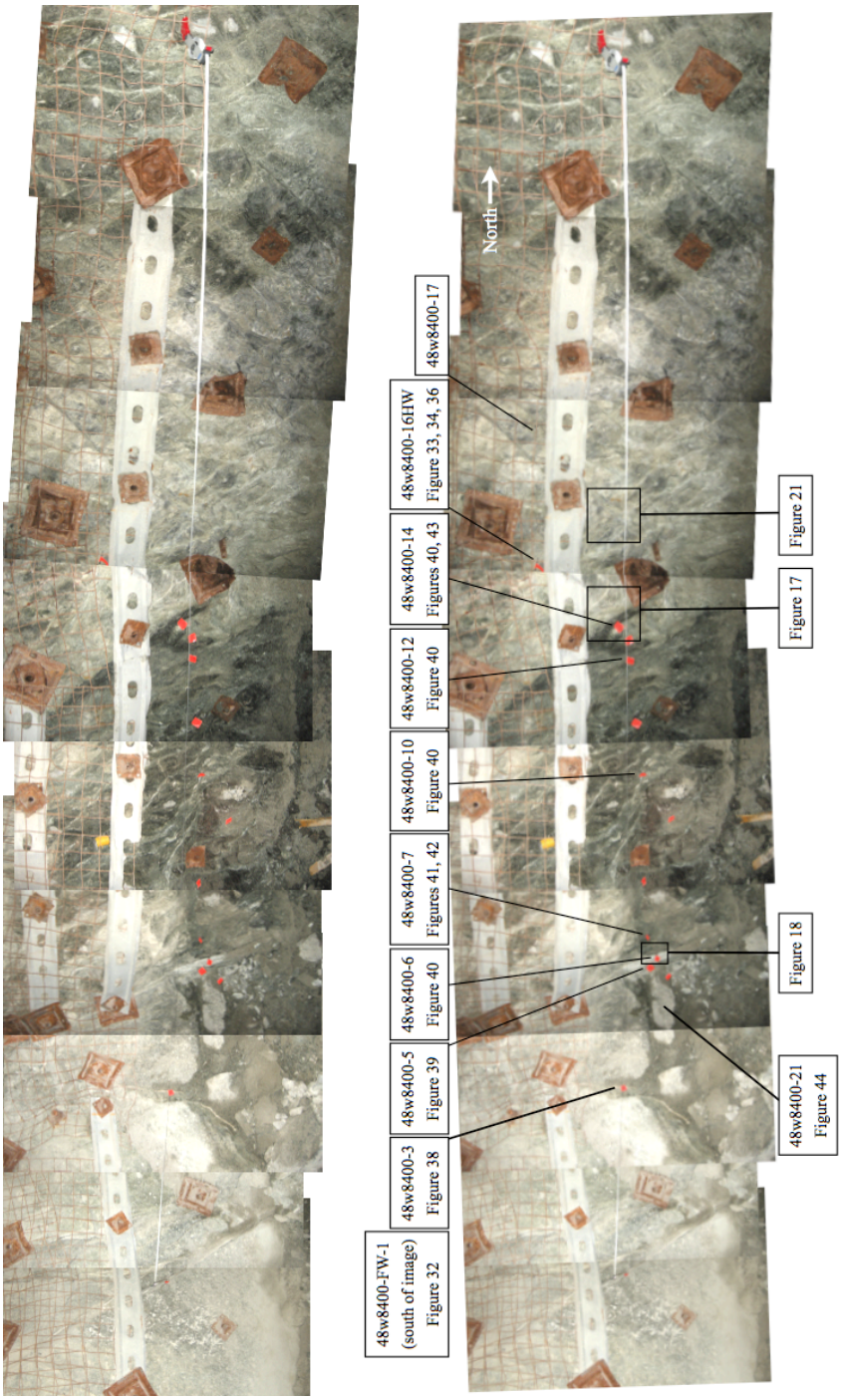


Figure 10: Left) Photo collage of the SPF at the 4800 level with orange flags showing sampling locations used for thin-sections. Width of tape is approximately 7.5 m. View is to the west. Right) Samples and corresponding figures mentioned in this study.

CHAPTER 6

RESULTS AND DISCUSSION

Geometry and Kinematics of the South Prairie Fault

Geometry

Laramide contractile structures correlate with an approximately NE-SW shortening direction (Blackstone, 1986; Brown, 1993; Bird, 1998; Neely and Erslev, 2009), resulting in thrust and reverse faults that trend approximately NW-SE (Figure 11). The SPF has an average strike azimuth of 286º and correlates well with this regional NW-SE Laramide shortening direction. In comparison with Figure 11, contractile and extensional structures at and near the Beartooth front also correlate well with published estimates of Laramide shortening in the direction of 040-065 (Figure 13). Features such as thrusts (north and south dipping, including the main Beartooth thrust) have a NW-SE trend (disregarding south of Red Lodge), as do the trends of anticlines and synclines to within a few degrees of each other. Likewise, extensional features (normal faults) trend orthogonal to compressive features and parallel the Laramide shortening direction, as expected. Sinistral and dextral strike-slip faults when considered together form a near perfect acute angle for a σ_1 direction of 060, and most likely represent conjugate shears with dextral strike-slip faults trending NE-SW sinistral strike-slip faults trending E-W. These conjugate shears and a shortening direction of 060 are consistent with Neely and Erslev's (2009) estimate of σ_1=065 for their study approximately 30 km (18 miles) south

of Red Lodge near the Clark's Fork Canyon. Also, it is likely that these conjugate structures are a result of slight regional sinistral motion in the area due to the Nye-Bowler lineament, the left-lateral basement-involved feature that spans from the Pryor Mountains to the Beartooth front near Nye (Wilson, 1936; Foose et al., 1961). The influence of this sinistral motion will be discussed in the following kinematics section of this chapter.

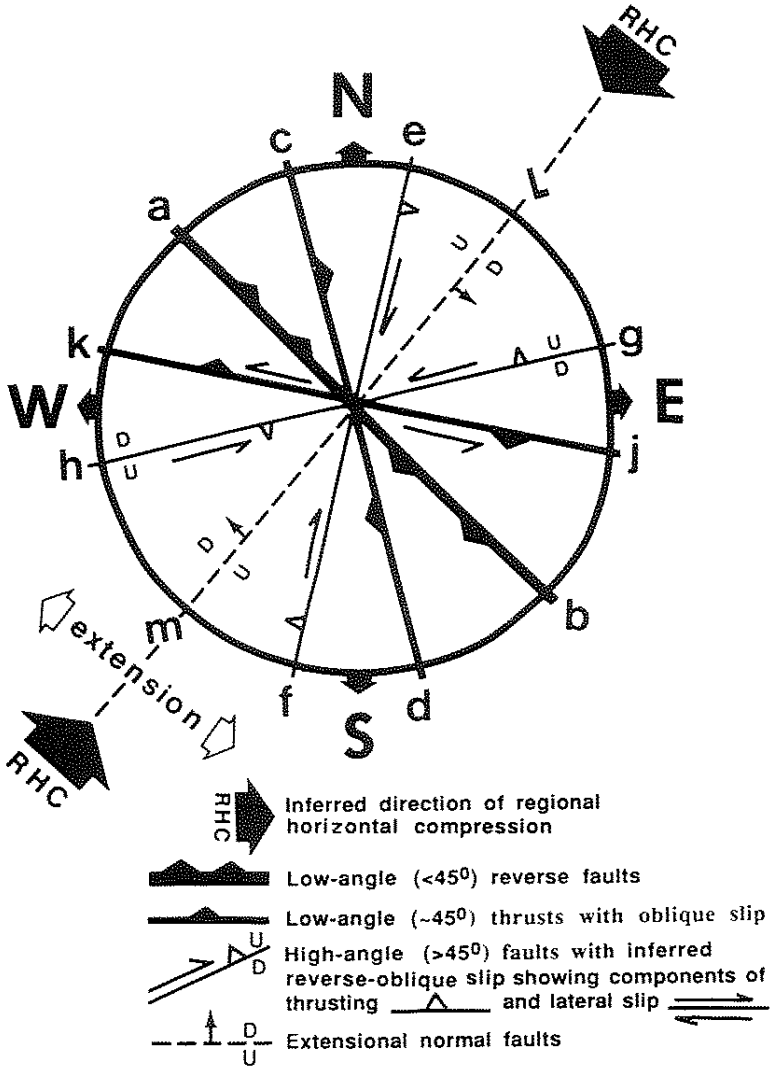


Figure 11: Laramide regional stress-strain diagram from Brown (1993) showing expected structures associated with a regional horizontal compression (RHC) azimuth of approximately 040 for the central Rocky Mountains.

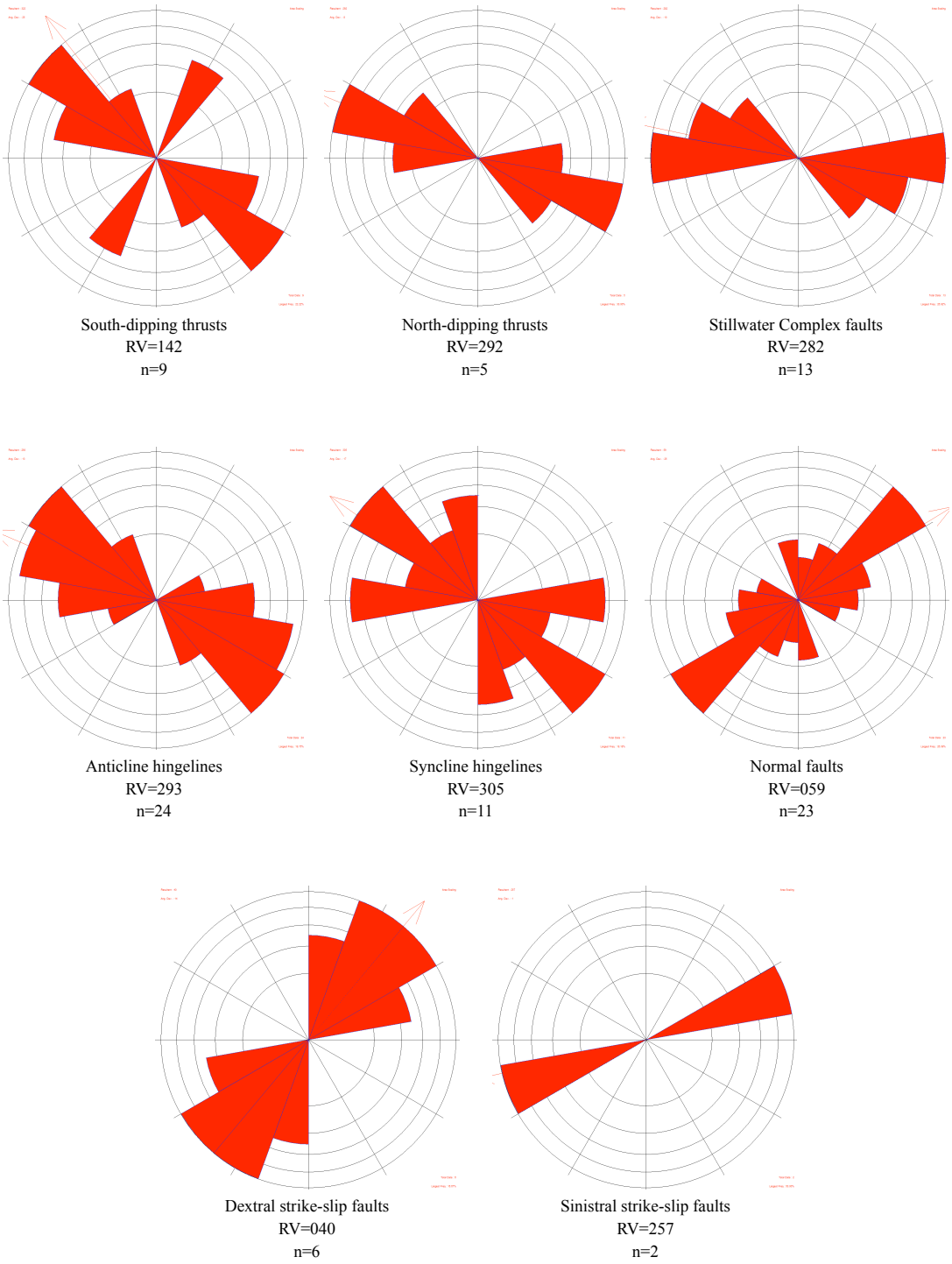


Figure 12: Area scaled Rose diagrams of strike of faults and trends of fold hingelines at and near the Beartooth front using the 1:100000 Red Lodge MBMG Map (Lopez, 2001). RV=resultant vector, n=number of data.

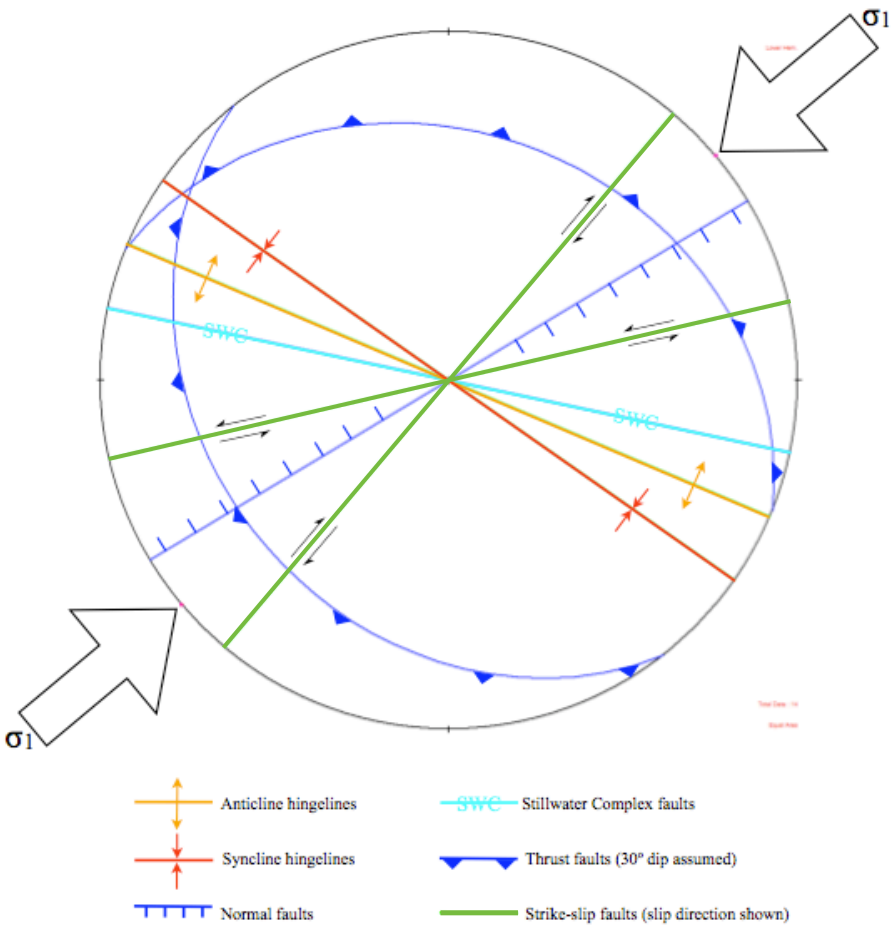


Figure 13: Schmidt stereonet plot of resultant vectors from Rose diagrams in Figure 12; compare with Brown's (1993) plot in Figure 11. This suggests Laramide movement for the SPF given its optimal orientation with the Laramide principle shortening direction. Dips of features are not shown except for an assumed 30º dip on thrust faults for the purpose of visual reference. An approximate Laramide shortening direction is shown here as 050, though it likely ranged between 040 to 065.

Kinematics

Slickenlines were rare at all locations except at the 2600 level face exposure. One slickenline from the 2900 level was also measured on a core zone gouge sample. These measurements give an average rake value of R=78º (n=17) from the west. Steps on the

face were smooth down towards the floor, consistent with reverse motion in absence of other data. As shown by the geometry and expected kinematics in Figures 11 and 13, the Beartooth front from Red Lodge to Livingston likely had an oblique slip that was slightly sinistral. This is likely due to the front's orientation slightly deviating from normal to the regional horizontal shortening direction. South of Red Lodge, the Beartooth front makes a NNE-SSW trend and has been shown to have an overall dextral oblique slip (O'Connell, 1996). Cross-sections constructed north of (this study, see Figure 15) and south of (Neely and Erslev, 2009; by the author) Red Lodge show decreasing amount of dip separation, while cross-sections at the Red Lodge corner are shown to have the greatest amount of dip separation (Lopez, 2001; Wise, 2001) with ≥5 km (16,500 feet) of heave (O'Connell, 1996). I interpret these observations to be consistent with an overall sinistral oblique slip direction on the northern segment of the Beartooth thrust and to, therefore, influence the characteristics of structures along this section of the front.

Sinistral motion for the Beartooth thrust is seemingly counter-intuitive considering the R=78º from W value, showing a dextral motion for the SPF instead of the sinistral en echelon faulting expected for NW-trending Beartooth frontal faults as mentioned above. This dextral movement is likely explained by the SPF's north-dipping geometry rather than south-dipping like the Horseman, Beartooth and other major frontal thrusts. Backthrusting of the SPF during the Laramide may have resulted from compression of the fault block between the Horseman thrust to the NE and Bluebird and Lake thrusts to the SW (see cross-section in Figure 15), causing the SPF block to "pop-

up" from slight transpression in a direction consistent with overall tectonic transport of this section of the Beartooth massif, but slipping obliquely in a sense opposing overall kinematics along the northern segment of the Beartooth front. This relationship can be visualized by considering that south-dipping thrusts with sinistral oblique slip would have rake measurements from the west as well, pushing the block towards the east and giving the Horsemen thrust an apparent sinistral motion and the SPF an apparent dextral motion (Figure 14). However, more work beyond the scope of this thesis would be required to prove or disprove this kinematic model.

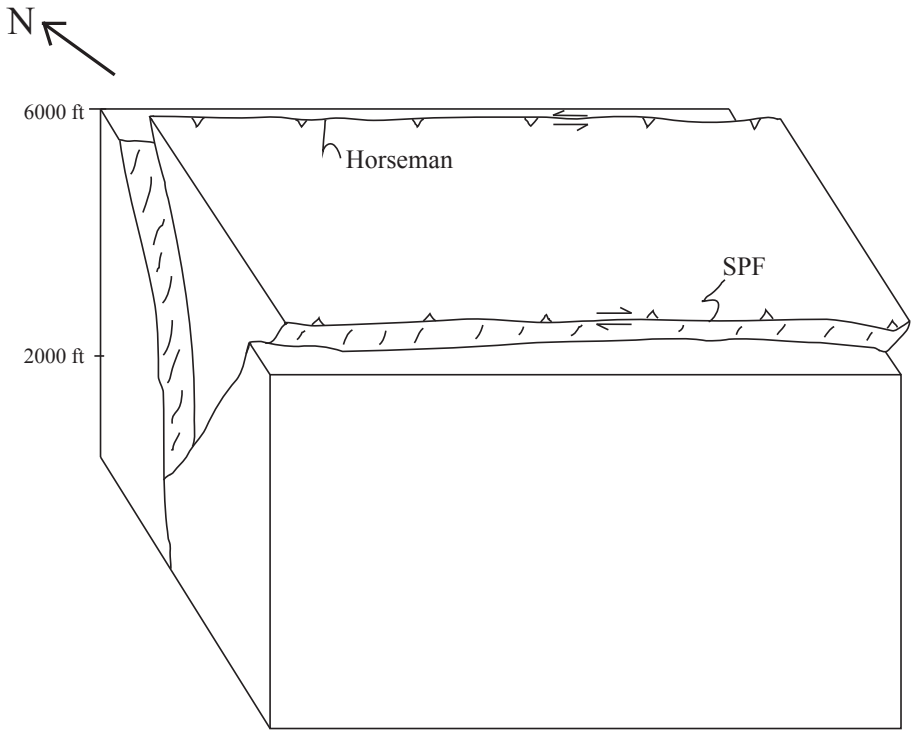


Figure 14: 3D schematic drawing showing relationship of the SPF to the Horseman thrust and generalized slickenlines (avg.=78º from west). Slight transpression may have caused the SPF block to be extruded up and out to the southeast by "squeezing" of the block between the Horseman and the Lake fault (see Figure 15 below).

Balanced Cross-section

An intricate series of faults is observed at the Beartooth front near Nye (Figure 15) in which the SPF is only a minor part of the entire fault system. Balancing of the cross-section suggests that the SPF is a true backthrust and is consistent with the geometry and kinematics discussed above. Drill data from Geraghty (2013) shows a complex duplex geometry beneath the Horseman thrust that partitions the heave on the Beartooth front substantially.

Cross-section restoration gives an approximate overburden range of 6-8 km above the SPF at the beginning of the Laramide orogeny, with a minimum overburden of 4-8 km during late stages of movement as evidenced by the balanced cross-section below. Assuming a geothermal gradient of 35ºC/km gives conditions at approximately sub-greenschist to greenschist facies at the start of the Laramide, placing the SPF at brittle to brittle-plastic conditions of 280ºC for 8 km burial. This geothermal gradient is an average of estimates by Mitra (1984) at 20ºC/km and Mitra and Frost (1981) at 50ºC/km for their work in the Wind River arch and correlates well with Beaudoin et al.'s (2011) estimate of 30ºC/km at Sheep Mountain anticline. Later stages of movement along the SPF at 4-8 km depth should show structures formed at brittle conditions. Early brittle-plastic features cut by brittle fractures were observed, and will be discussed later in this chapter.

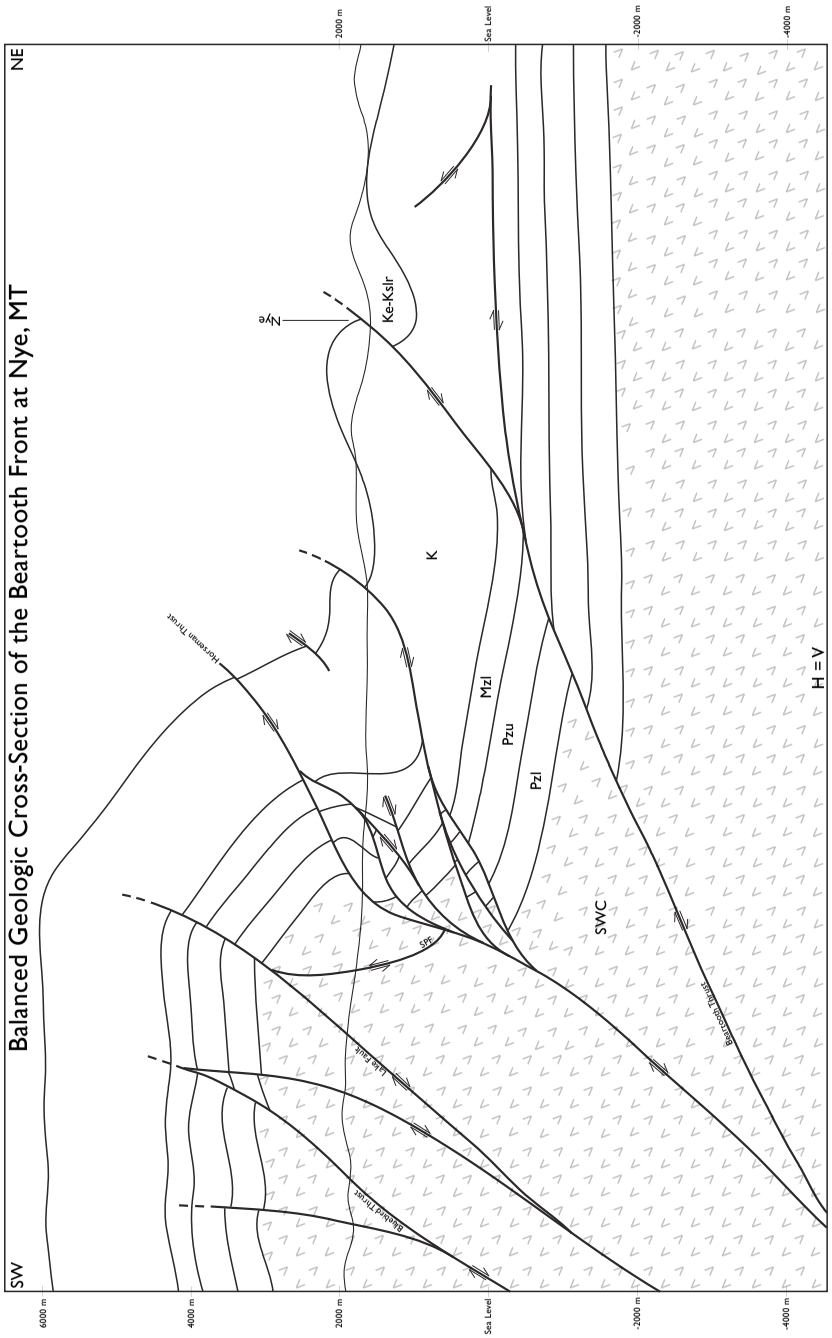


Figure 15a: Balanced cross-section of the Beartooth front near Nye, MT, west side of Stillwater River. A complex system of splay faulting partitioned the total heave of the Beartooth massif. SWC=Stillwater Complex rocks (undifferentiated); Pzl=Cambrian Wolsey Fm. to Devonian Three Forks/Jefferson Fm.; Pzu=Mississippian Madison Fm. to Permian Amsden Fm.; Mzl=Triassic Chugwater Fm. to Jurassic Morrison Fm.; K=Cretaceous Kootenai Fm. to Cretaceous Telegraphic Creek Fm.

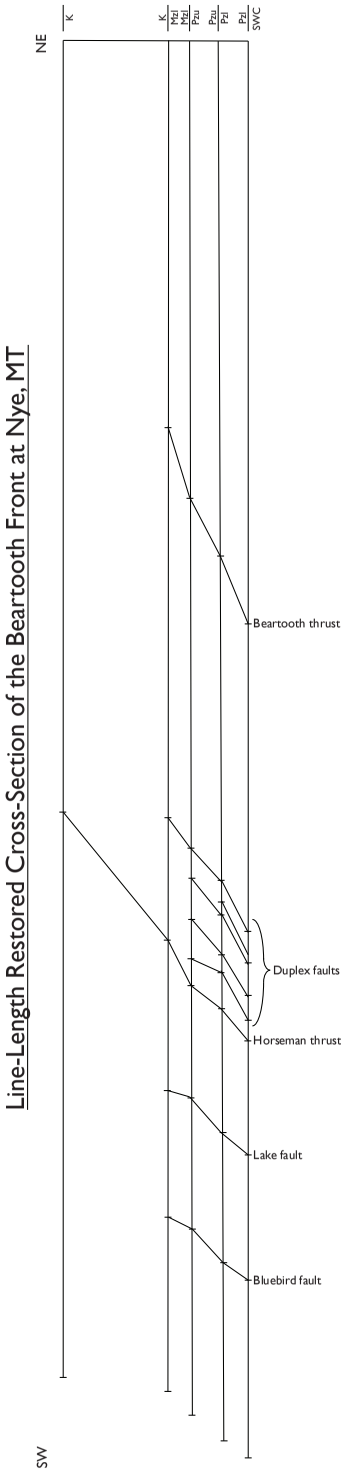


Figure 15b: Line-length restoration of Figure 15a shows an accurate and restorable geometry of geologic structures prior to Laramide deformation.

Extent of the Core and Damage Zone and the Architecture and Permeability of the SPF

Extent and Characteristics of the Core Zone and Damage Zone

At each location, the SPF's core and damage zones were observed to vary in width. At the floor of the 2600 level, the core zone was coincident with a single vein >5 cm wide which abruptly ended higher up the access as the core zone widened to approximately a meter wide (Figure 16). Within the core zone, abundant anastomosing fractures were observed. The contacts between the core zone and the FW-DZ and HW-DZ were sharp, and no through-going fractures were seen to penetrate into either zone from the other. This suggests slip was strictly localized to the core zone and was likely partitioned amongst the anastomosing fracture network. Due to the limited exposure, only a fraction of the HW-DZ was visible, so it's entire extent could not be fully measured. Likewise, drilling of the access parallel with the strike of the SPF obliterated any observation of the entire extent of the FW-DZ. Extensive wire mesh on the ceiling of the access also restricted any observation. However, a maximum extent can be estimated since the host rock at the southern end of the access was not disturbed. The distance from the core zone to the southern edge of the access was approximately 3-4 meters, though the non-brecciated southern wall and the competent nature of the FW-DZ (Figure 9 fractures) in comparison to the HW-DZ suggests that the FW-DZ did not extend this entire distance.



Figure 16: Close up view showing dying out of core zone vein and widening of the core zone at the 26w8000 locality. Note the anastomosing nature of fractures within the gouge and the competence of the FW-DZ. Systematic FW fractures are also evident.

The FW-DZ and HW-DZ at the 4800 level displayed a similar behavior as observed at the 2600 level, and was almost entirely visible due to a north-northeast cut across the SPF. The FW-DZ here was extremely competent with minimal fracturing visible. Only a single fracture at the southern end existed as the furthest extent of the fault

zone. A maximum width of 2.36 meters was recorded for the FW-DZ. Similar to the 2600 level, sharp contacts between the core zone and the FW and HW damage zones were observed (Figure 17). At the CZ/HW-DZ contact, a very dark zone of foliated gouge approximately 4 cm wide was observed and has been interpreted as a zone of localized slip, herein termed the HW-localized-shear zone (HW-loc-shear). The foliated nature in contrast to the non-foliated gouge within the central core zone and the darker material suggests slip localization. XRD and petrographic analysis of a core zone transect mentioned later in this chapter is consistent with this interpretation. Slip localization was also observed at the FW-DZ/core zone contact (FW-loc-shear), but was not as abrupt or apparent at the mesoscopic scale as the HW-loc-shear and was no wider than 1.5 cm (Figure 18). These observations are consistent with work by Chester and Logan (1986) who suggested that the boundaries between the damage zone and core zone are areas where the most significant differences in mechanical properties exist. Therefore, these zones would produce markedly different textures.

Between these two zones of slip localization, the gouge exhibited a flow-like/ foliated texture, but an overall lack of planar foliation was observed such as seen at the contacts. The presence of broken up vein material was also visible within the core zone. The second 4800 level location (which was subsequently shotcreted) also exhibited apparent internal folding cut by brittle fractures (Figure 19). Total width of the 4800 level core zone was approximately 2.51 meters.



Figure 17: Sharp contact between the core zone (left) and HW-DZ. Note bifurcation of the HW-localized shear zone at the level of the tape measure.



Figure 18: FW-localized shear zone at the FW-DZ/core zone contact (FW to left). Note dark clay smear along white interface. A vein (likely zeolitic) was also visible at this contact and could have implications for fluid-flow and fault slip relationships.



Figure 19: Apparent folding of gouge material within the core zone at the 4800 level. A) Internal flow of gouge material appears to have flowed around a nodule or resistant section of the JM Reef in the core zone. Yellow wire spool in top left is the size of a 1-liter water bottle. Orange flags are sampling locations. B) Shotcreted 4800 level location, arrow shows brittle fracturing of slightly folded material. Geologist is Lowell Miyagi.

The HW-DZ was extensive and heavily brecciated. A width of >2.63 meters was recorded, however the end of the access obscured a complete measurement and therefore this value represents a minimum width. The total measured width of the SPF at the 4800 level was approximately >7.5 meters, with each zone being sub-parallel with the dip of the fault.

A relationship was observed between the width of the core zone and the proximity of the JM Reef. At the 2600 level, the SPF was not coincident with the reef and the core

zone was less than a meter wide. The 4800 level core zone contained the JM Reef (as evidenced by sulfide minerals) and was up to 2.5 meters wide. This relationship may attest to the formation of the SPF as a competency contrast via the JM Reef (Turner et al., 1985), which is an olivine-rich unit contained between more competent norites and gabbronorites that dominantly lack olivine (McCallum, 2002). Experimental work by Borg and Handin (1966) shows serpentinized olivine-rich rocks are less than half as strong as rocks that do not contain olivine at 500ºC supports this claim.

Analysis of South Prairie Fault

Fracture and Vein Orientations

Fractures and veins measured in each zone of the SPF were analyzed with Rose diagrams, stereonets, and Kamb contoured plots to show the dominant fracture orientations and characteristics. As mentioned, not all exposures were ideal and partially exposed views allowed only an incomplete analysis of the fault-related fractures at a given location. However, these data are still considered in this study. Time restrictions in the mine and subsequent lack of access inhibited a more comprehensive fracture analysis. Orientations of veins are considered here along with fractures. Vein characteristics will be discussed in the following section.

Fractures observed were both systematic and non-systematic, though fractures observed in the hanging wall at the 4800 level and both the footwall and hanging wall of the 2600 level were dominantly systematic. Fractures at the 2900 level neither appeared systematic nor was this reflected in the measurements, though data was minimal.

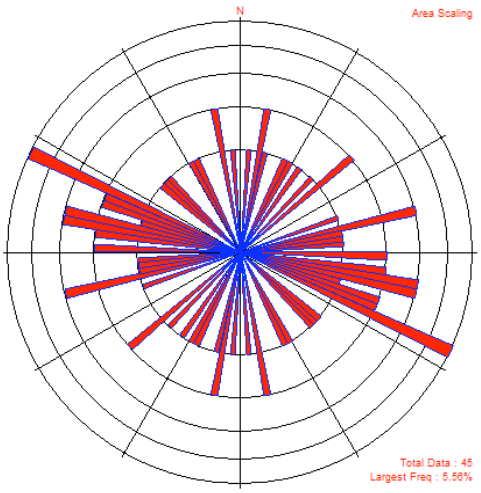


Figure 20: Area scaled Rose diagram of all fractures and veins measured at all levels. The majority of fractures are sub-parallel to the SPF strike. Class size=3

Fractures in the footwall of the 48w8400 location were non-systematic, though one set consisting of only two fractures did have coincident orientations. Hanging wall fractures at this location were dominantly systematic, with two sets dipping approximately 60ºN and approximately 60ºS. The systematic fracture set dipping 60ºS had an approximate spacing of 14-16 cm and an average strike azimuth of 085º (n=4), nearly parallel with the SPF's strike of 274-280º at this level. This fracture set likely represents R' Riedel fractures as discussed below. Fractures dipping 60ºN also had an approximate spacing of 15 cm and were observed to displace 60ºS dipping fractures up to 3 cm (Figure 21), suggesting these fractures are younger than the north-dipping fractures. The extent of this fracture set occurred up to 53 cm from the CZ/HW-DZ contact and did not persist further than this. Stick-slip movement of the SPF may have caused these fractures to form, thereby displacing the earlier south-dipping fractures.

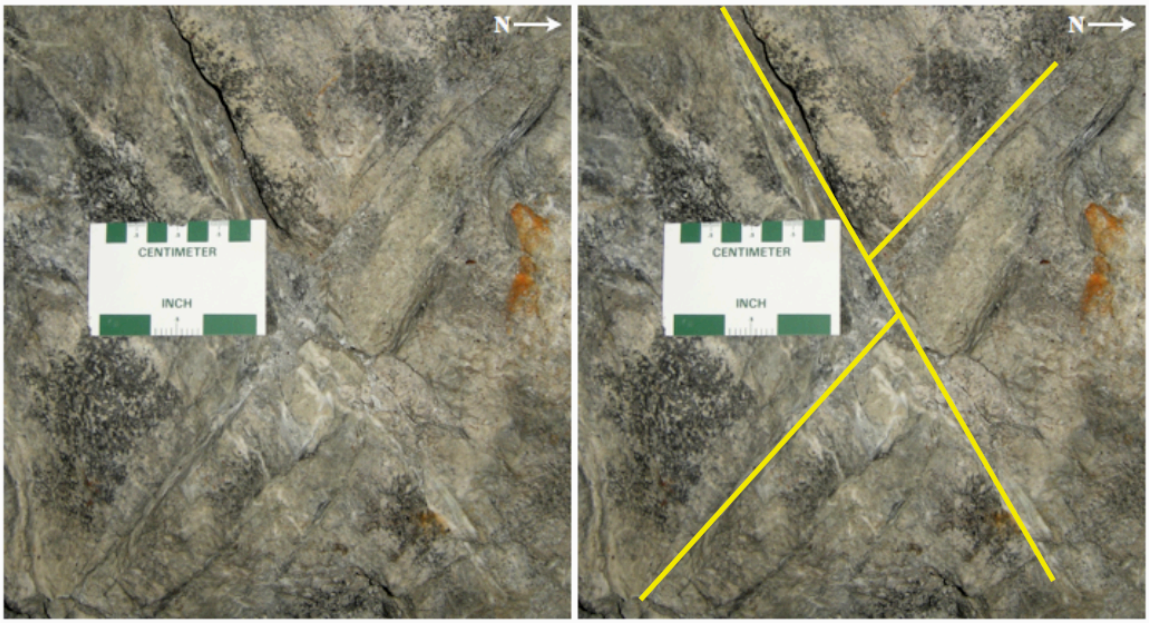


Figure 21: Displacement of ~60ºS dipping fractures by ~60ºN dipping fractures. Apparent dip separation is 3 cm. This picture was taken at the furthest extent of this fracture set and occurred 5.4 m north of the start of the fault zone in the FW (53 cm from the CZ).

Systematic fractures occurred in both the HW and the FW at the 2600 level (Figure 9) and were south-dipping in both zones. FW fractures dipped 32-56º and had a spacing of 6-10 cm, but were up to 20 cm. A single sighted dip measurement in the HW showed a 44º dip. Spacing was on the order of 20 cm. Extent of these fractures into the HW and FW was impossible to determine.

A characteristic pattern is observed in the fracture/vein data that correlates reasonably well with the strike and dip of the SPF (avg.=286º, 61ºN). Figure 22 shows all measured fractures and veins in the FW, HW and core zone of the SPF from all five locations visited during the study. Three major populations of fractures are observed in the Kamb contoured plot, two of which are similar to the strike of the SPF. These two

populations are interpreted to represent Riedel R- and R'-fractures. R-fractures are defined as being similar in dip to the main fault body (Scholz, 1990) to within approximately 15º. In this case, R-fractures dip with the SPF to the north. R'-fractures are antithetically oriented (Scholz, 1990), typically within 75º from the fault body. These SPF-related fractures are south-dipping and can be seen in the hanging wall of the 48w8400 location in Figure 29. More fracture data would be required to show if a stronger relationship existed for these fault-related fractures, but it is interesting to note the relatively strong relationship given a minimal amount of data.

Analyzing the fracture data individually by the fault's architecture shows slight characteristic patterns distinct to each zone, namely in the core zone. Figures 23-25 are stereonet plots showing the fractures of the FW-DZ, CZ and HW-DZ separately. All fractures exhibit a sub-parallel or antithetic geometry that is interpreted as being R- and R'-fractures, respectively, as described above. Fractures at the 2900 level and the HW of the 2600 level show an east-dipping geometry that is not observed in the other data. The 2900 level only exposed the FW-DZ and it is impossible to conclude whether the fractures measured are related to the SPF or the result of blasting. Interestingly, a set of fractures was observed to be sourced from a single fracture at the 2900 level. These splays are conspicuously oriented perpendicular to the 2900 level access, and it therefore seems likely that they formed during blasting of the access and are not syn-kinematically related to the SPF. The barely exposed HW of the 2600 level represents only one measurement and is not enough to make any statistical claims.

Fractures measured in the core zone at the 2600 and 4800 levels are dominantly sub-parallel to the strike and dip of the SPF when compared at each level separately (Figure 25) and together (Figure 27). Dip sub-parallel orientations of these fractures can also be seen in Figures 9 and 10. This result is interpreted as representing the anastomosing behavior of the core zone fractures and their behavior of partitioning total slip during fault movement. This result may be suggestive of a propensity for core zone fractures to form sub-parallel (synthetically) with a fault's orientation rather than antithetically as seen in the FW and HW damage zones. Dominance of synthetic fractures within a core zone could have implications for fluid-flow within the core zone, whether fluids are derived from within the core zone itself or are input from the surrounding host rock given the fault is not a total barrier to fluid-flow.

Figures 24-26 show collectively the fracture data at all levels as broken down into individual HW, CZ and FW zones. Overall, the FW and HW of the SPF appears to show a bimodal distribution of fractures, being the R- and R'-fractures discussed above, though some anomalous point concentrations that deviate from the strike and dip of the SPF do occur (such as the 2900 level fractures, possibly associated with blasting of the access). Again, the limited number of data makes it difficult to discuss definable relationships in the SPF fracture patterns and their potential for repeatability in other fault zones of various origins and host rocks. However, a noticeable statistical trend is evident and may warrant further investigation.

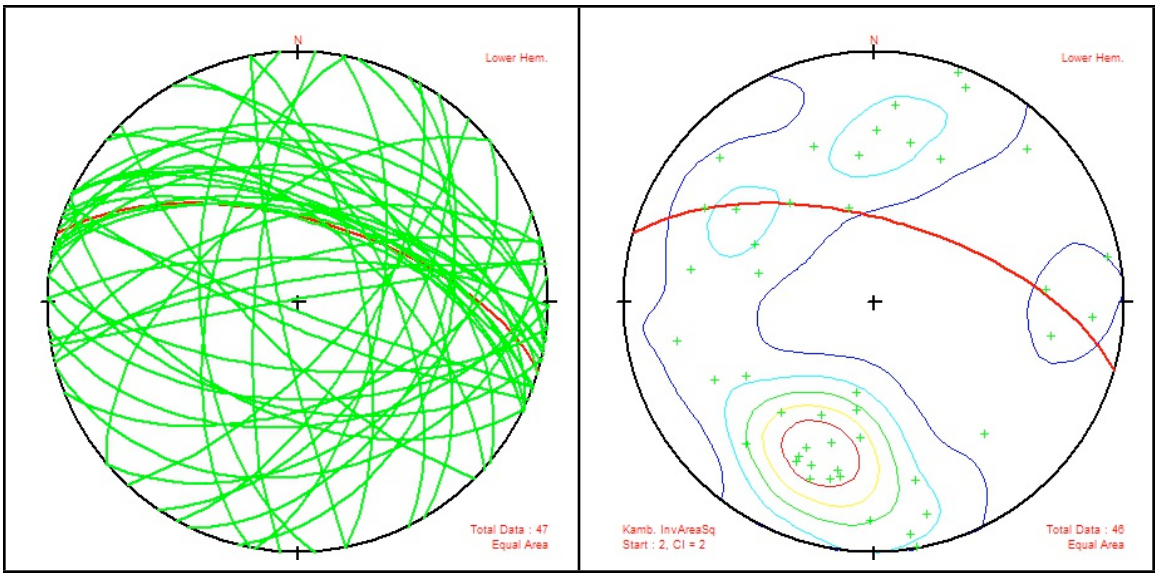


Figure 22: (Left) Lower hemisphere stereonet of all fracture and vein data from every location visited in the mine shows an array of orientations. (Right) Plot of poles to planes and contoured for density using Kamb contouring. There are three significant populations, two of which are sub-parallel to the SPF strike. Colored contour lines represent an increase in visibility of density contours. Yellow contours indicate relatively low density, red contours indicate a relatively high density (significant population). This shows that a high density of fractures measured are synthetic with the SPF. Red great circles in both represent average strike and dip of the SPF (286, 63ºN).

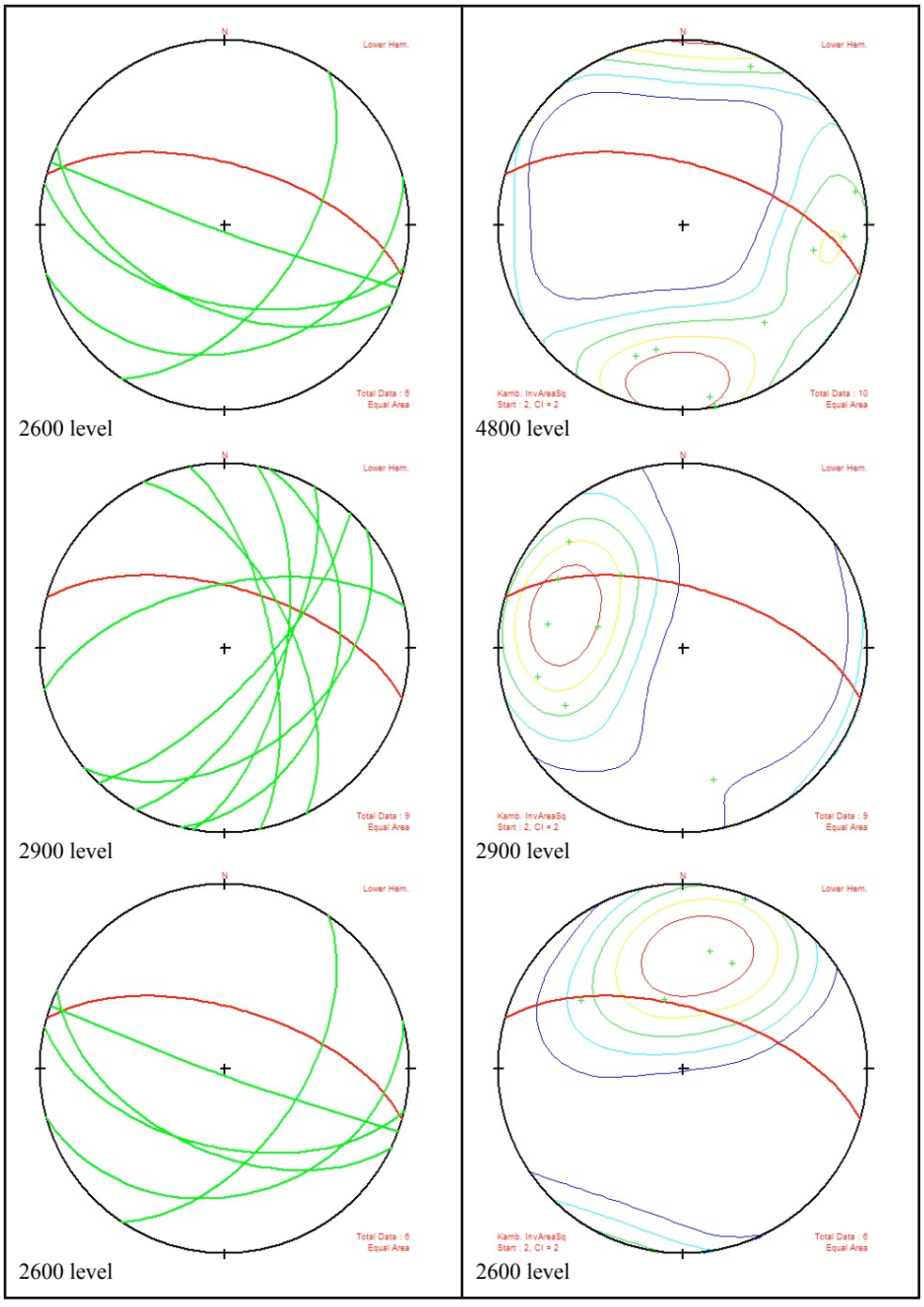


Figure 23: FW fractures from each level, red great circle shown is the average strike and dip of SPF (286, 63ºN). The 2900 level only exposed the FW-DZ and is shown here, unlike the other plots. Fractures at the 2900 level were likely the result of blasting. The 2600 and 4800 level fractures show a relatively high density of fractures sub-parallel with the SPF, though an anomalous SW-trending NW-dipping set does occur at the 4800 level.

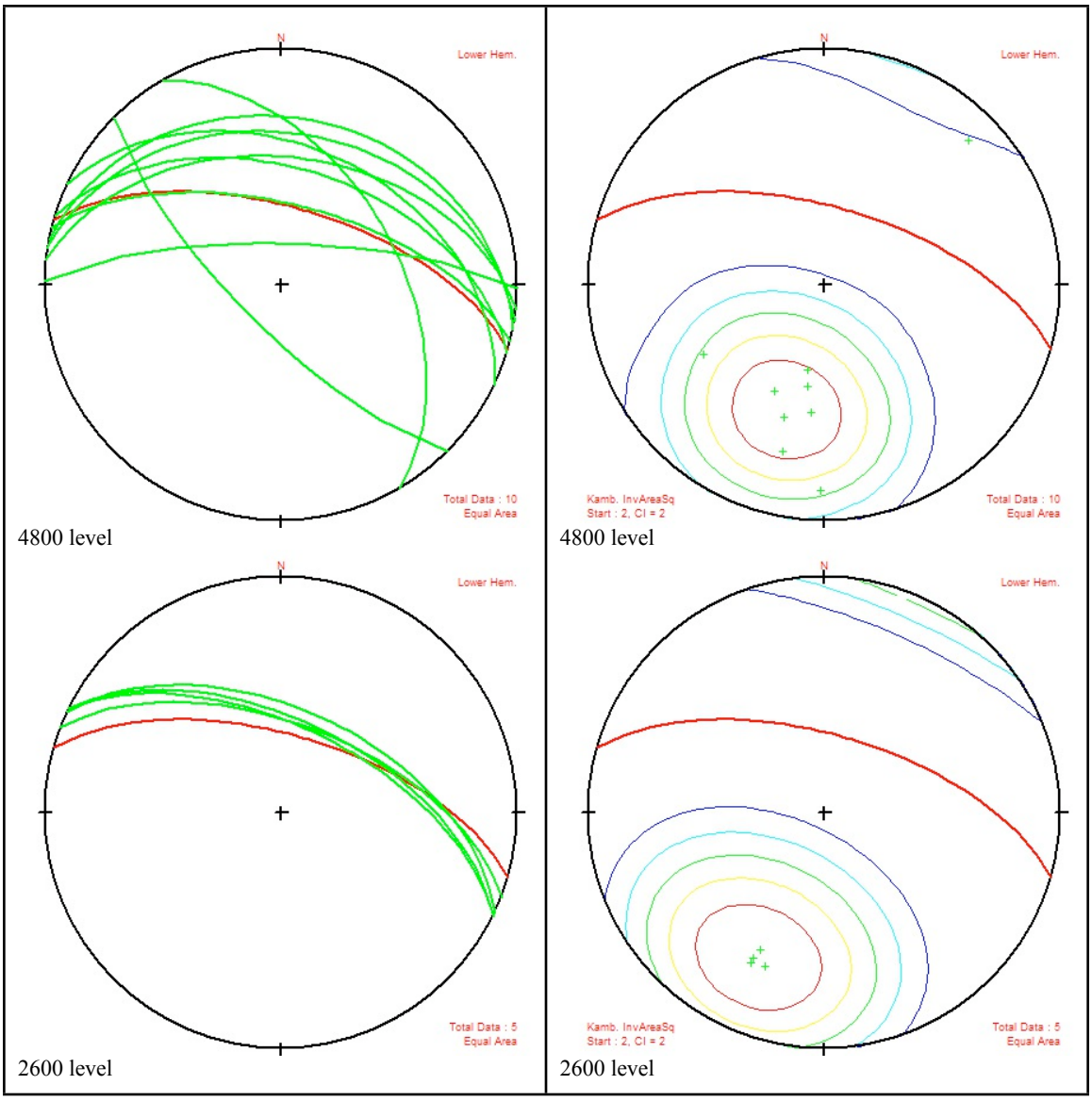


Figure 24: Core zone fractures from the 2600 and 4800 levels show a strong density of fractures sub-parallel with the SPF strike and dip (red great circles, avg.=286, 63ºN), and represents the anastomosing fracture network observed within the core zone. This suggests fractures in a core zone may be preferentially oriented synthetically to the main fault body, unlike the variation observed in the FW-DZ (Figure 23) and HW-DZ (Figure 25).

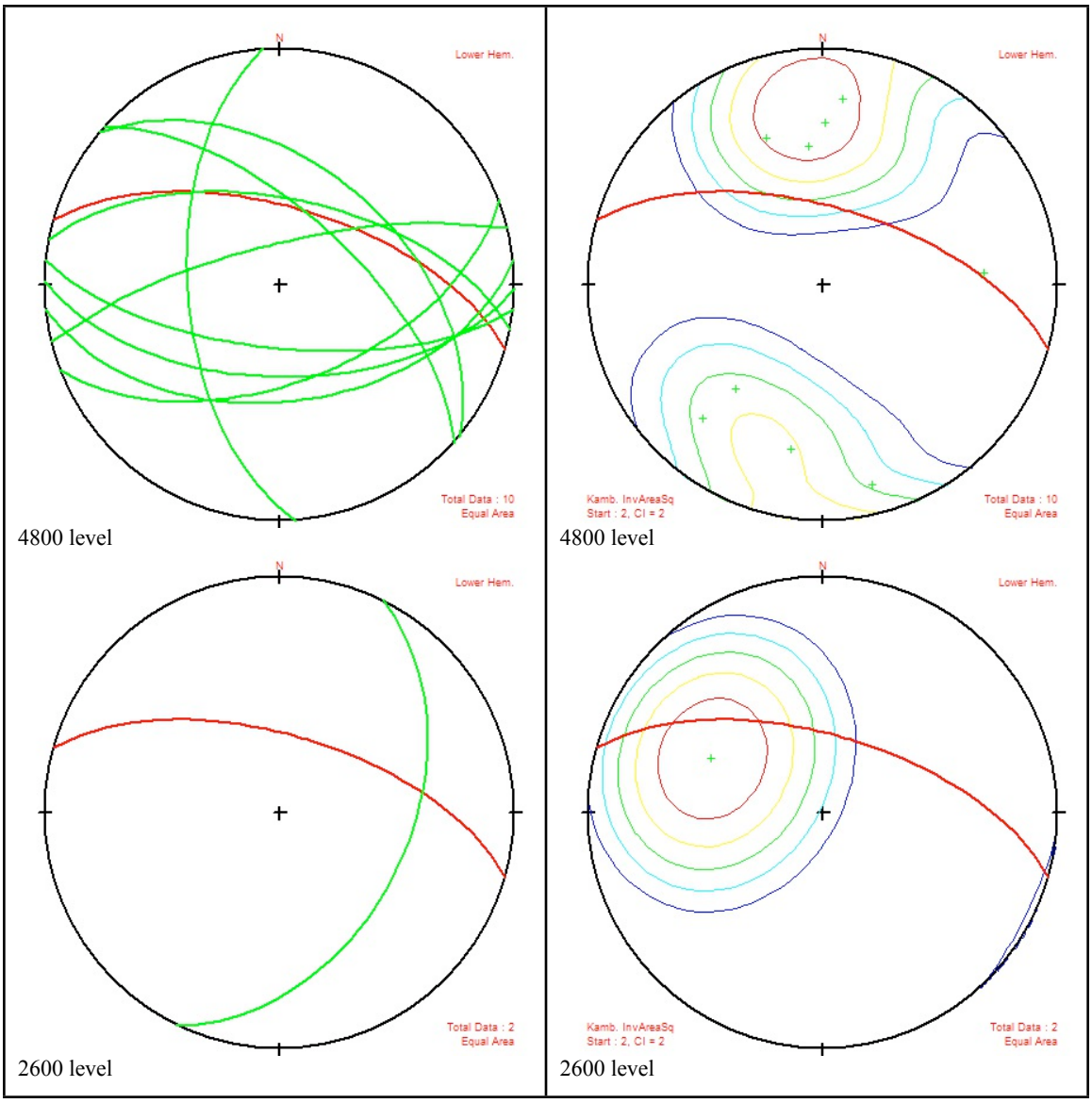


Figure 25: HW fractures from the 2600 and 4800 levels, red great circles are the average strike and dip of SPF (286, 63ºN). Fractures at the 4800 level strongly show synthetic and antithetic orientations as described above. The 2600 level was only one measurement from a section barely exposed and cannot represent any major significance.

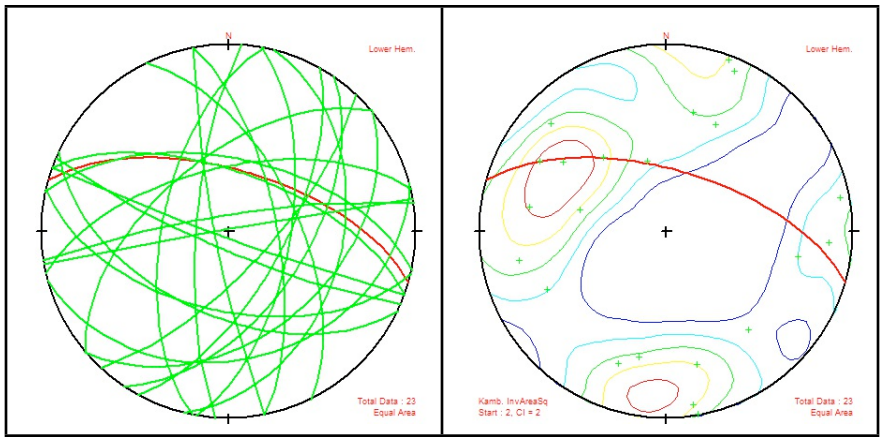


Figure 26: FW-DZ fractures from all three levels. Red is average SPF strike/dip.

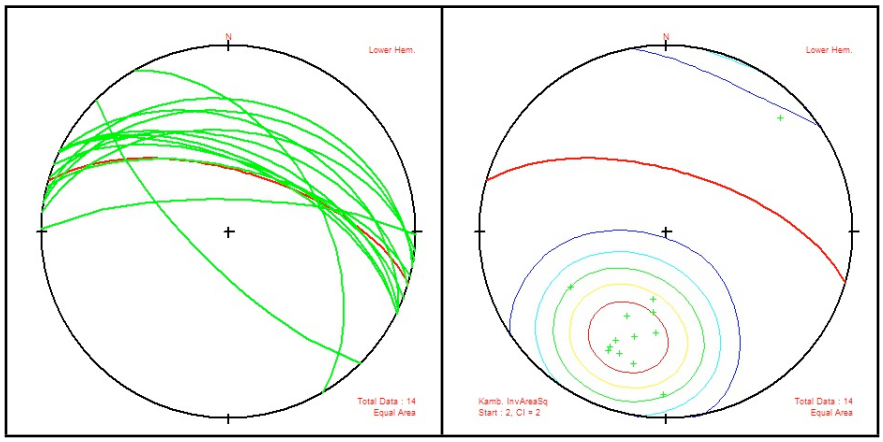


Figure 27: CZ fractures from 2600 and 4800 levels. Red is average SPF strike/dip.

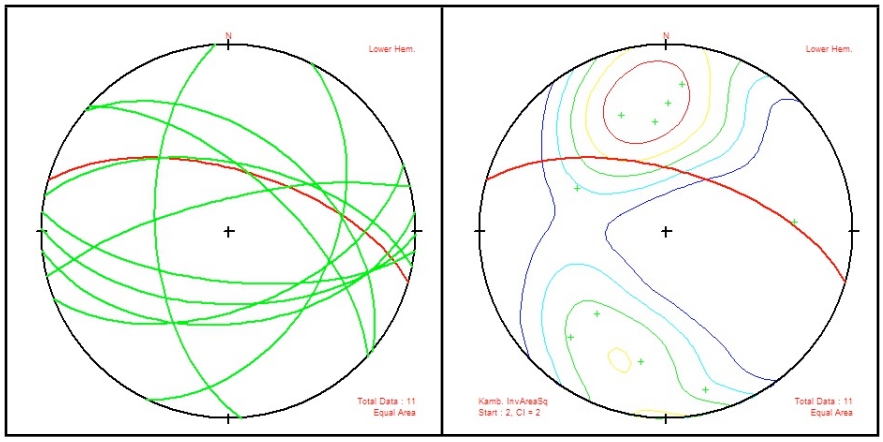


Figure 28: HW-DZ fractures from 2600 and 4800 levels. Red is average SPF strike/dip.

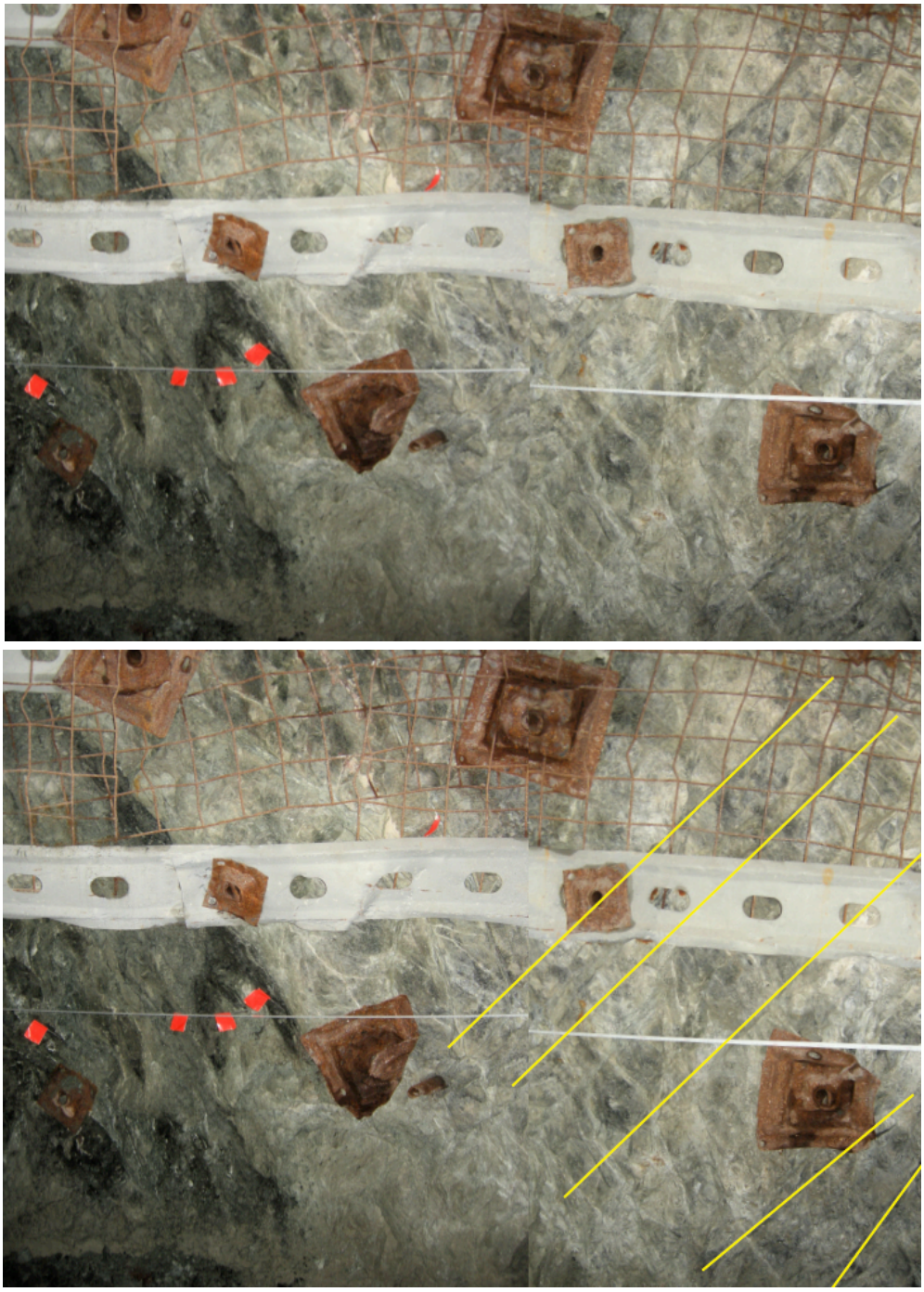


Figure 29: Hanging wall of SPF at the 4800 level, yellow lines on bottom photograph indicate fractures interpreted as R'-fractures given their antithetic orientation with respect to the dip of the SPF (core zone at left). Width of view is approximately 3 meters.

Vein Characteristics Within the South Prairie Fault

Veins were observed within the SPF damage zones at each level in the mine and varied from partially filled to fully sealed veins with no consistent aperture. Veins at the 4800 level were observed in the core zone, but not at the other two locations. Mesoscopic and microscopic observation of broken-up vein material within the 4800 core zone suggests a protracted fluid-flow history. Reaction of vein material to HCl was very minimal, though thin-section analysis shows this is not due to Fe-Mg rich carbonates as originally suspected, but rather was the result of zeolite vein fill with some late stage carbonate (possibly calcite according to XRD) growth.

Veining appears to have played a role at the CZ/DZ interface at the 4800 level, as well as within the core zone at the 2600 level, as mentioned above (Figure 16). The 2600 core zone vein had an aperture of 6 cm and was fully sealed, though it appears to be the result of two separate stages of growth and may represent crack-seal process. As mentioned, this vein dies out coincident with widening of the gouge zone to 1 m wide, whereas the core zone is <30 cm wide adjacent to the vein along the floor of the access.

Figure 18 shows the 4800 level vein at the FW-DZ/CZ contact. More specifically, the vein occurs at the FW-DZ/FW-loc-shear clay smear zone. Aperture of the vein ranged from 2-7 cm (approximately 4 cm wide in Figure 18). It is hypothesized that the location of these veins within and immediately proximal to the core zone is suggestive of a relationship between fluid-flow and fault slip, perhaps through stick-slip behavior caused by fluid overpressure (Scholz, 1992). Stick-slip is also suggested by the broken up veins

observed in the core zone at the 4800 level, showing that fluid was flowing and mineralization was taking place during interseismic periods.

Architecture and Permeability of the South Prairie Fault

Caine et al. (1996) developed a simple method for quantitatively estimating the permeability of a fault zone based on measurements of the fault's architecture (damage zone and core zone). This model is based on the disparate structural and hydrogeologic properties of a brecciated damage zone and a heavily comminuted gouge/core zone by assuming damage zones will likely behave as conduits for fluid-flow and core zones will behave as barriers to fluid-flow (Caine et al., 1996). Gudmundsson (2011) suggests that the damage zone permeability can be as much as 10,000 times higher than core and/or host rock. These vastly differing properties can have mechanical effects that inhibit fault movement via fluid overpressure at the DZ-CZ contact (Scholz, 1992; Babcock et al., 2013) and can be useful in estimating the likelihood of fluid (water, oil) movement in the vicinity around and through faults of differing lithologic compositions and geologic settings. In the case of typically low-permeability crystalline rocks, hydrologic properties of fault zones have been important for understanding potential fluid-flow near waste repository sites (Lützenkirchen, 2002). Initially for this study, a permeability estimate was calculated to qualitatively assess the likelihood of a fluid's role in the alteration mineralogy of the SPF zone (mentioned later in this chapter) (Chester and Logan, 1986),

but has since been used to consider the behavior of the SPF during pre- and syn-kinematic movement.

Damage zones are composed of brecciated fragments surrounded by interconnected fracture networks. This allows damage zones to behave as permeable units for fluids. Core zones, however, commonly act as fluid barriers due to the abundance of fine grained material. By measuring the width of a fault zone and the individual core and damage zones, one can therefore estimate the likelihood of fluid-flow in the vicinity of a fault by assuming these hydrologic properties. Caine et al. (1996) demonstrated this mathematically by the following equalities:

$$F_a = \text{damage zone width} / \text{total fault zone width} \quad (1)$$

$$= \text{damage zone width} / (\text{core zone width} + \text{damage zone width}) \quad (2)$$

$$F_m = \text{mean of } F_a \text{ values for a single fault zone} \quad (3)$$

where F_a is the fault zone architectural index. F_a is essentially a percentage of the likelihood of fluid-flow and ranges between 0 and 1 with 0 being a barrier to and 1 being a conduit for fluid-flow. A value in between these two end members results in a combined conduit-barrier system (Caine et al., 1996). The mean of F_a values is then calculated, giving F_m. Plotting F_m against the total fault zone width gives insight into the nature of faulting for things such as the mechanics during seismic slip and the response of the host rock types to deformation (Caine et al., 1996). This is especially of interest for the SPF since most fault studies have not been conducted on mafic-ultramafic host rocks.

Given the constraints of observation in this study, only the 4800 level was able to be completely measured from FW to HW. Therefore, F_m was not calculated for this study. The following widths were measured at the 48w8400 location (Figure 30):

FW-DZ to CZ:	2.36 meters
CZ width:	2.51 meters
CZ to HW-DZ:	>2.63 meters
Total DZ width:	4.99 meters
Total width:	>7.50 meters

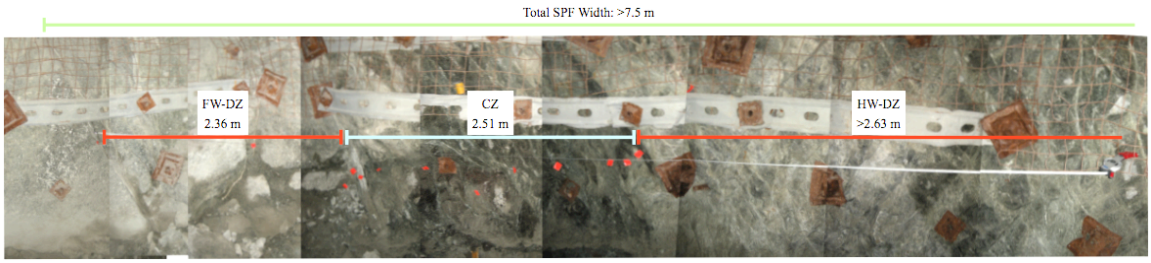


Figure 30: Widths of the SPF at the 48w8400 location. Photo collage is not of equal scale across due to close proximity of access wall behind photographer. View is to the west.

Using Equation (1):

$F_a = 4.99 \text{ m} / 7.50 \text{ m}$

$F_a = 0.67$

This gives a permeability of about 0.67 (67% permeable), and is almost 20% more permeable than a true combined conduit-barrier system. This value plotted against fault

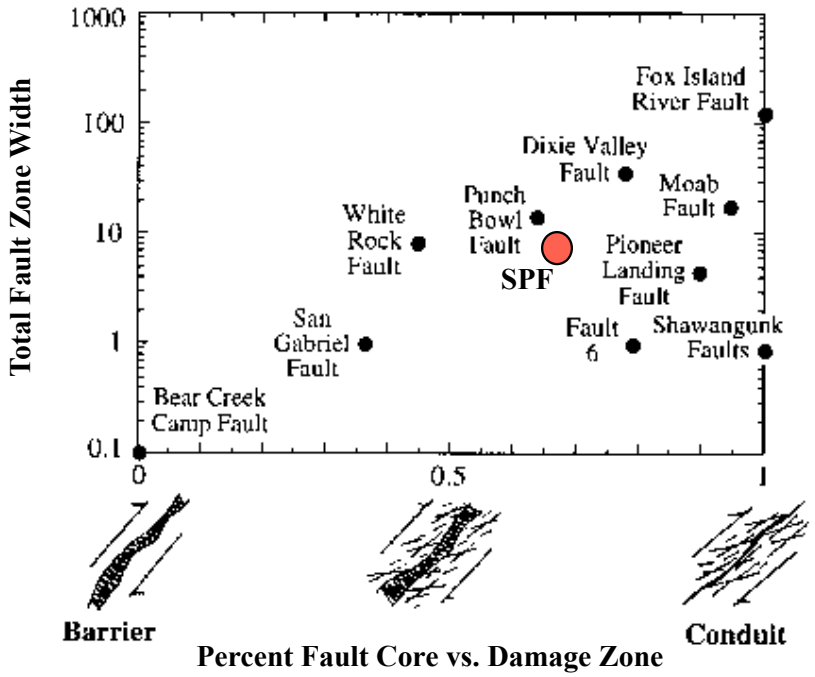


Figure 31: Plot of F_a as a function of total fault zone width. The SPF plots similar to other faults in various host rock lithologies. Another Laramide basement fault, the White Rock thrust, has a similar width but lower estimated permeability. Figure modified from Caine et al., 1996.

zone width (7.5 m) is above in Figure 31. A major Laramide basement fault, the White Rock thrust in the Wind River Mountains of Wyoming (Mitra, 1984), plots just 5% short of a true conduit-barrier system. The White Rock thrust likely had a recurring history of motion, and restored cross-sections give an approximate overburden of 10-12 km during Laramide deformation (Mitra, 1984). Similar to the SPF, the White Rock thrust formed at brittle to brittle-plastic conditions according to Mitra (1984). However, basement rock in this area of the Wyoming foreland is dominantly quartzofeldspathic granitic gneisses of the Archean Wyoming Province, and likely responded differently to Laramide

deformation. It is speculative to assume this lower permeability is a result of the differing host rock variety, but more research on various Laramide basement faults would be required to determine whether this lower value is truly based on lithology or on other factors.

Role of Fluids Within the South Prairie Fault

The presence of fluids in faulting mechanics is well studied and has quantitatively been shown to play a key role in rock failure (Hubbert and Rubey, 1959). Evidence suggests fluids played a large recurring role in the SPF. Broken-up vein material within the core zone along with veins coincident with the core zone are supportive of this claim. In addition, damage zone rock displayed a bleached appearance in comparison to host rock at the 2600 and 4800 levels. Furthermore, the 4800 HW-DZ showed the most defined bleaching. Herein, bleaching is described as the condition of a rock to exhibit a whitened and more easily breakable nature; occasionally, it was soapy to touch. Bleaching of the 2600 HW-DZ was also evident, but its limited exposure made it impossible to even qualitatively discuss to what degree bleaching occurred.

These observations suggest that fluids would prefer an upward path from the fault zone, thereby causing an evident color contrast between the HW and FW rocks. Bleaching by preferential fluid permeation into the HW-DZ, rather than the FW-DZ, seems consistent with claims of natural hydraulic fracturing proposed by W.J. Phillips (1972) who looked at natural hydrothermal brecciation phenomena in the hanging walls of normal faults in Wales. Faults in this study were in upper Ordovician- to Silurian-age

shales and turbiditic sandstones and were likely buried at a depth of 6 to 8 km at the time of faulting and mineralization. This is similar to the SPF's likely burial depth of 6-8 km at the start of Laramide orogenesis in what would become the Beartooth arch. Dip angles of normal faults in the study were 60º on average, also similar to the SPF. As stated by Phillips (1972):

> "The build up of the pressure of the hydrothermal solution at the top of the fault would set up a pressure gradient between the hydrothermal solution at the top of the fault and the pore water in the adjacent rocks. Hydrothermal solution would permeate into the pore spaces of the adjacent rock, and since the low density solute would tend to rise, the permeation zone would be more extensive in the hanging wall."

Given the model proposed by Hubbert and Rubey (1959), an extensional fault system should not change the process of fault rupture via fluid overpressure. Rather, an extensional fault system would only differ from a contractional fault system by the means of which the fluid enters the fault zone prior to rupture according to the orientation of Mode I fractures (when considering the Anderson Criterion for faulting and the formation of Mode I fractures parallel with the σ_1 direction) (Anderson, 1951). This, thereby, suggests a mechanism for which the hanging wall is more extensively brecciated and deformed than the footwall. This relationship is commonly observed in fault studies and particularly with the SPF. However, this model does require hydrothermal fluids and a source for them. Thin-section analyses of damage zone rock at the 2600 level show assemblages consistent with sub-greenschist to greenschist facies as evidenced by the assemblage tremolite-chlorite-serpentine-talc (Winter, 2010). Boschi (2006) suggests that this assemblage is indicative of metasomatism at greenschist conditions. Likewise, the

4800 HW-DZ shows extensive serpentinization of pyroxenes, a process that requires as little as 50% water/pyroxene concentrations (Eq. 18 of Frost and Beard, 2007). This is in addition to the relatively more extensive HW brecciation and visible bleaching. Though these observations do support the presence of hot water within the fault zone, fluid source has not been determined due to the composition of the vein mineralogy, as a preferred stable isotopic method of zeolites is not currently available.

A temperature range for fluids can be estimated from the zeolite mineralization found in SPF veins and the metasomatic mineral assemblage observed in the 2600 HW-DZ. Zeolite conditions have been cited in fault environments at 4-8 km depth, having temperatures of 180-200ºC (Lützenkirchen and Loew, 2011). This gives a range between 180º to <300ºC at the highest metasomatic conditions observed with the mineral assemblage (Boschi et al., 2006; Winter, 2010). More discussion on mineral assemblages and their formation conditions are described in the following section of this chapter.

Some veining outside of the core zone is likely post-kinematic, perhaps even relatively recent meteoric fluid-flow, and supports the permeability estimate of 0.67 and the general hydrologic properties of damage zones (Caine et al., 1996). Vein material within the core zone is undoubtedly the result of interseismic fluid-flow events and lends insight into the conditions of faulting for the SPF during the Laramide. The mineralogy of these veins as observed within gouge zone porphyroclasts will be discussed below.

Mineralogy of the South Prairie Fault and How it Varies

Stark color changes across a fault zone indicate variations in mineralogy within the fault's architecture. If one momentarily considers a fault zone as a closed system, it is intuitive that the alteration products within the fault zone will be compositionally homogeneous to the general chemical composition of the whole rock. This relationship was observed in the Fe-/Mg-rich rocks of the Stillwater Complex and their proclivity to produce Mg-rich phyllosilicates, rather than the Mg-poor alteration phyllosilicates illite and/or smectite commonly produced from quartzofeldspathic host rocks (Goddard and Evans, 1995; Solum et al., 2006; Boulton et al., 2012; Buatier et al., 2012). These previous fault zone studies include both Laramide and non-Laramide faults.

More appropriately considering a fault zone as an open system in terms of fluid-flow, as shown above, allows for the heterogeneity observed in fault zone mineralogy by the addition of H_2O and perhaps other elements or compounds found in the fluid. It was observed in this study that the addition of fluids consequently provided a catalyst by which some minerals began to alter (e.g., Opx to serpentine) at varying conditions.

As a matter of scale, chemical constituents appeared to remobilize at the grain scale rather than at the whole rock scale. Chemical compositions of different minerals were observed to produce alteration material rich in that grain's composition rather than distributing the whole rock Fe/Mg concentrations. For example: Ca-/Al-rich plagioclase, typically An_{70-80} for Stillwater Complex rocks, altered into the Al-rich epidote variety clinozoisite. This apparent behavior of single grain chemical remobilization is expected

to differ for faulting in rocks outside of the crystalline basement, and may have different results for faults in more porous (open system) sedimentary strata.

Alteration of mineral phases, though observed to be directly related to chemical composition, also appeared to be thermodynamically influenced as alteration conditions increased towards the core zone with a peak at the CZ-DZ contacts as evidenced by XRD (localized shear zones of Figures 17 and 18; Figure 40). This relationship was more zonal, however, than gradational. Damage zones did not exhibit complete alteration of host rock material as was observed in the core zone likely as a result of lower temperatures and less comminution of material. In a general sense, the DZ was a zone of incomplete alteration that typically occurred at or near the grain boundaries. Wholly serpentinized pseudomorphs after Opx were only observed in the 4800 HW-DZ within <35 cm from the core zone. Dissimilarly, the CZ was a zone of intense alteration and, at the microscopic scale, penetrative deformation. Mineral phases in the core zone could not be readily assigned to their protolith phase(s) and typically had a cataclastic flow texture at the microscopic scale. Sigma structure porphyroclasts were the only means by which some of the parent material could be identified in the most comminuted areas of the core zone. Less severely comminuted areas of the core zone (towards the middle) did show alteration and protolith material within a fluxion-style gouge matrix. Overall, the CZ was a zone of serpentine-chlorite gouge. XRD analysis suggests the chlorite to be the Clinochlore IIb polytype, as well as mixed-layer serpentine-chlorite.

Given the disparate mineralogic characteristics across the fault zone, the following discussion is organized by fault architecture and will describe each mineral phase separately for the damage zone and core zone.

Host Rock

The SPF occurs in the Lower Banded Series of the Stillwater Complex (Figure 2), an anorthositic, noritic and gabbronoritic zone of rocks that contain the Pt-/Pd-rich olivine-bearing JM Reef (OB-I, Figure 2). Johns-Manville corporations geologists, the first to find Pt/Pd in the Stillwater Complex in the 1970's, termed this the Troctolite-Anorthosite Zone I and divided it into four sub-units (Geraghty, 2013):

1) Gabbro Subzone - interlayered gabbronorite, norite, anorthosite, and troctolite; 60 m thick.
2) Anorthosite 1 Subzone (J-M Reef host) - dominantly anorthosite, troctolite, and leucotroctolite; 35 m thick.
3) Norite Subzone - often referred to as the "ragged-textured norite"; 10 m thick.
4) Anorthosite 2 Subzone – dominantly anorthosite and leuconorite; 15 m thick.

Exposure of the FW at the 2600 level seems most consistent with the Gabbro Subzone. Modal percentages of an undamaged FW sample (26w8000-FW-1) taken 2-3 m south of the core zone (right of the SPF in Figure 16) gives a composition of 50% plagioclase, 38% orthopyroxene, and 12% clinopyroxene (Figure 32A). This plots as a gabbronorite on the IUGS classification. Plagioclase compositions were estimated at An_{58-83}, with an

average of An_{71}. The HW sample was too altered to determine its original composition. Mine geologist Mike Pasecznyk interpreted the HW as a leucocratic troctolite.

At the 4800 level, the SPF was likely hosted at the upper extent of Anorthosite Subzone I. FW sample 48w8400-1-FW had an average modal percentage of 68% plagioclase, 29% orthopyroxene, and 3% clinopyroxene (Figure 32B). This gives the composition of the 4800 FW as a norite according to the IUGS classification. Plagioclase compositions here were estimated at An_{68-88}, and was An_{80} on average. Within the core zone, a lens of leucocratic troctolite was observed. This was interpreted as the JM Reef by the presence of sulfides. Interestingly, this was the most competent part of the core zone and a flow texture of gouge was observed around it (Figure 19). The HW consisted of oikocrystic anorthosite and was referred to by Mike Pasecznyk to be the "ragged-textured norite" mentioned above. This places the SPF at the contact of Anorthosite Subzone I and the Norite Subzone at the 4800 level. Only damaged and altered HW was able to be sampled. Relic host rock minerals were able to be interpreted (Figure 33), and gave a modal percentage of 63% plagioclase, 33% orthopyroxene, and 4% clinopyroxene. Anorthite concentrations will be presented in the damage zone discussion.

The SPF has been cited as commonly cutting out and doubling up parts of the JM Reef package at different levels within the Stillwater mine (Cooper et al., 2002; Cox and Holick, 2008) as the fault laterally migrated during slip. Location of the SPF likely within the Gabbro Subzone at the 2600 level and along the Anorthosite Subzone I/Norite

Subzone contact at the 4800 level represents a minimum lateral migration of 35 m (114 feet) over 670 vertical meters (2200 feet).

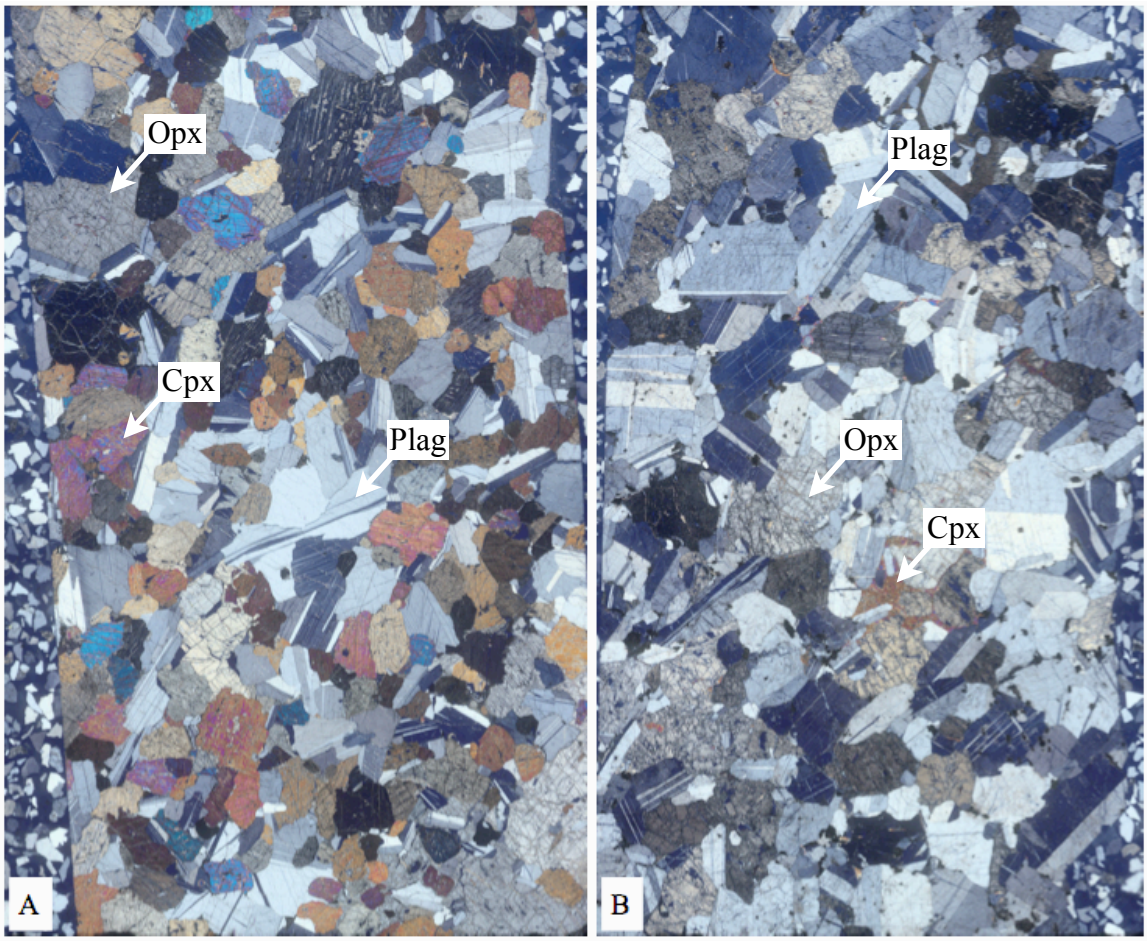


Figure 32: XPL thin-section scans of unaltered FW samples. A) 2600 FW. B) 4800 FW. Length of vertical axis is 36 mm (standard thin-section). Compare unaltered phases with photomicrographs of altered phases in the following discussions.

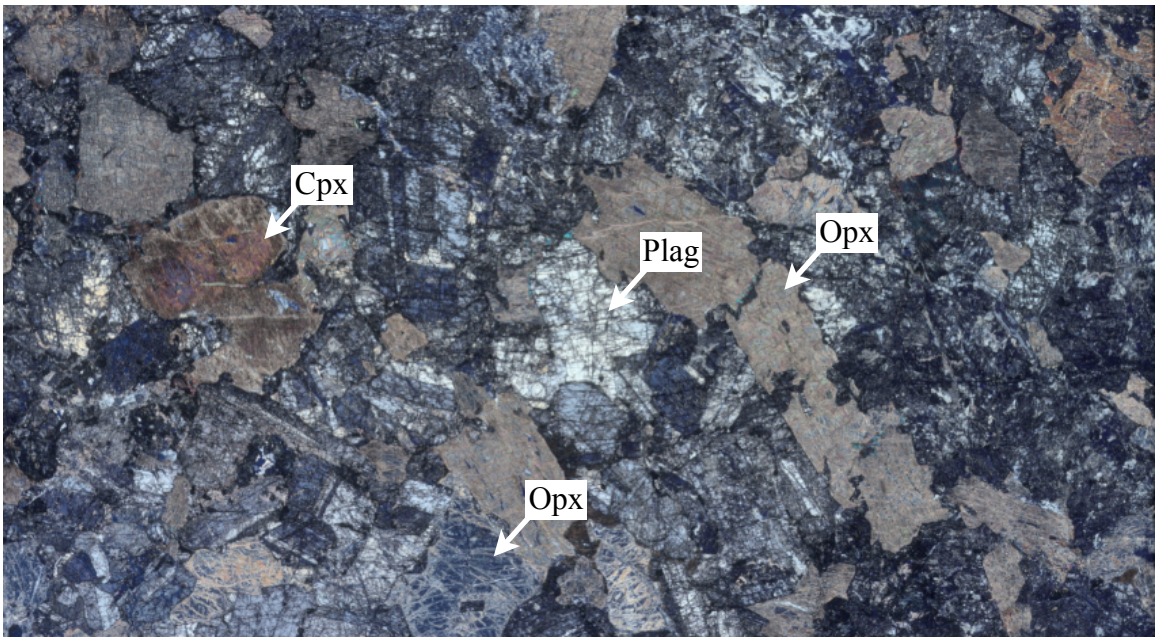


Figure 33: XPL thin-section scan of 4800 HW-DZ sample 48w8400-16HW. Note discernible relic mineral assemblage of Plag, Opx and Cpx. Length of horizontal axis is 36 mm.

Damage Zone

Damage zones appeared to behave as intermediate zones of alteration compared to the undamaged host rock and comminuted core zone. Consequently, damage zones record the physical-chemical alteration history of a fault. Progressive deformation in the form of fracturing behaved differently in varying mineral phases as expected. This relationship appeared consistent with the chemical compositions of certain mineral species. Orthopyroxenes (Opx) were noted to chemically alter most readily, despite plagioclase (Plag) grains being relatively more fractured than Opx in grains of the same sample. Clinopyroxene (Cpx) was the most resilient to alteration and proceeded by cleavage plane fracturing before complete alteration.

Grain fracturing occurred as both stable and unstable fractures. These two varieties of fracturing indicate brittle and brittle-plastic conditions. Unstable fractures are continuous transgranular fractures that cut across grains of differing composition and orientation and lack any sign of internal plastic processes. Lack of plastic processes in these fractures suggest instantaneous stress relief following fracturing and, therefore, are indicative of brittle processes (Mitra, 1984; Miller, 1987; Smith, 1991). Dissimilarly, stable fractures are intragranular fractures that die out within the grain or at mineral grain boundaries. Stress at the fracture tip of stable fractures is likely dissipated by plastic deformation in adjacent grains (Mitra, 1984; Miller, 1987; Smith, 1991).

Quartzofeldspathic basement rocks of the Wyoming province have been shown to deform brittlely and plastically concomitantly at the grain scale (Miller, 1987). This relationship was also observed in the heterogeneous mineralogy of this study as already mentioned by plagioclase's propensity to fracture more readily than Opx within grains only millimeters apart. The dissipation of stable fractures by meeting a zone of plastically deformable material may be explained by grain-boundary alteration phases altering to more ductile material, as seen by the deformation of feldspars in a study by Janecke and Evans (1988). Alternatively, conditions of faulting were also observed to have occurred earlier at more plastic conditions with later-stage brittle fractures cross-cutting brittle-plastic structures such as CS fabrics. This observation likely suggests more brittle processes beginning to occur as more overburden was stripped from the Beartooth Massif. These observations will be discussed more fully in the CZ mineralogy section.

Evidence of fluid-flow alteration was observed in the HW of the 4800 level by the presence of fully serpentinized Opx grains (Figure 36). The 2600 HW and FW displayed hydrothermal fluid-flow characteristics by the mineral assemblage tremolite-chlorite-serpentine-talc (Boschi et al., 2006). This characteristic assemblage was most pervasive at the 2600 level. However, mineral phases in the damage zone appeared to alter to specific alteration phases consistently at the 2600 and 4800 levels and are discussed by individual phase below.

Plagioclase: Plag was the dominant mineral phase of the SPF host rocks and was the second most resilient to alteration. Fracturing was observed to begin even at the most distal locations of the FW-DZ at the 4800 level (2.5 m from core zone), though alteration did not readily occur until more pervasive fracturing towards the CZ. Fracturing within Plag grains occurred as both stable and unstable fractures. The FW sample consisted of stable fractures dominantly, though some unstable fractures strictly between grains of like phases were observed. No unstable fractures were observed between Plag and Opx/Cpx 1.55 m into the fault zone (≈0.8 m from CZ). Multi-phase unstable fractures however were observed in the more brecciated HW-DZ (Figure 34). Cleavage planes were possibly the most dominant catalyst for fracture formation, though shear fractures deviating from cleavage angle were also observed.

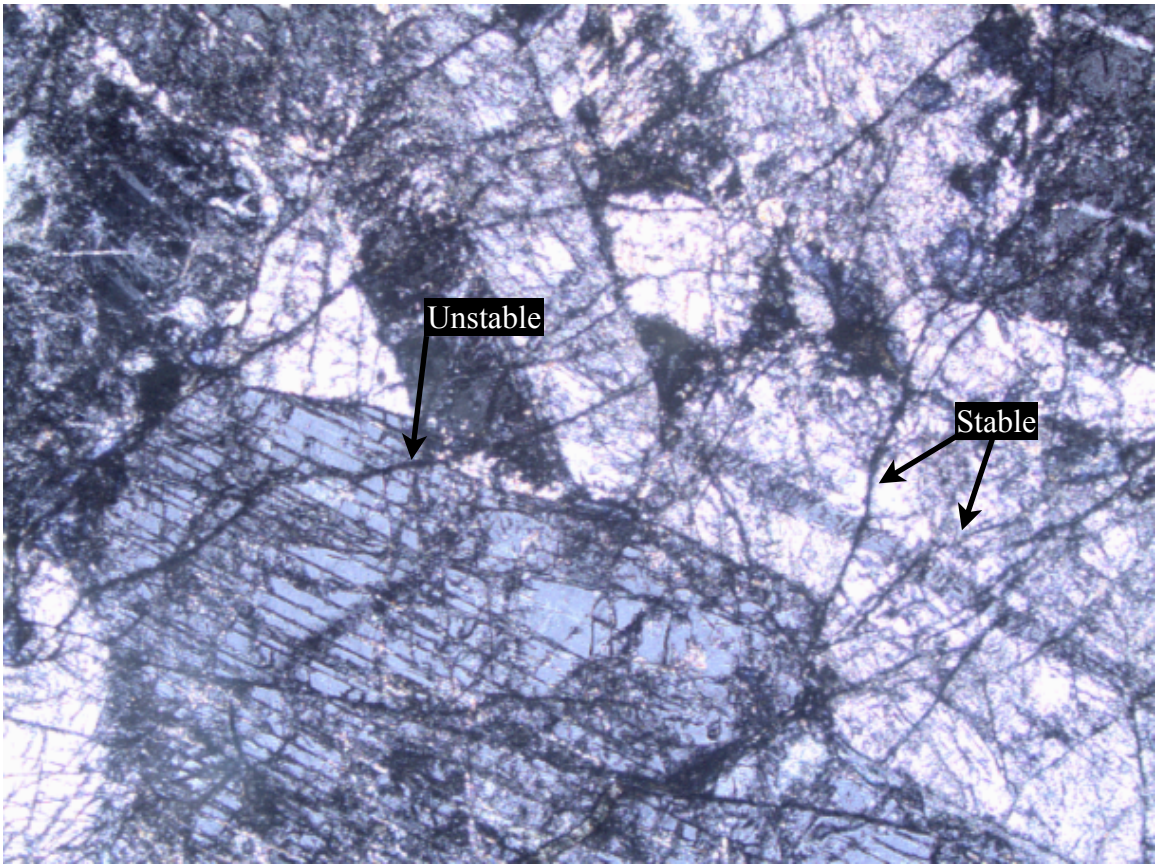


Figure 34: 4800 HW-DZ sample showing unstable and stable fractures across Plag and Opx grains. Note stable cleavage plane fractures of Opx. Length of horizontal axis is approximately 2 mm. XPL.

Alteration of Plag was dominantly to the Ca-/Al-rich epidote variety clinozoisite and occurred initially at the grain boundaries. More advanced alteration and deformation exhibited patchy internal disintegration of Plag and alteration to clinozoisite (Figure 35). Clinozoisite occurred as anhedral granules; no euhedral grains were observed.

Epidote formation from Plag is expected, as it commonly occurs from the hydration of tectonically fractured Plag (Miller, 1987; Miller and Lageson, 1993). Miller (1987) found epidote to be the most common alteration phase associated with Laramide

deformation of plagioclases (An_{30}) in his quartzofeldspathic rocks from the Bridger and Gallatin ranges. Conditions of deformation in his study were T≥200ºC.

Anorthite concentrations of DZ Plag's were observed to decrease towards the core zone (Appendix B). The term albitization is herein used to describe a decreasing An content towards compositions of more sodic Plag. Plag grains did not consistently decrease as a whole, and estimations of An-content varied. I interpret the coincident albitization of Plag in relation to increased clinozoitization to be directly related to the release and remobilization of Ca^{2+} and Al^{3+} from Plag to clinozoisite. Formation of clinozoisite from albitization of Plag was experimentally shown to be possible at T<525ºC by Moody et al. (1985). They state that epidote "is commonly found co-existing with the sodic plagioclase, and forms owing to the release of Ca^{2+} and Al^{3+} during the breakdown of plagioclase." The breakdown of Plag to form clinozoisite can be shown by the reaction:

$$\text{labradorite} + SiO_2(aq) + H_2O = \text{albite} + \text{clinozoisite} + H^+ \qquad (4)$$

as modified from Moody et al. (1985). This reaction assumes constant aluminum concentration and a positive or negative flux of calcium or silica as needed. A requirement for water in this reaction is congruous with the above discussion on fluids within the SPF. HW samples at the 4800 level appeared more clinozoitized than FW samples, perhaps suggesting more fluids in the HW-DZ. Pure albite did not occur as discernible crystals, though it is possible that alteration groundmass could have precipitated albite.

Prevalence of clinozoisite after Plag is consistent with both Moody et al.'s (1985) experiments and Miller's (1987) and Miller and Lageson's (1993) observations of epidote in tectonically deformed Plag. Based on Miller's (1987, 1993) results, it is postulated that the low initial calcic Plag compositions of his study are expected to form Ca-/Al-deficient varieties of epidote, as observed in his study, since there is not an excess of Ca^{2+} and Al^{3+} constituents. Prior to thin-section analysis, it was expected that Ca/Al release remobilized into chlorite. This relationship may still hold true but to a lesser degree, suggesting that faulting conditions within the SPF DZ's were more conducive to clinozoisite formation.

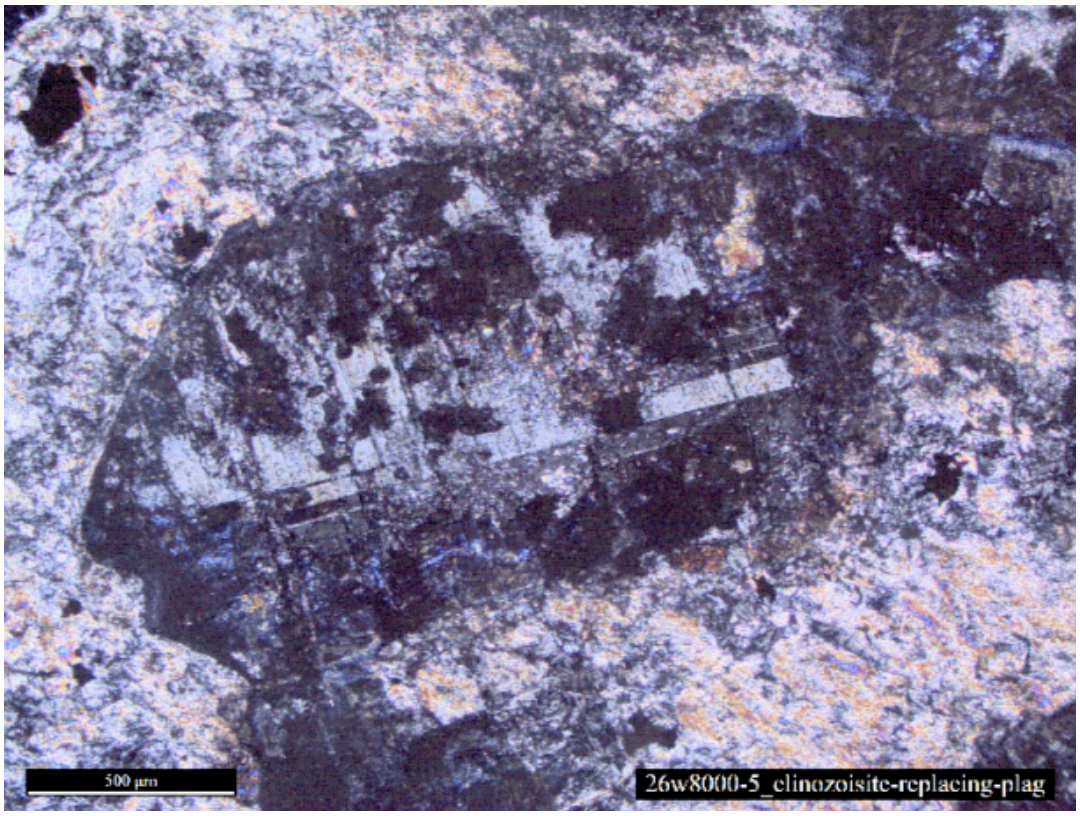


Figure 35: Extensive clinozoitization (anomalous blue) of a Plag grain from the 2600 FW-DZ. Note occurrence of alteration phases mostly at the grain boundaries, though internal disintegration and alteration had started to occur (<30 cm from CZ). XPL.

Orthopyroxene: A more complex alteration history was observed within Opx. Opx was the most readily altered mineral phase, and would show extensive alteration even in the FW-DZ up to 1.5 m from the core zone. Characteristic irregular fracturing of Opx grains commonly observed in unaltered samples appears to have been the source for much of the syn-kinematic fracturing and likely the cause for easier alteration.

Alteration of Opx in some instances appeared to be directly replaced pseudomorphically by serpentine (Figure 36A) by liberation of SiO_2 and hydration of Opx. This can be shown by the reaction:

$$3Mg_2Si_2O_6 + 4H_2O = 2Mg_3Si_2O_5(OH)_4 + 2SiO_2 \quad (5)$$

This reaction assumes a starting composition of enstatite which concurs with work by McCallum (2002), suggesting Opx compositions of $En_{75\text{-}83}$ in rocks just below the JM Reef. Release of SiO_2 was observed in the form of quartz (Figure 37). Mafic/ultramafic rocks totally lack quartz as a primary phase and, therefore, the presence of this mineral indicates its formation entirely through alteration. Quartz commonly occurs in low-grade metamorphosed mafic/ultramafic rocks starting at the higher end of the prehnite-pumpellyite facies where chlorite also becomes stable (Winter, 2010). Undulose extinction suggests that quartz formed prior to the latest stages of deformation.

In some grains alteration appears to have resulted through hydration of Opx. The presence of talc was observed in some Opx grains (Figure 36) within twins, as well tremolite on the grain boundaries. This relationship was not consistent with all Opx grains, and may represent a partial reaction prior to full serpentinization.

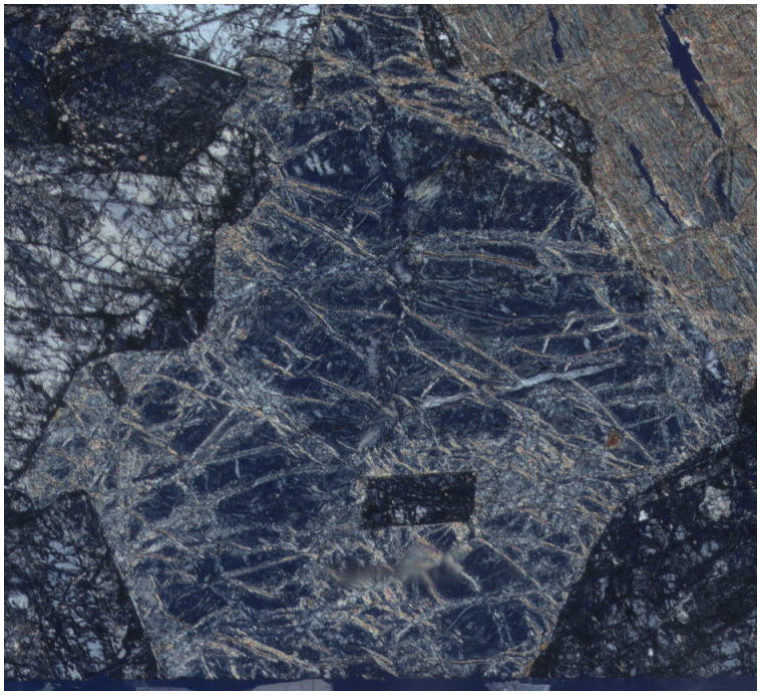


Figure 36: 48w8400-16HW sample, XPL. Pseudomorphically formed serpentine after Opx. Length of horizontal axis is 4 mm. Opx at upper right exhibits partial alteration with talc and tremolite visible.

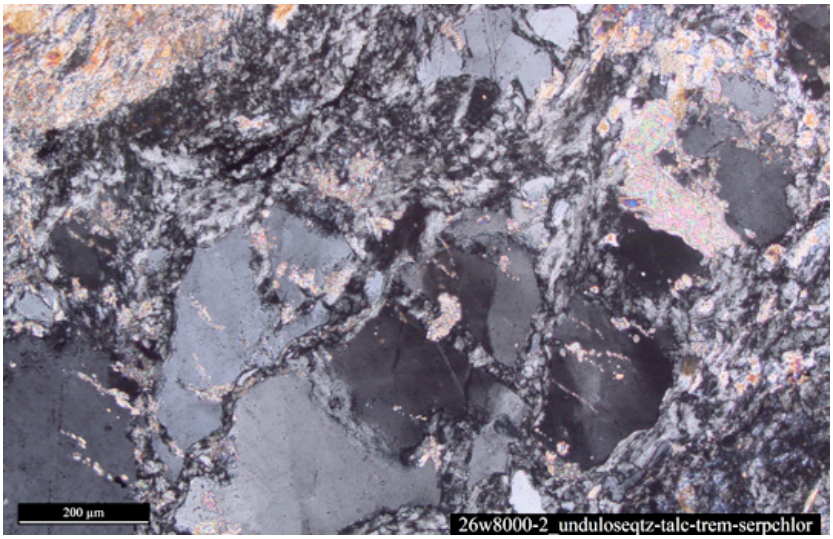


Figure 37: Undulose extinct quartz from the 26w8000 CZ/DZ area amidst a groundmass of tremolite and serpentine-chlorite. Talc is also present as the high-order phase to the right of the photograph. XPL.

Clinopyroxene: Cpx was the most resistant phase to chemical alteration, often remaining mostly free from alteration while Plag was heavily fractured and altered to clinozoisite and Opx was fully altered to serpentine. Fracturing occurred substantially along cleavage planes, dominantly along the {110} plane. No extensive shear fractures deviated from the cleavage plane were observed. Alteration was likely to serpentine and may have progressed along the cleavage plane fractures. Figure 38 shows a Cpx grain in a FW-DZ vein altering to serpentine. This may suggest that alteration of Cpx was strongly favored by extensive fluid-flow, but is inconclusive given the lack of Cpx grains.

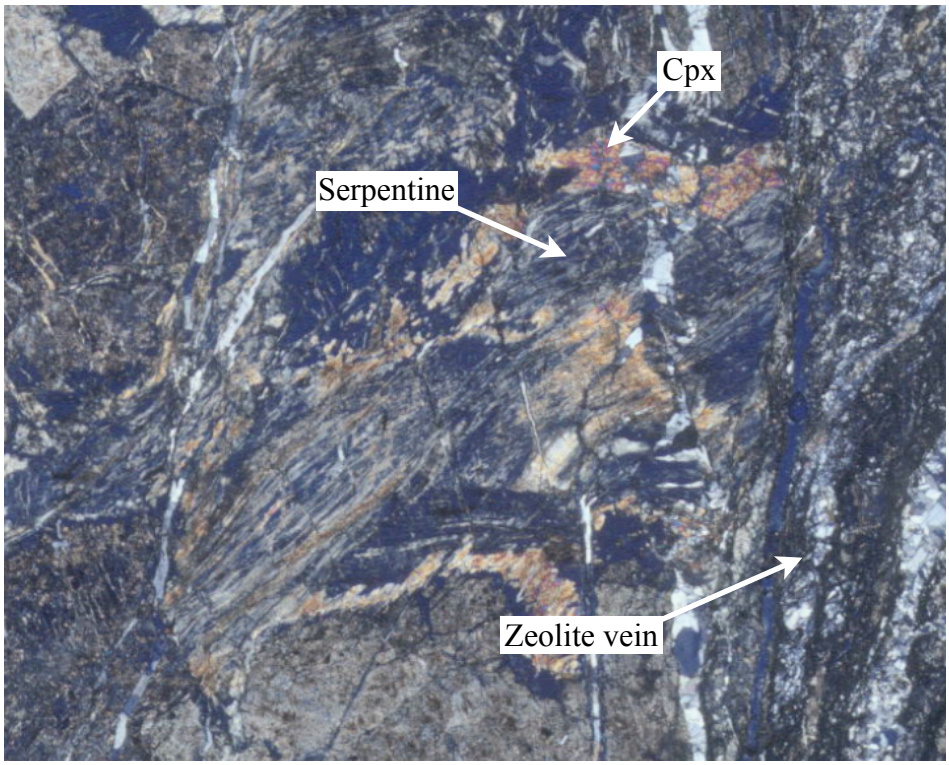


Figure 38: FW-DZ sample 48w8400-3 showing alteration of Cpx to serpentine preferentially along cleavage plane fractures. Sample is from a vein about 1.5 m south of the core zone. Main body of vein is at right of photograph. XPL.

Veins

Zeolites were the most prevalent mineral phase found in veins within both the core and damage zones. Evidence of repeated interseismic fluid-flow and mineralization events were observed by broken up clasts of vein material within gouge porphyroclasts in the core zone. These clasts varied in size and texture, further suggesting a protracted fluid-flow history within the SPF.

Lützenkirchen (2002) similarly found zeolites in veins associated with faults in the Gotthard Massif of Switzerland in his study. Like the SPF, his study was conducted in underground exposures. However unlike the SPF, the Gotthard Massif faults are hosted in quartzofeldspathic rocks, though interesting similarities do occur. Stilbite and laumontite were the most common zeolites observed in the Gotthard Massif faults. Zeolites within veins of the SPF appeared to dominantly consist of stilbite, as suggested by one plane of cleavage and XRD analysis. Laumontite is a common alteration product of anorthite (Lützenkirchen and Loew, 2011). No laumontite (three planes of cleavage) was observed in thin-section, however XRD analysis does suggest its presence. XRD analysis also suggests the calcium variety of stilbite (Stilbite-Ca) to be the dominant zeolite present within vein material. This finding is consistent with the excess calcium from break down of plagioclase. Late stage veins showed well developed subhedral to euhedral grains of stilbite growing outwards antitaxially into the vacant fracture (Figure 39). Lützenkirchen (2002) observed this same characteristic in stilbites of his study.

A lack of carbonate vein fill was observed in all thin-section and XRD samples. Thin-section analysis shows carbonate to have formed late stage in the vein fill, typically filling interstices between zeolites that lined the walls of the fracture (Figure 39). Due to this lack of carbonate, previously planned stable isotopic studies of vein fill material were abandoned as there is currently no good method for stable isotope analysis of zeolites. Talc was also found in association with the veins, and appears to have formed at later stages than carbonate within these zeolite veins.

Lower grade subhedral-euhedral mineral assemblages compared to higher grade assemblages in the core zone (discussed below) suggest that fluid-flow precipitated at ambient temperature conditions lower than synkinematic conditions. Euhedral zeolite grains did not appear to display major undulose extinction, though some were noticed to have a slight undulose extinction, indicating that not much strain accumulation or recovery had taken place. This could support that zeolite mineralization post dated seismic (syn-kinematic) events and/or the latest stages of deformation within the SPF.

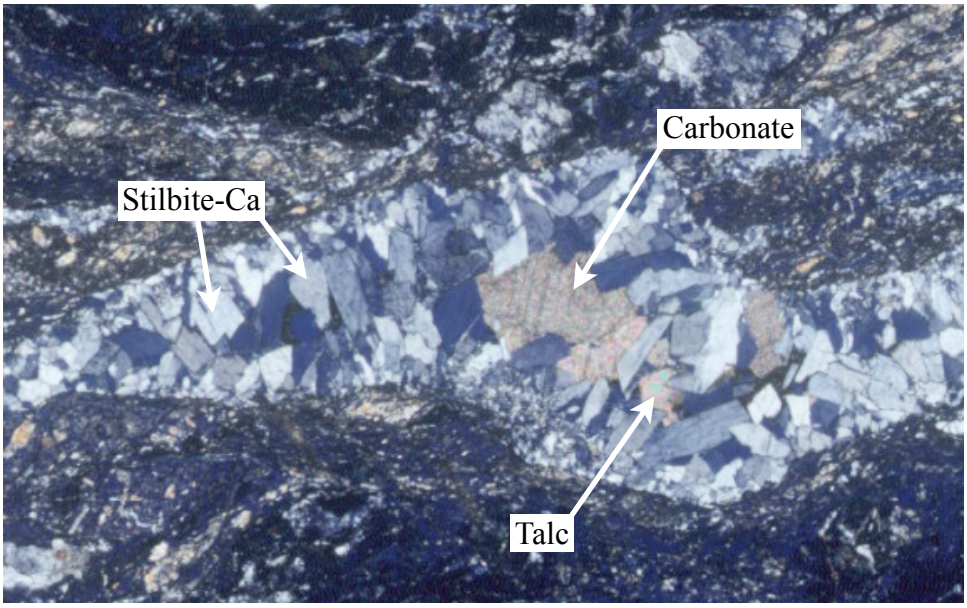


Figure 39: Zeolite vein from FW-DZ/CZ sample 48w8400-5. Subhedral to euhedral phases are stilbite, note late stage infilling of carbonate into interstices. Minor talc is also present as high order phase at center right. Length of vertical axis is 2 mm. XPL.

Core Zone

The most comminuted and completely altered areas of the core zone occurred at the contacts of the FW-DZ/CZ and CZ/HW-DZ. Gouge at the contacts had a slight foliation and a strong visible preferred orientation of gouge material. Internally, the core zone had a flow-like, folded texture at the mesoscopic scale. Microscopically, core zone gouge exhibited a more "tumbled" appearance. Mineral phases within the core zone were extensively serpentinized/chloritized. XRD analysis suggests clinochlore-chlorite, serpentine and mixed layer serpentine-chlorite are the major phases in the core zone. Formation of chlorite may have been from the continual release of Al^{3+} from Plag giving

way from clinozoitization to chloritization. Aluminum's general lack of mobility suggests that any Al^{3+} required to form chlorite was directly sourced from Plag.

A transect of core zone samples was examined using XRD. These results (Figure 40) suggest the highest alteration at the FW-loc-shear where the gouge consisted of only serpentine-chlorite (Figure 40A). Samples within the core zone were less altered and still showed sign of zeolite, plagioclase and clinozoisite (Figure 40B, C). Similar to the FW-loc-shear, serpentine-chlorite was the dominant phase at the HW-loc-shear, but a minor amount of zeolite was detected (Figure 40D). Tremolite was also detected by XRD, though thin-section analysis of this sample did not show any observable or well-formed crystals. The presence of tremolite is consistent with the pervasive fluid-flow in the HW and likely formed from metasomatic conditions as presented in the discussion above. These results are suggestive of hotter conditions at the FW-DZ/CZ contact than at the CZ/HW-DZ contact and therefore marks a distinct mechanical boundary.

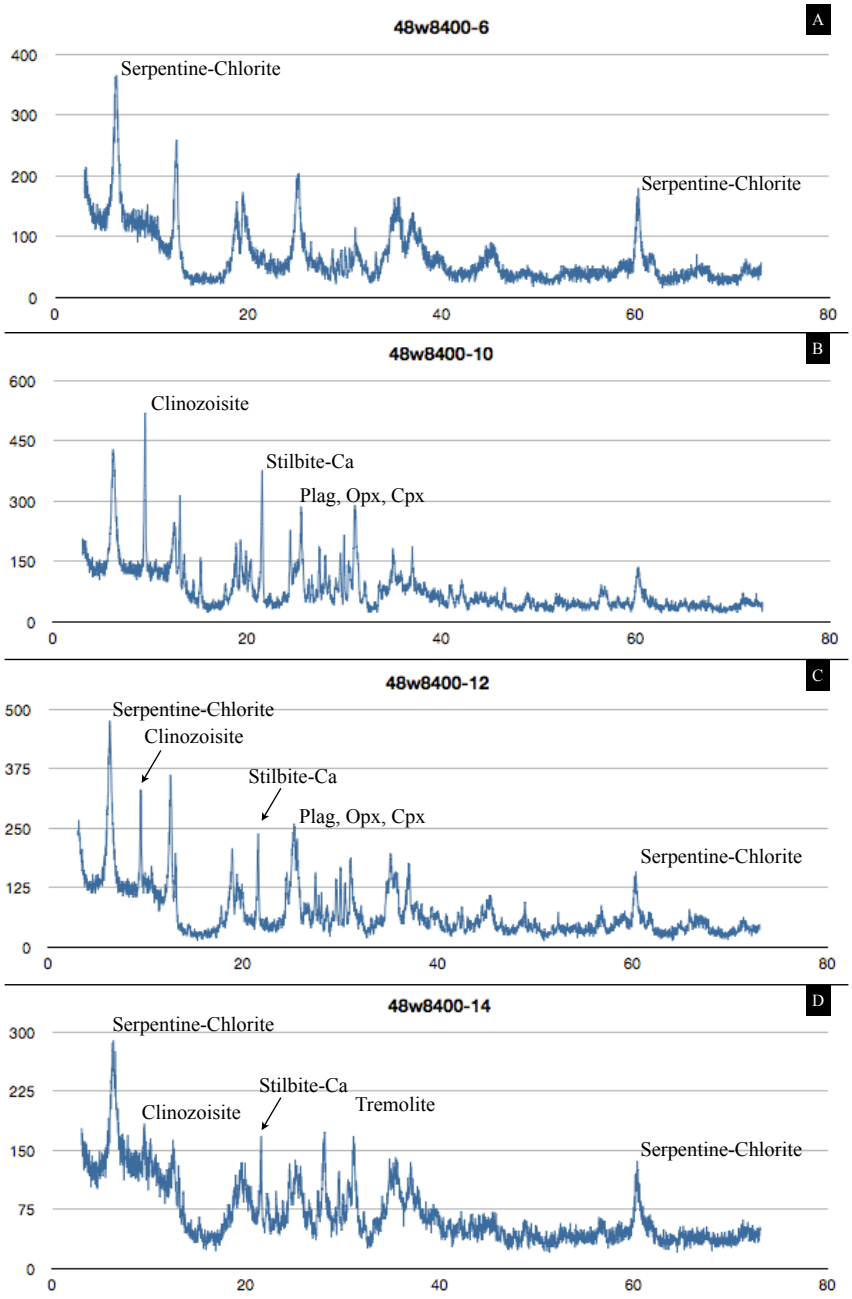


Figure 40: XRD results of 4800 CZ transect. FW and HW localized shear zone samples 48w8400-6 and -14 are strikingly similar. A) Dominant serpentine-chlorite at FW-loc-shear. B) Center of CZ, serpentine-chlorite, zeolites, albite/plagioclase and clinozoisite. C) Approximately 30 cm from CZ/HW-DZ contact. Similar mineralogy to 48w8400-10. D) HW-loc-shear shows a more complex assemblage compared to FW-loc-shear, but dominantly serpentine-chlorite.

Some of the most comminuted samples of gouge at the CZ boundaries exhibited a cataclastic flow texture at the microscopic scale with an evident CS fabric (Figure 41). At the HW-loc-shear, an interpreted CS fabric was observed to be cut by later stage brittle fractures (Figure 42), suggesting both brittle and ductile conditions during fault motion on the SPF. Sigma structure porphyroclasts within the flow matrix were abundant and contained relic vein fill material. An average of 93.4% of all porphyroclasts between samples 48w8400-7a and -7b were positively identifiable as relic vein fill material (zeolite, carbonate, talc). The size of porphyroclasts varied from <1 mm to up to 4 mm in diameter. The incorporation of vein material into the gouge suggests it was spatially closest to the core zone and was easily brecciated into the gouge matrix. This could be indicative of a relationship between fluid-flow processes and fault slip.

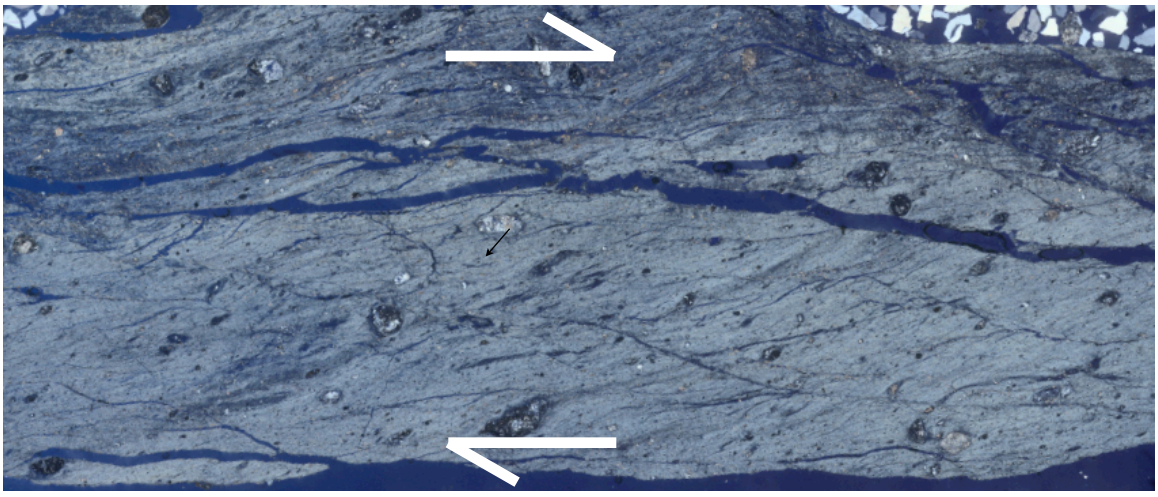


Figure 41: XPL thin-section scan showing gouge with CS fabric in 48w8400-7b sample. Dominant serpentine-chlorite mineralogy. Sigma structure porphyroclasts are composed of broken up vein fill material and give a top to right shear sense. Length of horizontal axis is approximately 35 mm.

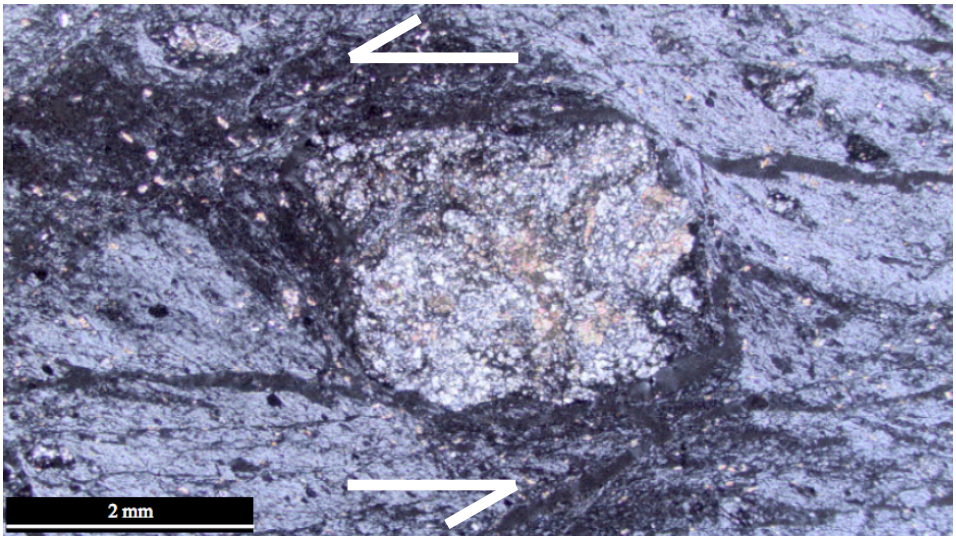


Figure 42: XPL photomicrograph of sigma structure porphyroclast from 48w8400-7a sample. Top is to the left in this sample. Material inside porphyroclast is relic vein fill material of zeolites and carbonate/talc.

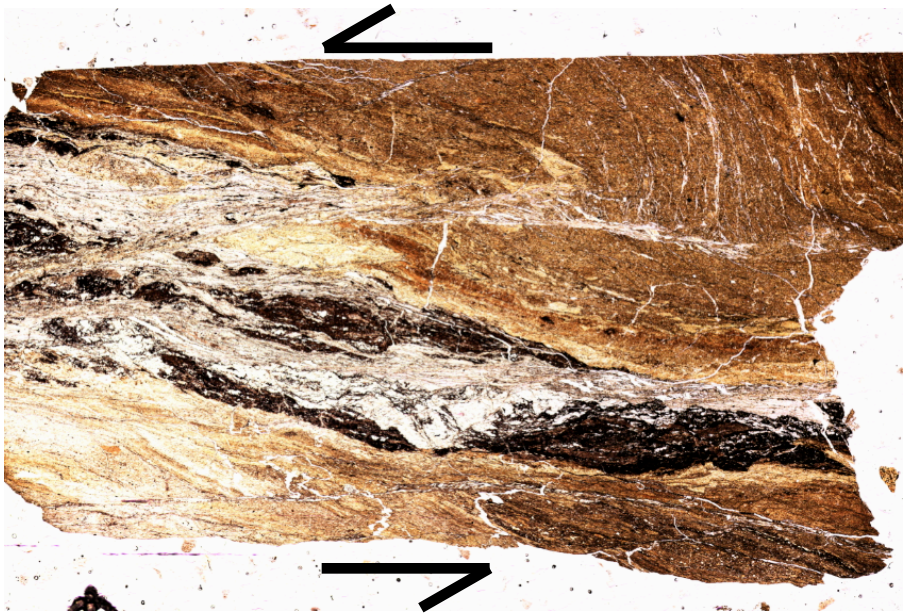


Figure 43: PPL thin-section scan of HW-loc-shear from 48w8400-14 sample showing pervasive cross cutting of brittle fractures through plastic structures. CS fabric in bottom left. Note microthrust at the top of the image and folded material at right. Length of horizontal axis is 36 mm.

Synkinematic Temperature/Pressure Conditions and the Deformation Mechanisms

T/P Conditions Within the South Prairie Fault

Multiple lines of evidence suggest that the maximum T/P conditions experienced during faulting were low greenschist facies, equating to T≈300ºC and P≈250-400 MPa (Winter, 2010). This maximum temperature is observed in the core zone mineralogy consisting dominantly of serpentine and serpentine-chlorite and the disappearance of laumontite at the FW- and HW-loc-shears (as evidenced by XRD). At increasing grades from zeolite facies through prehnite-pumpellyite, zeolites become less stable and break down at the expense of more stable minerals such as chlorite and quartz (Winter, 2010). This relationship could represent either the difference in early and late stage T/P conditions, and/or disparate prekinematic and synkinematic conditions. The presence of quartz at the 2600 level is consistent with this break down process and remineralization at higher conditions. Quartz's undulose extinction also supports a maximum temperature at T≤300ºC (Miller, 1987; Smith, 1991; Miller and Lageson, 1993; Lützenkirchen, 2002). Furthermore, the hydrated mineral assemblage of talc-tremolite-chlorite-serpentine observed at the 2600 and slightly at the 4800 level gives a temperature range consistent with greenschist conditions (Boschi et al., 2006; Winter, 2010). These mineralogical characteristics are consistent with the geothermal gradient estimates mentioned in the Geometry section of this chapter, where an assumed gradient of 35ºC/km gave a

maximum ambient temperature of T=280ºC for 8 km burial depth of the SPF at the start of Laramide orogenesis in the Beartooth arch. It is likely this is a maximum value.

Scholz (1990) attributes greenschist conditions to be securely in his "semi-brittle" field, within the brittle to plastic transition. Petrographic analyses support this claim with the presence of CS fabrics found within the foliated gouge of the core zone. The presence of stable fractures within grains of the FW- and HW-DZ further suggests brittle/plastic behavior to have occurred within the SPF (Mitra, 1984; Smith, 1987; Miller, 1991). It is likely that both brittle and plastic mechanisms operated early in the SPF's motion history, however subsequent unroofing during arching of the Beartooth massif would have reduced the conditions observed from early brittle/plastic to more brittle towards the end of the Laramide orogeny. This relationship is directly observed and discussed above (Figure 43) where later-stage brittle fractures are shown to crosscut earlier formed CS fabrics.

Evidence within the alteration mineralogy can also be used to estimate a minimum temperature experienced in the SPF. Alteration of plagioclases to epidote establishes temperature conditions at less than 525ºC (Moody et al., 1985). This estimate can further be refined by the presence of clinozoisite, as epidote has been shown to be indicative of T≥200ºC (Miller, 1987; Lützenkirchen and Loew, 2011 and references therein). Prior studies citing this temperature range were conducted in hydrothermally altered environments. No evidence of clinozoitization was observed to occur at vein boundaries and thereby suggests that alteration of plagioclase was strictly related to

conditions during motion on the SPF. Therefore, minimum conditions within the SPF's damage zones during seismic periods had to be in the range of T≥200-220ºC. Lack of a relationship between clinozoisite and veining does not preclude formation of clinozoisite formation from metasomatism or hydrothermal fluids, as it has already been shown that fluids are required for their formation. Observation of sample 48w8400-17 within the 4800 HW-DZ being pervasively clinozoitized could be evidence in support of hydrothermal and/or metasomatic fluid-flow within the HW during faulting. More evidence is needed to prove or disprove this claim, though the above discussion based on Phillips (1972) does lend support.

Minimum estimates on temperatures within the fault are best suggested by the post-kinematic vein mineralogy. Zeolite facies requires T≥150ºC (Winter, 2010). The abundant presence of euhedral zeolites (stilbite-ca) as the dominant vein-fill material therefore records at least minimal temperatures of fluids after the latest stages of movement on the SPF. Caution must be taken, however, as the presence of stilbite and laumontite may represent two phases of zeolite growth as both of these minerals represent both ends of the zeolite facies. Stilbite is common at lower conditions (T≤190ºC at 10 MPa; Lützenkirchen, 2002) in the zeolite facies, whereas laumontite represents higher grade conditions (T=190-210ºC at 10 MPa; Lützenkirchen, 2002) up to the prehnite-pumpellyite facies. Euhedral stilbite (Figure 39) strongly supports its growth as post-kinematic. Laumontite, though observed by XRD, was not readily apparent, and therefore may be present as the smaller and broken up grains found within veins or

cataclasized material. Lützenkirchen (2002, 2011) had similar results in his study, and suggests that laumontite formed synkinematically. He proceeds to use laumontite for his estimates on syn-kinematic T/P conditions. I suggest that the use of clinozoisite after plag is the best method in this study for determining minimum faulting conditions in the SPF. If laumontite was a product of syn-kinematic fluids, it would positively show the presence of fluids during faulting and likely indicate a cooling down phase immediately following motion on the fault.

Relic vein material within the gouge of the core zone, however, does suggest that zeolite conditions did occur for at least some time during the SPF's deformation history. The metasomatic mineral assemblage does suggest hotter fluids did permeate through at least the HW of the SPF, perhaps synkinematically as mentioned above. However, euhedral stilbite crystals and broken up vein material within CZ porphyroclasts strongly suggests that the minimum temperature of fluids flowed strictly during post-kinematic or interseismic periods.

Platinum/Palladium Mobility
Within the South Prairie Fault

In many areas of the mine, the SPF intercalates with the Pt/Pd JM Reef mined by the Stillwater Mining Company. This makes the presence (or absence) of the SPF a considerable obstacle during production, as it has the tendency to double or reduce production at a given location by a spatially undeterminable amount. Doubling-up and depletion is achieved by a pseudo ramp-flat geometry produced by the SPF's layer-

parallel geometry. In this study, the 4800 level was the only location that the SPF contained the reef within the actual fault zone, as determined by the presence of sulfide mineralization within the lens of rock near the FW-loc-shear. The SPF at the 2600 and 2900 levels did not cut into the reef and was located just shy of it by a few meters. It is unknown at these latter two locations if the SPF doubled-up or cut the reef.

Assays run on SPF gouge have locally shown Platinum Group Elements (PGE) mineralization to be sometimes double that of what is observed in unfaulted JM Reef strata immediately adjacent to the fault (Cox and Holick, 2008). In other areas, mine geologists frequently mark zones for production that are seemingly unfaulted, yet return on the area is unprofitable as ore is depleted seemingly for no reason at all (Mike Pasecznyk, personal communication). To the best of my knowledge there has been no attempt to study and describe the absence of the reef and/or the doubling of PGE mineralization within SPF gouge. However Cox and Holick (2008) do suggest remobilization and possible enrichment coincident with alteration, and work conducted in this study may have implications for this process.

Concentration of PGE's into fault gouge can be explained by two processes: (1) physical grain remobilization via cataclasis, and (2) chemical remobilization by fluid-flow processes. Though grain remobilization is likely, it is well understood that fluids commonly assist in ore mineralization and remobilization (Cathles, 1981; Winter, 2010) and thereby suggests a chemical process. Within the mine, the lack of PGE mineralization in ore zones that are apparently unaffected by faulting suggests a process that does not

require concentration by cataclasism, but rather by chemical remobilization. Furthermore, the hydrous phyllosilicate mineralogy of the SPF core zone strongly warrants consideration of fault-zone fluids as a catalyst for the reaction and remobilization process of ore into the SPF gouge.

Fluid-assisted remobilization of PGE minerals has been documented in a variety of environments (Hsu and Lechler, 1991). In all cases, hydrothermal fluids of T≥300ºC are cited. Experiments conducted on remobilization (Hsu and Lechler, 1991; Barnes and Liu, 2012) also cite minimum temperatures at T≥300ºC. A recent study by Barnes and Liu (2012) was conducted modeling potential remobilization in sulfur-rich and sulfur-poor komatiites from various locations. They found that Pt/Pd remobilization up to 50 ppb in sulfur-rich environments was readily possible at low water/rock (W/R) ratios on the order of W/R=10. Dissimilarly, when sulfur-poor to sulfur-absent environments were theoretically examined, unrealistic W/R ratios were required for remobilization to occur. However, more work on the nature and composition of the fluids must be conducted to determine the likelihood of Pt/Pd remobilization via bisulfide ion since pH and eH plays a strong role in the mobility of metals.

Earlier experiments by Hsu and Lechler (1991) suggested that remobilization of PGE minerals could be easily done by formation of a Pt/Pd compound with a chloride ion. Barnes and Liu (2012) were able to successfully model remobilization via a Pt/Pd compound with bisulfide ions. They were also able to show that remobilization by bisulfide compounds required moderate acidic-neutral solutions, whereas chloride

compounds require extremely acidic or oxidized solutions. Therefore, reaction and remobilization of PGE's could have been a relatively easy process given the conditions found within the SPF. Being that the JM Reef is a sulfide-rich unit, it is very likely that remobilization of PGE's could have proceeded by formation of Pt-/Pd-bisulfide compounds during metasomatic conditions.

A requirement of low W/R ratios (Barnes and Liu, 2012) is also satiated by observation of the SPF, as it is evident fluids were most likely present while the fault was active. It was discussed that the reaction of Opx to serpentine requires at least 50% water to one part Opx. If this is representative of the W/R ratio, then remobilization of PGE's was likely readily possible within the SPF. Hydrothermal temperatures of T≈300ºC are extremely favorable as well, as work suggests remobilization is more extensive at low to moderate temperature hydrothermal solutions (Lechler and Hsu, 1988) given a pH between 5.4 (Barnes and Liu, 2012) and 6.5 (Hsu and Lechler, 1991). In all studies, palladium was shown to be the most soluble.

Determination of the geochemical parameters for PGE remobilization was beyond the scope of this thesis. However, further research should be conducted as hydrothermal remobilization of PGE's has been noted elsewhere, such as at the New Rambler Mine in the Medicine Bow Mountains of Wyoming (McCallum et al., 1976) and the Lac des Iles mine in northern Ontario, Canada (Hinchey and Hattori, 2005). Assays correlated with a fault zone architecture and permeability estimate as done in this study could be used to assess the likelihood of fluid-flow in areas where SPF gouge has high PGE

concentrations. Estimates on pH-eH levels and stable isotopic analyses for fluid-flow history and characteristics would further refine whether hydrothermal fluids were derived syn-kinematically or post-kinematically. Given palladium's propensity for solubility at low to mid hydrothermal conditions (≈300ºC), it seems more likely that remobilization, if in fact hydrothermally remobilized into SPF gouge, would have occurred during elevated temperatures recorded in the talc-tremolite-chlorite-serpentine fluid-derived assemblages rather than the interseismic stilbite formation phases. Assay reports considering both Pt and Pd would also be needed.

Deformation Mechanisms

The conditions at which faulting took place have formed a variety of deformation mechanisms that span from strictly brittle to brittle-plastic mechanisms. These mechanisms reflect the unroofing of the sedimentary veneer during arching of the Beartooth massif during the Laramide orogeny. Mesoscopic observation of the SPF shows brittlely deformed material through pervasive fracturing, mostly in the HW-DZ's. The core zone is heavily comminuted and slip localization was likely in a process of gouge flow via an anastomosing network of Riedel R-fractures subparallel to the main fault body.

Microscopically, brittle and plastic mechanisms were observed in the overall deformation process of the SPF. These processes include fracturing, cataclasis, cataclastic flow and pressure solution/dissolution. Increasing alteration towards the core zone suggests that dissolution was an important process during the overall deformation history

whereby fracturing of grains and whole rock provided a path for fluid transport leading to subsequent alteration. The following discussion is broken up into the damage zone and core zone given the differing mechanical properties.

Damage Zones: Grains within the damage zones were observed to fail by unstable as well as stable fracturing. At distal (furthest from the core zone) portions of the damage zone, stable fracturing was observed within different mineral grains. Unstable fractures were only present in grains of the same phase (Plag and Plag). This shows the different rheological behavior of grains and suggests that brittle and brittle-plastic mechanisms operated concurrently in different parts of the fault zone, such as was seen with Miller (1987) and Miller and Lageson (1993). Polyphase unstable fracturing was only observed in the HW-DZ and at areas closest to the core zone. Some areas showed stable fracturing and microfaulting dying out into a more ductile matrix (Figure 44).

Intergranular fractures, fractures formed along grain boundaries (Davis et al., 2012), were likely the initial means by which fluids permeated through the damaged material, leading to alteration. Alteration appeared initially as a closed system within the damage zone phases (Plag to clinozoisite; Opx to serpentine), likely from intragranular stable fractures. Opx's characteristic non-kinematic irregular fracturing was probably the reason for its quick alteration, as fluids were more likely to permeate before fractures had occurred in Plag and Cpx. Continued fracturing allowed more alteration to take place by permeation of fluids into individual grains (Evans, 1988). Occasionally these fractures

were crystallographically controlled by cleavage (Cpx), but shear fractures deviating from cleavage angle were detected.

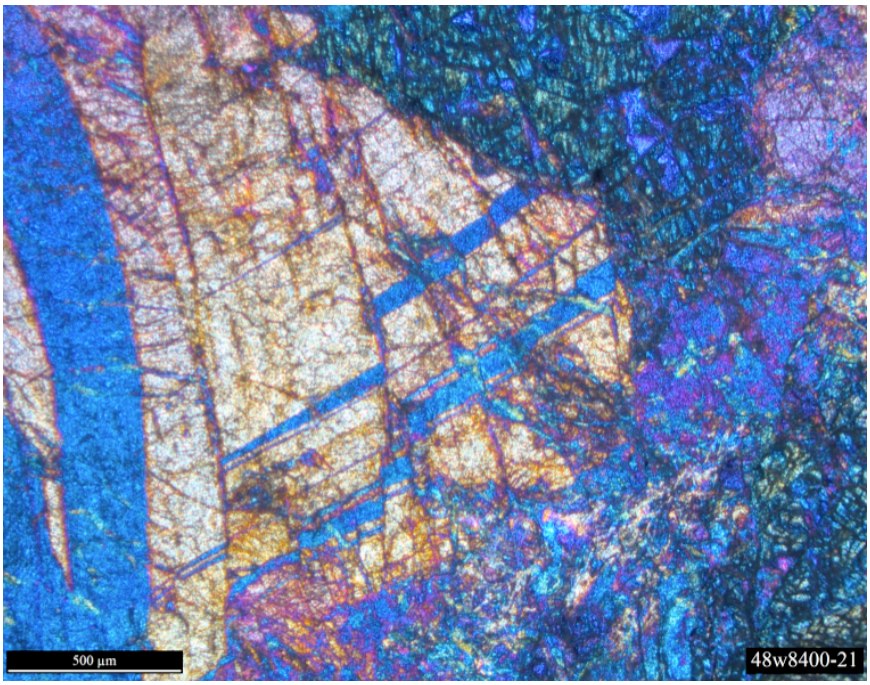


Figure 44: Dying out of stable microfaults into a more ductile matrix at the bottom, Opx crystal at top. XPL, condenser plate used. This sample was taken in the 4800 FW-DZ approximately 0.8 m away from the FW-loc-shear (south of CZ).

Core Zone: Mesoscopically, the core zone was entirely composed of fully comminuted gouge. Discrete fracture surfaces were visible within the core zone at both the 2600 and 4800 levels, showing slip was partially through fracturing within the gouge rather than strictly by cataclastic flow. Cataclastic flow was observed at the microscopic scale however (Figure 45). Cataclasis, cataclastic flow, and pressure solution were all observed within the core zone of the SPF. However, as opposed to the damage zone, the core zone dominantly consisted of the alteration material serpentine-chlorite. Relic grains

surrounded by cataclastically flowed material were observed to persist into the core zone. These relic minerals were heavily altered across the entire grain. Cataclastic flow at the microscopic scale appeared to have a fractal behavior (self-similar) to the anastomosing nature of the core zone gouge at the mesoscopic scale.

These observations suggest that within the SPF, core zone material was not caused strictly by comminution within the core zone. Rather, a gradient of alteration aided in the development of core zone material that was eventually entrained into the plane of slip localization. Once taken up by the core zone, comminution and alteration continued to the point of true gouge formation with a microscopic cataclastic flow texture. The damage and core zone are mechanically and compositionally distinct, however.

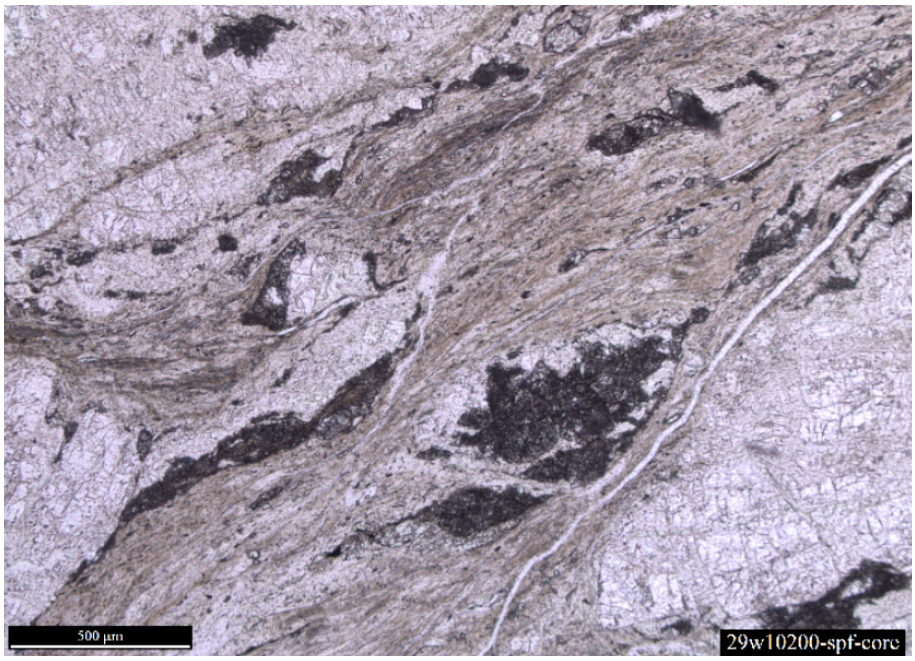


Figure 45: PPL photomicrograph of anastomosing cataclastic flow within 29w10200 CZ. Heavily fractured Plag at right. Dark material is altered and comminuted ultracataclasite.

Preferred Orientation of Fault
Zone Rock and Material

Two samples from core (Figure 45) were examined for preferred orientation at Sector 11-ID-C of the Advanced Photon Source at Argonne National Laboratories. These samples were likely from one of the SPF damage zones, as no gouge was present. A section of core approximately <0.5 m wide was missing from the core box, and may have been gouge from the core zone. An apparently chloritized and an anomalous white sample were taken and cut perpendicular to the SPF. Results indicate an overall lack of preferred orientation for these two samples at m.r.d.<2. Petrographic analysis supports this as it is apparent that the damage zones do not even contain a visible alignment of grains and are essentially randomly oriented in this part of the Stillwater Complex (though rhythmic layering is observed elsewhere). Had gouge samples been available at the time of these analyses, it is likely that a higher preferred orientation would have been measured.

Rudy Wenk (personal communication) suggests that gouge material has a tendency to tumble, and therefore does not produce a strong preferred orientation. Other studies that have quantified gouge preferred orientation have consistently shown m.r.d.≤7 with most samples being m.r.d.≈2 (Buatier et al., 2012), further suggesting tumbling of the gouge during deformation. Tumbling was clearly evident for gouge in the interior of the core zone at the 4800 level. However, it is postulated that the localized shear zones may produce higher preferred orientation measurements based on their visible foliation. This would be indicative of different mechanical processes occurring at the core zone

boundaries, perhaps by a clay smear mechanism. Strongly preferred alignment of gouge material would have hydrological effects on a fault zone (Buatier et al., 2012), and therefore understanding the properties of these localized shear zones could have implications on the ability of fluid-flow within fault zones.



Figure 46 (following page): Core box showing areas of core taken for synchrotron diffraction. Missing section may represent core zone gouge. Left side of box is likely the hanging wall based on drill log data. Width of box is approximately one meter.

CHAPTER 7

CONCLUSIONS

Geometry and Kinematics of the South Prairie Fault

Geometric and kinematic analyses show that the SPF's strike is coincident with other Laramide faults and fits well within the interpreted Laramide regional shortening direction (040-065). A balanced cross-section across the Beartooth front at Nye, MT, shows a complex system of fault splays in which the SPF is only a minor part of the system. Slight transpression of the SPF block between the Horseman thrust and south-dipping thrusts above the SPF may have caused the block to pop-up towards the east, giving an apparent dextral oblique motion that is opposite the expected sinistral motion along Beartooth front following the kinematic model of Brown (1993). This is a result of the SPF's north-dip and still follows a sinistral motion overall along the Beartooth range front during Laramide orogenesis.

Extent of the South Prairie Fault's CZ and DZ and its Architecture and Permeability

The extent of the core and damage zone varies per location in the mine, and appears to be related to the fault's proximity with the JM Reef. The 4800 level was a total width of 7.5 m with a ~2.5 m core zone that contains the reef. The FW-DZ/HW-DZ were also ~2.5 m. The 2600 CZ is outside the reef, and thickens from <30 cm to ≥1 m, while the FW-DZ is <3 m. The HW-DZ is not fully exposed and was unable to be determined.

The 2900 level did not show a full exposure and determination of zone widths was not possible.

Fractures associated with the SPF show a bimodal relationship and are oriented either sub-parallel or antithetically to the main fault body. These fractures were interpreted to represent Riedel R- and R'- fractures. R-fractures are within 10º of the dip of the SPF; R'-fractures are oriented about 75º antithetically to the SPF. A set of anastomosing fractures was observed within the core zone at the 2600 level. Fractures in the 4800 CZ were also measured. Both sets are shown to be oriented dominantly with the main fault body and likely represent partitioned slip within the SPF.

The architecture values measured at the 4800 level give an estimated permeability of 67% that plots as a combined-conduit barrier system, similar to another basement fault, the Wind River Range's White Rock thrust, shown by Caine et al. (1996). Evidence for fluid-flow within the SPF was observed at the meso- and microscopic scales and was consistent with the permeability estimate calculated. Fluids likely ranged from metasomatic and/or hydrothermal fluids at the time of faulting to post-kinematic fluids, possibly derived from meteoric waters. Veins within and at the FW-DZ/CZ contact on the 2600 and 4800 levels, respectively, are hypothesized as being suggestive of a fluid-flow/ fault slip behavior. Such a relationship within SPF could have caused fluid-overpressure and eventual fault rupture, as discussed by Scholz (1990).

Mineralogy of the South Prairie Fault and How It Varies

Host rock in the vicinity of the SPF was gabbronorites and norites of the Lower Banded Series, specifically in the vicinity of Anorthosite I Subzone (Geraghty, 2013). The dominant mineral phase was plagioclase, followed by orthopyroxene, and minor to moderate clinopyroxene.

Damage zones acted as intermediate zones of alteration, showing partially altered minerals and vein-fill material. Orthopyroxene succumbed to alteration to serpentine likely due to irregular cracking and subsequent infiltration of fluids. Intermediate alteration of orthopyroxene to cummingtonite before total pseudomorphic serpentinization was observed. Plagioclase was the second most resistant phase to alteration, even while heavily fractured and orthopyroxene was nearly entirely altered. Decreasing anorthite concentrations suggest that Ca-/Al-remobilization led to clinozoitization of plagioclase through albitization (Moody et al., 1985), and is consistent with prior studies of tectonically deformed plagioclase to epidote (Miller, 1987). Clinopyroxene was the most resistant to alteration, appearing to alter to serpentine by extensive fluid-flow. Cleavage plane fractures dominated in clinopyroxene and precluded alteration. Alteration phases appeared to form as the mafic counterparts of alteration phases observed in quartzofeldspathic rocks (plagioclase to an epidote variety, gouge forming Mg-rich phyllosilicates in mafic rocks and illite/smectite in quartzofeldspathic rocks).

A metasomatic mineral assemblage of tremolite-chlorite-serpentine-talc (Boschi et al., 2006) was observed to be pervasive in the 2600 HW-DZ, and minor at the 4800 CZ/ HW-DZ contact. These fluids suggest the presence of hydrothermal fluids likely at the time of faulting, and left a bleached appearance of the rock. The FW-DZ's showed minor to no bleaching, suggesting fluids permeated up from the fault zone, similar to what was observed in Phillips (1972) study that caused hydrothermal brecciation.

Gouge within the severely comminuted core zone consists dominantly of serpentine, chlorite, and serpentine-chlorite, as evidenced by XRD. Towards the center of the core zone, damage zone phases such as zeolite, albite/plagioclase, and clinozoisite were observed in XRD and thin-section. The FW-loc-shear consists of cataclastically flowed serpentine-chlorite and contains porphyroclasts of relic vein material, suggesting protracted fluid-flow events. The HW-loc-shear is also dominantly serpentine-chlorite, but minor tremolite did occur, likely from the metasomatic mineral assemblage.

Zeolites are the dominant vein-fill material, and likely formed during late stage deformation. Euhedral veins in the DZ and CZ are most likely stilbite-Ca, evidenced by one plane of cleavage and XRD, and formed post-kinematically. Laumontite was suggested by XRD analysis, though none was directly observed in the petrographic analysis and may have made up some of the groundmass material. It is possible that laumontite formed as a late syn-kinematic fluid-flow material, as was seen in Lützenkirchen's (2002) study.

Syn-kinematic T/P Conditions and the Deformation Mechanisms

Physical-chemical evidence suggests that the SPF experienced motion in the brittle-plastic region early in its history, and purely brittle conditions later in its history. Ambient conditions were likely in the range of T≥150ºC, evidenced by zeolite veins. The presence of the epidote variety clinozoisite suggests syn-kinematic conditions in the range of T≥220ºC, while serpentine-chlorite and the metasomatic assemblage suggest lower greenschist conditions of T≤300ºC. Undulose extinct quartz also supports this upper limit.

These conditions of faulting were favorable for fluid-induced remobilization of JM Reef PGE minerals. Sulfides associated with the JM Reef may have formed bisulfide compounds that dissolved and remobilized the ore at low W/R ratios into the fault zone gouge at the hydrothermal conditions of T≈300ºC (Lechler and Hsu, 1988; Hsu and Lechler, 1991; Barnes and Liu, 2012). This may explain the high concentrations of PGE's shown by assays run on SPF gouge and the disappearance of ore in areas seemingly unaffected by faulting (Cox and Holick, 2008). This warrants further investigation, however, to better understand the mechanism.

Fracturing, cataclasis, cataclastic flow, and pressure solution (dissolution) deformation mechanisms were all observed within the SPF and is consistent with the brittle and brittle-plastic conditions suggested by the mineralogy and micro-mesoscopic physical characteristics. Unstable (brittle) and stable (plastic) fractures were evident in the damage zones. Unstable fracturing between plagioclase-orthopyroxene was only

observed in heavily brecciated samples near the CZ or in the HW-DZ. Besides these, unstable fracturing was only observed to occur between like-phases. Alteration (dissolution) within the damage zones started at the grain boundaries by intergranular fractures, and continued via stable fractures within grains. Cataclastic flow was observed only within the core zone.

Preferred orientation of fault zone rock and material was consistent with other studies and showed low m.r.d. values (Buatier et al., 2012). However, samples of damage zone rock were only available at the time of analysis, and it is expected that fluxion core zone material would exhibit a stronger preferred orientation measurement.

REFERENCES CITED

Anderson, E.M., 1951, The Dynamics of Faulting and dyke formation with applications to Britain: Edinburgh, UK, Oliver and Boyd, 2nd ed, 191 pp.

Babcock, L.N., Chadwick, J., Corthouts, T., Easley, E., Jeffrey, S., Kay, L., Mangini, S., Moore-Nall, A.L., Reid, C.R., and Thacker, J., 2013, A new look at the classic Hubbert-Rubey Beer Can Experiment: Laboratory analogue to fault displacement mechanisms: Geological Society of America Abstracts with Programs, v. 45, no. 7.

Barnes, S.J., Liu, W., 2012, Pt and Pd mobility in hydrothermal fluids: Evidence from komatiites and from thermodynamic modeling: Ore Geology Reviews, v. 44, p 49-58.

Beaudoin, N., Bellahsen, N., Lacombe, O., Emmanuel, L., 2011, Fracture-controlled paleohydrology in a basement-cored, fault-related fold: Sheep Mountain Anticline, Wyoming, United States: Geochemistry Geophysics Geosystems, v. 12, n. 6, Q06011, doi: 10.1029/2010GC003494.

Bird, P., 1998, Kinematic history of the Laramide Orogeny in latitudes 35 degrees-49 degrees N, western United States, Tectonics, v. 17, p. 780-801.

Blackstone, D. L. Jr., 1986, Structural geology – northwest flank of Bighorn Basin: Park County, Wyoming and Carbon County, Montana, in Geology of the Beartooth Uplift and adjacent basins, Montana Geological Society and Yellowstone Bighorn Research Association joint field conference and symposium, p.125-135.

Borg, I. and Handin, J.W., 1966, Experimental deformation in crystalline rock: Tectonophysics, v. 3, p. 251-323.

Boschi, C., Früh-Green, G.L., Delacour, A., Karson, J.A., Kelley, D.S., 2006, Mass transfer and fluid flow during detachment faulting and development of an oceanic core complex, Atlantis Massif (MAR 30ºN), Geochemistry Geophysics Geosystems, v. 7, n. 1, Q01004, doi:10.1029/2005GC001074.

Boulton, C., Carpenter, B.M., Toy, V., Marone, C., 2012, Physical properties of surface outcrop cataclastic fault rocks, Alpine Fault, New Zealand: Geochemistry Geophysics Geosystems, v. 13, n. 1, p. 1-13.

Brown, W. G., 1993, Structural style of Laramide basement-cored uplifts and associated folds, *in* Snoke, A.W., Steidtmmann, J.R., and Roberts, S.M., eds., Geology of Wyoming: Geological Survey of Wyoming Memoir Number 5, p. 312-371.

Brozdowski, R.A., 1985, Cumulate xenoliths in the Lodgepole, Enos Mountain and Susie Peak intrusions: A guide, *in* Czamanske, G.K., and Zientek, M.L., eds., The Stillwater Complex, Montana: Geology and guide: Montana Bureau of Mines and Geology Special Publication 92, p. 368-372.

Buatier, M.D., Chauvet, A., Kanitpanyacharoen, W., Wenk, H.R., Ritz, J.F., Jolivet, M., 2012, Origin and behavior of clay minerals in the Bogd fault gouge, Mongolia: Journal of Structural Geology, v. 34, n. 1., p. 77-90.

Caine, J.S., Evans, J.P., Forster, C.B., 1996, Fault zone architecture and permeability structure: Geology, v. 24, n. 11, p. 1025-1028.

Cathless, L.M., 1981, Fluid flow and genesis of hydrothermal ore deposits; Economic Geology, 75th Anniversary Volume, p. 424-457.

Chester, F.M., and Logan, J.M., 1986, Implications for the mechanical properties of brittle faults from observations of the Punchbowl fault zone, California: Pure and Applied Geophysics, v. 124, n. 1/2, p. 79-106.

Cooper, R.W., Zientek, M.L., Boudreau, A.E., McCallum, I.S., Miller, J.D., Geraghty, E.P., Mooney, D.G., editors, 2002, Stillwater Complex, 9th International Platinum Symposium, Geology and Guide, July 2002, 182 p.

Cox, B.E., Holick, P., 2008, Reverse fault duplication of the J-M Pd/Pt Reef - opportunities for enhanced mine production in the Stillwater Complex, Montana: Northwest Geology, v. 37, 2008, p. 41-44.

Davis, G.H., Reynolds, S.J., Kluth, C.F., 2012, Structural Geology of Rocks and Regions: New York, USA, John Wiley & Sons, Inc, 3rd ed., 839 p.

DePaolo, D.J., Wasserburg, G.J., 1979, Sm-Nd age of the Stillwater Complex and the mantle evolution curve for neodymium: Geochimica et Cosmochimica Acta, v. 43, p. 999-1008.

Erslev, E.A., 1993, Thrusts, back-thrusts, and detachment of Rocky Mountain foreland arches, in C.J. Schmidt, R.B. Chase, and E.A. Erslev, eds., Laramide basement deformation in the Rocky Mountain foreland of the western United States: Geological Society of America Special Paper 280, p. 339-358.

Evans, J.P., 1988, Deformation mechanisms in granitic rocks at shallow crustal levels: Journal of Structural Geology, v. 10, n. 5, p. 437-443.

Finn, C., Zientek, M.L., Bloss, B.R., Wintzer, N.E., Parks, H.L., 2013, Geophysical imaging of the Stillwater Complex and relation to platinum group element exploration: Geological Society of America Abstracts with Programs, v. 45, no. 7.

Foose, R.M., Wise, D.U., and Garbarini, G.S., 1961, Structural geology of the Beartooth Mountains, Montana and Wyoming: Geological Society of America Bulletin, v. 72, p. 1143-1172.

Frost, B.R., Beard, J.S., 2007, On silica activity and serpentinization: Journal of Petrology, v. 48, n. 7, p. 1351-1368.

Geissman, J.W., Mogk, D.W., 1986, Late Archean tectonic emplacement of the Stillwater Complex along reactivated basement structures, northern Beartooth Mountains, southern Montana, U.S.A., *in* Proceedings of the 6th International Conference on Basement Tectonics, Santa Fe, p. 25-44.

Geraghty, E., 2013, Geologic map of the Stillwater Complex within the Beartooth Mountains Front Laramide triangle zone south-central Montana: MBMG Open File Report 645, 22p., 1 sheet, 1:48,000.

Goddard, J.V., Evans, J.P., 1995, Chemical changes and fluid-rock interaction in faults of crystalline thrust sheets, northwestern Wyoming, U.S.A.: Journal of Structural Geology, v. 17, n. 4, p. 533-547.

Gudmundsson, A., 2011, Rock Fractures in Geological Processes: Cambridge, UK, Cambridge University Press, 1st ed., 578 p.

Hinchey, J.G., Hattori, K.H., 2005, Magmatic mineralization and hydrothermal enrichment of the High Grade Zone at the Lac des Iles palladium mine, northern Ontario, Canada: Mineralium Deposita, v. 40, p. 13-23.

Hsu, L.C., Lechler, P.J., 1991, Hydrothermal solubility of Palladium: Nevada Bureau of Mines and Geology Newsletter, Spring 1991 (in press).

Hubbert, M.K., Rubey, W.W., 1959, Role of fluid pressure in the mechanics of overthrust faulting: Geological Society of America Bulletin, v. 70, p. 115-166.

Janecke, S.U., Evans, J.P., 1988, Feldspar-influenced rock rheologies: Geology, v. 16, p. 1064-1067.

Jones, C.H., Farmer, G.L., Sageman, B., Zhong, S., 2011, Hydrodynamic mechanism for the Laramide orogeny: Geosphere, v. 7, n. 1, p. 183-201.

Jones, W. R., Peoples, J. W., and Howland, A. L., 1960, Igneous and tectonic structures of the Stillwater complex, Montana: U. S. Geol. Survey, Bull. 1071-H, p. 281-340.

Kleinkopf, M.D., 1985, Regional gravity and magnetic anomalies of the Stillwater Complex area, in Czamanske, G.K., and Zientek, M.L., eds., The Stillwater Complex, Montana: Geology and guide: Montana Bureau of Mines and Geology Special Publication 92, p. 33-38.

Lechler, P.J., Hsu, L.C., Hudson, D.M., 1988, Anomalous platinum associated with hydrothermal manganese mineralization at the Gibellini Mine, Fish Creek Range, Nevada: Nevada Bureau of Mines and Geology Open-File Report 88-4, 7 p.

Lijun, L., Gurnis, M., Seton, M., Saleeby, J., Müller, R.D., Jackson, J.M., 2010, The role of oceanic plateau subduction in the Laramide orogeny: Nature Geoscience, v. 3, no. 5, p. 353-357.

Lopez, D.A., 2001, Preliminary geologic map of the Red Lodge 30’ x 60’ quadrangle south-central Montana, Montana Bureau of Mines and Geology: Open File Report 423, 1 sheet, 1:100,000.

Lützenkirchen, V.H., 2002, Structural geology and hydrogeology of brittle fault zones in the central and eastern Gotthard Massif, Switzerland [PhD Dissertation]: Phillips-Universität Marburg, 247 p.

Lützenkirchen, V., Loew, S., 2011, Late Alpine brittle faulting in the Rotondo granite (Switzerland): deformation mechanisms and fault evolution: Swiss Journal of Geosciences, v. 104, n. 1, p. 31-54.

Lynn, H.B., 2012, Structural controls on subsurface fluid migration through thrust sheets of the Stewart Peak Culmination, northern Salt River Range, Wyoming [Master's thesis]: Montana State University, 306 p.

Marshak and Mitra, 1988, Basic Methods of Structural Geology: Englewood Cliffs, NJ, Prentice Hall Publishers, 448 p.

McCallum, I.S., 2002, The Stillwater Complex: a review of the geology, *in* Stillwater Complex, 9th International Platinum Symposium, Geology and Guide, July 2002, p. A-1-A-25.

McCallum, M.E., Loucks, R.R., Carlson, R.R., Cooley, E.F., Doerge, T.A., 1976, Platinum metals associated with hydrothermal copper ores of the New Rambler Mine, Medicine Bow Mountains, Wyoming: Economic Geology, v. 71, p. 1429-1450.

Miller, E.W.B., 1987, Laramide basement deformation in the northern Gallatin Range and southern Bridger Range, Southwest Montana [Master's Thesis]: Montana State University, 78 p.

Miller, E.W.B. and Lageson, D.R., 1993, Influence of basement foliation attitude on geometry of Laramide basement deformation, southern Bridger Range and northern Gallatin Range, Montana, in C.J. Schmidt, R.B. Chase, and E.A. Erslev, eds., Laramide basement deformation in the Rocky Mountain foreland of the western United States: Geological Society of America Special Paper 280, p. 73-88.

Mitra, G., and Frost, B.R., 1981, Mechanisms of deformation within Laramide and Precambrian deformation zones in basement rocks of the Wind River Mountains: Contributions to Geology, University of Wyoming, v. 19, n.2, p. 161-173.

Mitra, G., 1984, Brittle to ductile transition due to large strains along the White Rock thrust, Wind River mountains, Wyoming: Journal of Structural Geology, v. 6, n. 1/2, p. 51-61.

Mogk, D.W., Geissman, J.W., 1984, The Stillwater Complex is allochthonous: Geological Society of America Programs with Abstracts, v. 16, no. 6, p. 598.

Mogk, D.W., 1988, Archean allochthonous units in the northern and western Beartooth Mountains, Montana, in Lewis, S., Berg, R.B., 1988, Precambrian and Mesozoic plate margins: Montana, Idaho and Wyoming, with field guides for the 8th International Conference on Basement tectonics, Montana Bureau of Mines and Geology: Special Publication 96, p. 43-51.

Moody, J.B., Jenkins, J.E., Meyer, D., 1985, An experimental investigation of the albitization of plagioclase: Canadian Mineralogist, v. 23, p. 583-596.

Mueller, P.A., Wooden, J.L., Mogk, D.W., Henry, D.J., Bowes, D.R., 2010, Rapid growth of an Archean continent by arc magmatism: Precambrian Research, v. 183, p. 70-88.

Neely, T.G., Erslev, E.A., 2009, The interplay of fold mechanisms and basement weakness at the transition between Laramide basement-involved arches, north-central Wyoming, USA: Journal of Structural Geology, v. 31, n. 9, p. 1012-1027.

O'Connell, P.J., 1996, Kinematics of the Eastern flank of the Beartooth Mountains, Montana and Wyoming, *in* Bowen, C.E., Kirkwood, S.C., Miller, T.S., Resources of the Bighorn Basin: Casper, Wyoming Geological Association, 47th Annual Field Conference, Guidebook, p. 189-220.

Page, N. J., and Nokleberg, W. J., 1974, Geologic Map of the Stillwater Complex, Montana: U.S. Geological Survey, scale 1:12000, 5 sheets.

Page, N. J., 1977, Stillwater Complex, Montana : Rock succession, metamorphism, and structure of the complex and adjacent rocks: U.S. Geological Survey Professional Paper 999, 79 p.

Page, N.J., and Zientek, M.L., 1985, Geologic and structural setting of the Stillwater Complex, in Czamanske, G.K., and Zientek, M.L., eds., The Stillwater Complex, Montana: Geology and guide: Montana Bureau of Mines and Geology Special Publication 92, p. 1-8.

Phillips, W.J., 1972, Hydraulic fracturing and mineralization: Journal of the Geological Society of London, v. 128, p. 337-359.

Poppe, L.J., Paskevich, V.F., Hathaway, J.C., Blackwood, D.S., 2002, A laboratory manual for X-ray powder diffraction: USGS Open File Report 01-041, 88 p.

Reid, H.F., 1913, Report of the committee on the nomenclature of faults: Geological Society of of America Bulletin, v. 24, p. 163-183.

Scholz, C.H., 1990, The mechanics of earthquakes and faulting: Cambridge, Cambridge University Press, 439 p.

Scholz, C.H., 1992, Weakness amidst strength: Nature, v. 359, p. 677-678.

Scholz, C.H., 1996, Faults without friction?: Nature, v. 381, p. 556-557.

Segerstrom, K., Carlson, R.B., 1982, Geologic map of the Banded upper zone of the Stillwater Complex and adjacent rocks, Stillwater, Sweet Grass, and Park Counties, Montana: U.S. Geological Survey, scale 1:24000, 2 sheets.

Sibson, R.H., 1977, Fault rocks and fault mechanisms: Journal of the Geological Society, v. 133, p. 191-213.

Smith, Daniel J., 1991, Structural Geology and History of the Buck Mountain Fault and Adjacent Intra-Range Faults, Teton Range, Wyoming [Master's Thesis]: Montana State University, 143 p.

Solum, J.G., Hickman, S.H., Lockner, D.A., Moore, D.E., van der Pluijm, B.A., Schleicher, A.M., Evans, J.P., 2006, Mineralogical characterization of protolith and fault rocks from the SAFOD Main Hole: Geophysical Research Letters, v. 33, n. 21.

Turner, A.R., Wolfgram, D., Barnes, S.J., 1985, Geology of the Stillwater County sector of the J-M Reef, including the Minneapolis Adit, in Czamanske, G.K., and Zientek, M.L., eds., The Stillwater Complex, Montana: Geology and guide: Montana Bureau of Mines and Geology Special Publication 92, p. 210-230.

Van der Pluijm, B.A., Marshak, S., 2004, Earth Structure: New York, USA, W.W. Norton & Company, Inc., 2nd ed., 656 p.

Wenk, H.R., Voltolini, M., Mazurek, M., Van Loon, L.R., Vinsot, A., 2008, Preferred orientations and anisotropy in shales: Callovo-Oxfordian shale (France) and Opalinus clay (Switzerland): Clays and Clay Minerals, v. 56, n. 3, p. 285-306.

Wilson, C.W., 1936, Geology of Nye-Bowler lineament, Stillwater and Carbon counties, Montana: AAPG Bulletin, v. 20, n. 9, p. 1161-1188.

Wilson, J.T., 1936, The geology of the Mill Creek - Stillwater Area, Montana [PhD. Dissertation]: Princeton University, 131 p.

Winter, J.D., 2010, Principles of Igneous and Metamorphic Petrology: New York, USA, Pearson Education Inc., 2nd ed., 702 p.

Wise, D. U., 2000, Laramide structures in basement and cover of the Beartooth Uplift near Red Lodge, Montana: AAPG Bulletin, v. 84, no. 3., p. 360-375.

Wooden, J.L., Mueller, P.A., Mogk, D.A., Bowes, D.R., 1988, A review of the geochemistry and geochronology of the Archean rocks of the Beartooth Mountains, Montana and Wyoming *in* Lewis, S., Berg, R.B., 1988, Precambrian and Mesozoic plate margins: Montana, Idaho and Wyoming, with field guides for the 8th International Conference on Basement tectonics, Montana Bureau of Mines and Geology: Special Publication 96, p. 23-51.

Zoback, M., Hickman, S., Ellsworth, W., 2011, Scientific drilling into the San Andreas fault zone - An overview of SAFOD's first five years: Scientific Drilling, no. 11, March 2011, p. 14-28.

APPENDICES

APPENDIX A

ORIENTATION MEASUREMENTS OF BEARTOOTH FRONT TECTONIC FEATURES

Orientations of Tectonic Features Near the Beartooth Front							
South Dipping Thrusts	North Dipping Thrusts	Normal Faults	Dextral Strike Slip Faults	Sinistral Strike Slip Faults	Anticline Hingelines	Syncline Hingelines	Stillwater Complex Faults
305	298	062	000	258	300	294	278
308	270	078	039	255	305	300	306
290	295	022	065		300	305	270
285	299	020	056		300	315	275
330	302	048	045		288	320	270
032		055	035		288	278	315
032		095			300	270	SWC S-Dipping Thrusts
313		168			270	350	
312		062			270	278	
		165			280	308	292
		090			318	344	288
		048			315		273
		118			288		269
		008			288		290
		056			310		265
		040			275		283
		050			292		
		048			270		
		052			292		
		052			330		
		040			280		
		052			328		
		040			300		
					255		
n=9	n=5	n=23	n=6	n=2	n=24	n=11	n=13

Resultant Vectors Orientations							
South Dipping Thrusts	North Dipping Thrusts	Normal Faults	Dextral Strike Slip Faults	Sinistral Strike Slip Faults	Anticline Hingelines	Syncline Hingelines	Stillwater Complex Faults
322 (142)	292	059	040	257	293	305	282

APPENDIX B

ESTIMATED ANORTHITE CONCENTRATIONS

48w8400 Samples

48w8400-1 FW

Plag compositions:

1: 268-230 = 38 An_{68}
2: 304-262 = 58 An_{86}
3: 281-222 = 59 An_{86}
4: 238-176 = 62 An_{88}
5: 087-035 = 52 An_{81}
6: 083-044 = 39 An_{68}

Average: An_{80}

48w8400-21 (FW-DZ sample)

Plag compositions:

1: 210-193 = 17 An_{36}
2: 285-248 = 37 An_{66}
3: 268-240 = 28 An_{52}
4: 270-231 = 39 An_{69}
5: 211-176 = 35 An_{64}
6: 362-322 = 40 An_{71}
7: 203-187 = 16 An_{35}

Average: An_{56}

48w8400-16 HW

Plag compositions:

1: 345-303 = 42 An_{72}
2: 269-222 = 47 An_{76}
3: 180-149 = 31 An_{56}
4: 122-084 = 38 An_{66}
5: 236-202 = 34 An_{64}
6: 129-104 = 25 An_{45}

Average: An_{63}

26w8000 Samples

26w8000b-SPF-5 (FW-DZ sample)

Plag compositions:

1: 150-103 = 47 An_{78}
2: 139-096 = 43 An_{72}
3: 134-083 = 51 An_{81}
4: 337-304 = 33 An_{60}
5: 265-234 = 31 An_{58}
6: 270-239 = 31 An_{58}

Average: An_{68}

26w8000-FW-1

Plag compositions:

1: 304º-252º = 52º An_{81}
2: 243-210 = 33 An_{58}
3: 300-268 = 32 An_{58}
4: 263-208 = 55 An_{83}
5: 266-210 = 56 An_{83}
6: 208-172 = 36 An_{65}

Average: An_{71}